Scientific report ; WR 2009-02

# Improving potential wind for extreme wind statistics

*Nander Wever and Geert Groen*

De Bilt, 2009

De Bilt, 2009

PO Box 201
3730 AE De Bilt
Wilhelminalaan 10
De Bilt
The Netherlands
http://www.knmi.nl
Telephone +31(0)30-220 69 11
Telefax +31(0)30-221 04 07

Authors: Wever, N
Groen, G.

KNMI Scientific Report: WR2009-02

# Improving potential wind for extreme wind statistics

Nander Wever and Geert Groen
Netherlands Royal Meteorological Institute (KNMI)

March 5, 2009

**Acknowledgements**
We especially thank Jacco Groeneweg, Houcine Chbab, Marcel Bottema, Sofia Caires, Hans de Waal and Douwe Dillingh from Rijkswaterstaat Waterdienst and Deltares for their cooperation. We also thank Arnout Feijt, Henk van den Brink, Fred Bosveld, Rudmer Jilderda, Jitze van der Meulen and Adri Buishand for their support. Finally, we thank Sander Tijm, Anton Beljaars and Peter Baas for reviewing and commenting our work.

**Omslag**
Houtsnede uit het boek van W. Scheidig: *die Holzschnitte des Petrarca - Meisters*. Berlijn, Henschelverlag, 1955. Het origineel dateert uit 1532.

# Abstract

It is legally required to monitor the main Dutch water defences for their level of protection every five years. For this action, so-called Hydraulic Boundary Conditions (HBC) are needed to quantify the hydraulic loadings on these flood defences. Extreme winds are one of the key inputs for the hydraulic models used to evaluate these HBC. The programme *Strength and Load of Water Defences* (SBW: Sterkte en Belasting Waterkeringen) has the task of improving the knowledge underpinning the HBC. The wind-related aspects are investigated in *SBW Wind*. This report describes the result of the first SBW Wind task: improving the KNMI time series of wind. Subsequent tasks will focus on extrapolation of measured data to extremes, and on spatial coherence of extremes.

Many wind data underpinning the present HBC are based on the 1962-1976 time series and so-called Rijkoort Weibull model (see: *Wieringa and Rijkoort* (1983)). The KNMI HYDRA-project (1998-2005) aimed at extending these time series whilst improving the methods to estimate wind extremes. However, the HYDRA-results were not accepted for the HBC as it yielded a physically implausible result: land-based wind extremes were estimated to be higher than those over the sea, referred to as *curvature problem*.

To correct measured wind for local roughness at the station location, exposure correction factors can be calculated, which convert measured wind into potential wind. Recent KNMI investigations found indications that the exposure correction factors calculated from mean wind speed and wind gusts (referred to as *gustiness analysis*), were too large in the west to north sector in winter. This effect contributes to the curvature problem. Both *Wieringa and Rijkoort* (1983) and *Verkaik* (2006) used gustiness analysis to approximate the standard deviation of the wind speed, due to limited data availability. However, they also suggested to calculate exposure correction factors using 10 minute-data with direct use of standard deviation ($\sigma_u$) and average wind (referred to as $\sigma_u$-*analysis*). Since 2003, for most KNMI wind stations 10 min samples of mean wind speed and standard deviation are stored. Therefore, we now have access to an interesting new data set to compare both methods. It is argued that in winter time with north-westerly winds, possible stability changes in a polar air mass within the timeframe of an hour influences the exposure correction factors based on 1-hour gustiness analysis. By comparing both methods, it is shown that a strong improvement in omnidirectional analysis and spatial gradient of exposure correction factors is achieved when $\sigma_u$ is used. The latter exposure corrections are successfully fitted to the gustiness-derived exposure corrections. In this way, the more consistent characteristics of the exposure correction factors calculated from $\sigma_u$ analysis can be applied onto historical time series.

The improved exposure corrections yield about 1-5% reduction in the 1000 year extreme wind speeds following a relatively simple extreme wind analysis of a Gumbel-fit to yearly maxima of hourly mean wind speed squared. The largest reductions occur at sheltered locations inland. These preliminary estimates show spatial patterns in agreement with *Wieringa and Rijkoort* (1983), although extremes of the present 1993-2007 time series are 10-30% lower than similar estimates (*Wieringa and Rijkoort*, 1983) for the period 1962-1976. However, careful choosing an extreme value distribution is important (*Palutikof et al.*, 1999). Further research (step 2 of Plan of Approach) will focus on extreme wind statistics and contribute to the further analysis of the curvature problem.

# Nederlandse samenvatting

Het is wettelijk vereist iedere vijf jaar een analyse van het veiligheidsniveau van de hoofdwaterkeringen uit te voeren. Hiervoor zijn zogenaamde *Hydraulische Randvoorwaarden* nodig, om de hydraulische belasting op de waterkeringen te kwantificeren. Kennis over extreme windomstandigheden is nodig als invoer voor de hydraulische modellen die gebruikt worden voor de bepaling van die Hydraulische Randvoorwaarden. Het doel van het programma *Sterkte en Belasting Waterkeringen* (SBW) is het verbeteren van de kennis die de basis vormt voor de Hydraulische Randvoorwaarden. Het windgerelateerde onderzoek valt onder *SBW Wind*. Dit rapport beschrijft de resultaten van de eerste taak van SBW Wind: het verbeteren van de KNMI tijdreeksen van wind. Aansluitend zal nog onderzoek volgen naar de extrapolatie van gemeten data naar extreme waarden en de ruimtelijke correlatie van extreme wind.

Veel windgegevens die op dit moment voor de Hydraulische Randvoorwaarden gebruikt worden, zijn gebaseerd op metingen uit de periode 1962-1976 en het zogenaamde Rijkoort Weibull model (zie: *Wieringa and Rijkoort* (1983)). Het doel van het KNMI-HYDRA project (1998-2005) was het verlengen van deze tijdreeksen en het tegelijkertijd verbeteren van de methode om extreme wind te bepalen. De resultaten van HYDRA werden echter niet geaccepteerd als bruikbaar binnen de Hydraulische Randvoorwaarden, omdat er een fysisch niet te verklaren resultaat opdook: schattingen van windextremen boven land waren hoger dan boven zee. Dit probleem wordt sindsdien aangeduid met de term *krommingsprobleem*.

Om de reeksen gemeten wind te corrigeren voor verschillen in lokale ruwheid op een meetstation, kunnen beschuttingsfactoren berekend worden. Beschuttingsfactoren zetten gemeten wind om in potentiële wind. Recent onderzoek van het KNMI heeft aanwijzingen gevonden dat de methode om beschuttingsfactoren te berekenen uit de gemiddelde wind en de windstoten (de zogenaamde *vlaaganalyse*), te hoge beschuttingsfactoren leek op te leveren in de west- tot noordsector in de winter. Dit effect draagt bij aan het krommingsprobleem. Vanwege de beperkte databeschikbaarheid gebruikten zowel *Wieringa and Rijkoort* (1983) als *Verkaik* (2006) in hun onderzoek vlaaganalyse op uurlijkse periodes om de standaarddeviatie van de wind te benaderen. Ze gaven echter al aan dat het gebruik van 10-minuut periodes en directe waarnemingen van de standaarddeviatie van de wind een robuustere schatting van de beschuttingsfactoren zal opleveren.

Sinds 2003 zijn voor bijna alle KNMI stations gegevens van windsnelheid, windstoten en standaarddeviatie, op 10-minuutbasis beschikbaar. We hebben nu dus voldoende gegevens om de verschillende methodes te kunnen vergelijken. In dit rapport wordt beargumenteerd dat met name in de winter bij noordwestelijke aanvoer de beschuttingsfactoren gebaseerd op vlaaganalyse op uurvakken worden beïnvloed door veranderingen van stabiliteit in polaire luchtmassa's binnen een uurvak. Uit de vergelijking van beide methodes (vlaaganalyse op uurvakken en standaarddeviatie op 10-minuutvakken), blijkt dat het gebruik van de standaarddeviatie van de wind een sterke verbetering laat zien van de richtingsafhankelijke beschuttingsfactoren en de landelijke gradiënt. Daarnaast blijkt het mogelijk een goede relatie te vinden tussen beschuttingsfactoren berekend met behulp van de vlaaganalyse en die berekend met behulp van de standaarddeviatie. Daarmee kunnen de consistente eigenschappen van de beschuttingsfactoren op basis van de standaarddeviatie vertaald worden naar de gehele historische meetreeks.

De verbeterde beschuttingsfactoren laten via een relatief eenvoudige extreme waardenanaly-

se (Gumbel-fit op windsnelheid in het kwadraat) een reductie van 1-5% zien voor de eens in de 1000 jaar windextremen. De grootste verschillen treden op beschutte locaties in het binnenland op. Deze voorlopige resultaten van extreme windstatistiek laten ruimtelijke patronen zien die in overeenstemming zijn met *Wieringa and Rijkoort* (1983) voor de periode 1962-1976. De absolute waarden van de huidige analyse voor de periode 1993-2007 liggen echter 10-30% lager dan *Wieringa and Rijkoort* (1983). Er zal zorgvuldig omgegaan moeten worden met het kiezen van een extreme-waardedistributie te kiezen (*Palutikof et al.*, 1999). Verder onderzoek (stap 2 in het Plan van Aanpak) zal zich richten op de extreme wind statistiek en bijdragen aan de verdere analyse van het krommingsprobleem.

# Contents

# Preface

## Background SBW-Belastingen

The Flood Defences Act (*Wet op de Waterkering*, WWk (1995)) demands that the primary flood (sea, lake and river) defences in the Netherlands are monitored every five years (2001, 2006, 2011, etc.) for the required level of protection. This assessment is based on the Hydraulic Boundary Conditions (HBC) and the Safety Assessment Regulation (VTV: Voorschrift op Toetsen op Veiligheid). The HBC are derived every five years and approved by the Minister of Transport, Public Works and Water Management. The programme *Strength and Loads of Water Defences* (SBW: Sterkte en Belasting Waterkeringen) has the task of improving the quality of the methods used in the assessment to enable the managers and experts to have sufficient confidence to use these tools for the five-yearly assessment. The SBW project *Belastingen* focuses on the knowledge underpinning the HBC determination in general. The SBW project *Wind* is one of the sub-projects of SBW *Belastingen*.

## Problem statement

Wind is the driver for many of the models used to evaluate the Hydraulic Boundary Conditions (HBC). For this, one also requires knowledge about wind speed that might occur in very rare conditions, corresponding to for example return times of 10000 years. Most HBC wind data are now based on the Rijkoort-Weibull model of *Wieringa and Rijkoort* (1983). New HBCs are to be developed and calculated in 2010, preferably with updated wind statistics. The HYDRA project (1998-2005) aimed at improving the statistical and extrapolation techniques and spatial interpolation techniques, but the HYDRA results were not accepted because inland wind extremes were estimated to be higher than those over sea. This problem is referred to as *curvature problem*. In the present Plan of Approach SBW Wind (*KNMI and Deltares wind modeling team*, 2008), three steps are defined:

- Deriving improved time series of potential wind (exposure-corrected wind).
- Deriving techniques to extrapolate these time series to extremes with return times up to order 10000 years.
- Devise methods for spatial interpolation and spatial consistence of these extremes.

The present study focuses on the first step mentioned above.

## Objective of this study

The objective of this study is to introduce a new technique for evaluating exposure correction factors for the KNMI time series of hourly wind, based on the relatively modern 10 minute data sets, and evaluate its effect, including its effect on previously applied extreme value analysis.

## Outline of the report

The outline of this report is as follows:

- Chapter 1 introduces the concepts of potential wind and the curvature problem and gives the background to the present research task.
- Chapter 2 discusses the current techniques to evaluate the local roughness
- Chapter 3 discusses the available wind measurements
- Chapter 4 compares the different techniques for exposure correction factors
- Chapter 5 discusses the implications of the present findings for extreme wind estimates
- Chapter 6 summarizes the conclusions and recommendations for further research.

# Chapter 1

# Introduction to Potential Wind

*The potential wind speed is a reference wind speed, free of local effects.*

## 1.1 Potential wind

Rijkswaterstaat Waterdienst has the obligation (Wet op de Waterkering, 1995) to perform a risk assessment of the Dutch dike systems every five years. To derive hydraulic conditions for extreme water levels, meteorological input of wind is needed, because wind drives waves and has a strong impact on water levels.

According to WMO standards, wind measurements should be carried out at $10$ m above the ground in a free landscape with a typical roughness length of $3$ cm over land. In practice it is often difficult to find locations meeting these standards. Therefore, the principle of potential wind was introduced to correct for differences in measuring height and local roughness in the upstream sector (*Wieringa and Rijkoort*, 1983). The theory was elaborated and implemented during the HYDRA-project (*Verkaik*, 1998-2005) for the Netherlands.

In $1983$ Wieringa and Rijkoort's assessment of the Dutch wind climate was published. This book has become a standard work for the Dutch wind engineering community. The assessment was mainly based on wind speed records measured from $1962$-$1976$. In their 1983-assessment Wieringa and Rijkoort derived local roughness lengths and exposure corrections from gustiness analysis. From the local roughness length, the wind speed at the blending height ($60$ m), where variations in local roughness are neglectable, can be computed. Using the assumption that the temperature profile has a neutral stratification when the average wind speed during an hour is at least $5$ m/s (*Tennekes*, 1973), a logarithmic wind profile can be assumed. The wind speed at the blending height can in turn be used to compute the wind at $10$ m above a hypothetical measuring site of open terrain with grass, with a roughness length of $3$ cm (WMO requirements). This resulting wind speed is now corrected for *local* roughness (*Wieringa*, 1986) and therefore is referred to as *potential* wind. The potential wind does not correct for the influence of so-called landscape or meso roughness on scales of several kilometres. The meso roughness has significant influence on the wind profile above $60$ metres height and on the spatial trends in potential wind (see Figure 4.8 of *Wieringa and Rijkoort* (1983)). Only the so-called macro wind at the top of the atmospheric boundary layer (at roughly $0.2 - 2$ km height) is insensitive to these roughness effects.

The ratio between the potential wind speed ($U_{\mathrm{p}}$) and the measured wind speed ($U_{\mathrm{m}}$) is the exposure correction factor (ECF). The exposure correction factor (ECF) is then calculated with Equation 1.1:

$$ECF = \frac{U_{\mathrm{p}}}{U_{\mathrm{m}}} = \frac{\ln\left(z_{\mathrm{b}}/z_0\right)\ln\left(z_{\mathrm{ref}}/z_{0,\mathrm{ref}}\right)}{\ln\left(z_{\mathrm{m}}/z_0\right)\ln\left(z_{\mathrm{b}}/z_{0,\mathrm{ref}}\right)} \tag{1.1}$$

with $z_{\mathrm{b}}$ the blending height (m), $z_{\mathrm{m}}$ the sensor height (m), $z_{\mathrm{ref}}$ the reference height (10 m), $z_0$ the local roughness length and $z_{0,\mathrm{ref}}$ the reference roughness length[1].

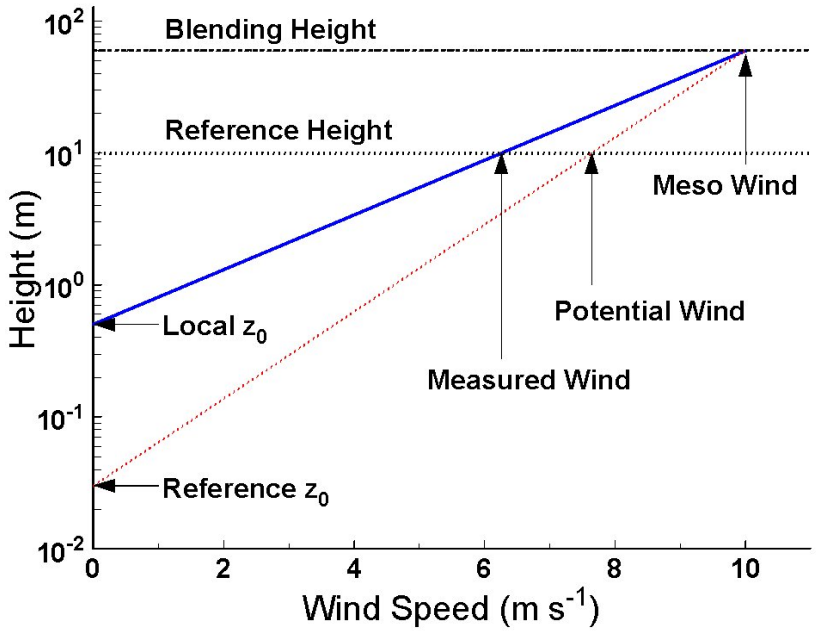


Figure 1.1.1: *The transformation process from measured wind with local roughness length to potential wind with standard roughness length under neutral conditions.*

Figure 1.1.1 illustrates the process: The exposure correction factor (ratio between measured and potential wind) can be found using the calculated local roughness length and a fixed blending height. In figure 1.1.1, the measuring height is 10 m above the ground, the calculated local roughness length is 0.5 m, the blending height is 60 m, and potential wind is calculated for a WMO-standard of a roughness length (over land) of 3 cm.

Key element in the concept of potential wind is the determination of the roughness length at the station location. The roughness length is the theoretical height at which the wind speed becomes 0 m/s under assumption of a logarithmic wind profile. It is mainly determined by the height and distance of the objects surrounding the station, although the porosity and movement of the objects also play a role. The roughness length is always smaller than the height of the roughness elements itself.

Several methods to derive roughness have been developed (*Wieringa and Rijkoort*, 1983). The roughness can be derived from variations in wind speed. The most direct approach is calculating the standard deviation ($\sigma_{\mathrm{u}}$) from the wind speed measurements. The larger the roughness, the larger $\sigma_{\mathrm{u}}$ will be. However, direct measurements of $\sigma_{\mathrm{u}}$ are only available from 1995 onwards. Therefore, *Wieringa* (1993) and *Verkaik* (2000) used an (indirect) approach to estimate $\sigma_{\mathrm{u}}$ from the ratio wind gust over average wind, based on 1 hour intervals. This approach is called *gustiness analysis*. As now direct observations of $\sigma_{\mathrm{u}}$ are available, one might expect an increased accuracy in the estimation of $z_0$ (*Verkaik*, 2000).

[1] In the HYDRA project, the standard roughness length of 3 cm was used for stations on land and a roughness length of 2 mm was assigned to stations at the North Sea and other large water masses (252, 253, 254, 285, 311, 312, 313, 316, 320, 321 and 331), approximating a roughness length typical for a wind speed of 15 m/s above water, following the Charnock relation. Coastal stations (310, 330 and 225) were treated as land stations, using a roughness length of 3 cm.

## 1.2 Review on current time series of potential wind

Time series of potential wind constructed during the HYDRA project, were based on roughness lengths derived from gustiness analysis of hourly data per sector of 20 degrees (20=5-25, 40=26-45, etc) for hourly periods with average wind speeds of at least 5 m/s. They were not accepted as useful to determine extreme potential winds (in the order of the wind speeds once per century or more), because return values of extreme potential wind appeared to be higher inland than for some coastal stations. This problem is referred to as *curvature problem* (Figure 1.2.1). The problem was identified during the HYDRA project. It appeared to be a complex problem, due to influences of

- the original measurement chain, like anemometer behaviour, characteristics of data recording systems used and data processing.
- the methodology of calculating potential wind
- the large change of roughness between sea and land
- the statistical analyses applied on the potential wind series (*Verkaik et al.*, 2003a).

The increase of extreme potential wind inland is intuitively not acceptable as, in general, measured wind decreases over land due to friction. Analyses of the curvature problem revealed features in the exposure correction factors (*KNMI and Deltares wind modeling team*, 2008), that could have an influence on the curvature problem. This report will focus on the concepts of deriving local roughness for calculating potential wind, in order to better understand the features found in the exposure correction factors.

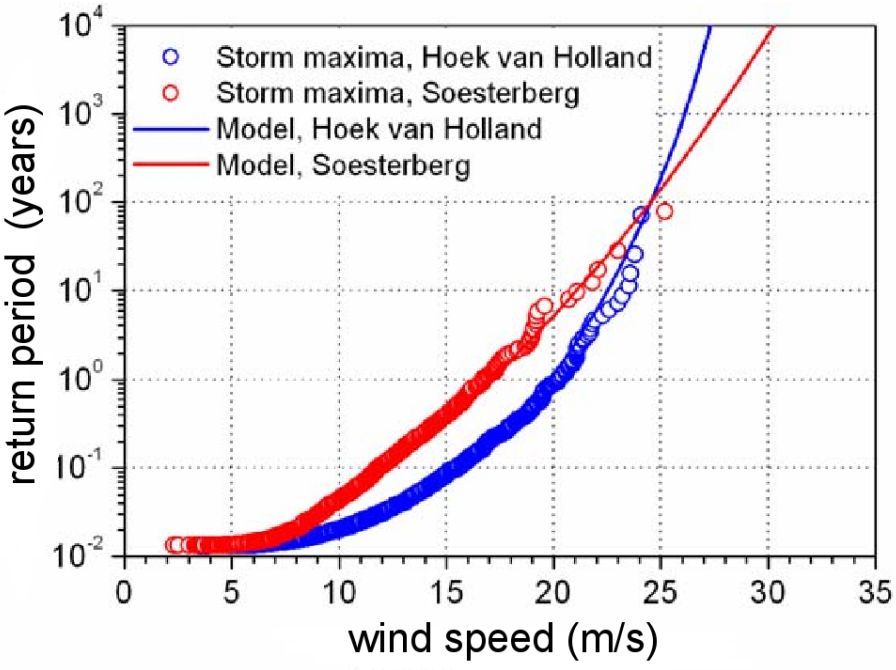


Figure 1.2.1: *Return periods of potential wind speed (using peaks over a 2 m/s wind speed threshold in a 48 hour interval) for stations Hoek van Holland (North Sea coast) and Soesterberg (central Netherlands), showing both measurements and a CWD fit (conditional Weibull distribution), illustrating the curvature problem in potential wind for extreme winds. Reprint from Verkaik et al. (2003b)*

Figure 1.2.2 illustrates the exposure correction factors for Schiphol in the period 2004-2008, divided in a summer (May-September) and winter period (October-April). At this measurement

site, environmental objects like buildings and nature, which are causing turbulence and increasing gustiness, are mainly present in northerly directions. Those objects require a 10 to 15% increase on top of the measured hourly average wind speed in order to get potential wind speed. Note in Figure 1.2.2 that in the winter period in southerly direction the exposure correction factor is lower than in summer, possibly caused by nature (leaves on trees and presence of crops) having higher roughness in summer than in winter. However, why are the factors higher in northerly directions in winter than in summer? Do we see this effect on other stations? Does this increasing effect change on higher wind speed thresholds?

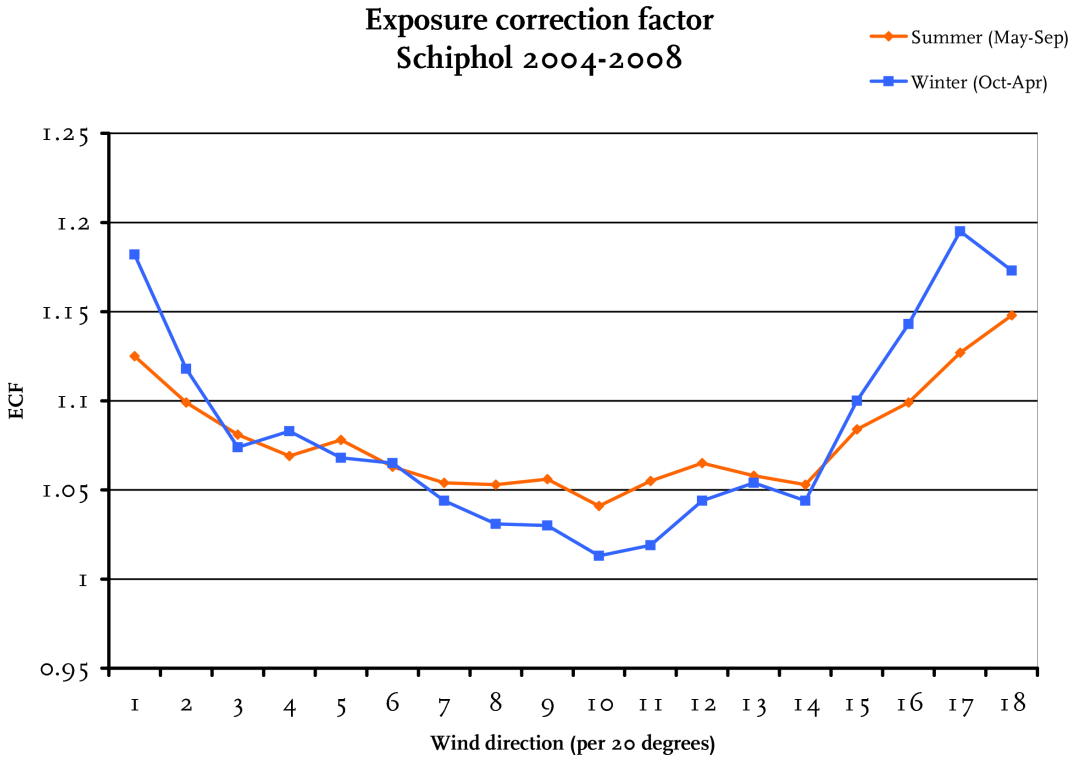


Figure 1.2.2: *Exposure correction factor, based on gustiness analysis for Schiphol, period 2004-2008, divided in a summer and winter period.* 1 *denotes sector* $5 - 25$ *degrees, etc.*

Analysing all wind stations in the same period indicates that the enhanced winter season signal in the exposure correction factors in northwesterly directions occurs on most stations. Figure 1.2.3 shows the average value of the exposure correction factor of 51 stations per wind direction sector of 20 degrees. In the analysis of hourly data of all wind stations for the period 2004-2008 the exposure correction factors are systematically higher for sectors around northwest in winter than for other directions or in summer (see section 4.2). Analysis of an independent three-year period (2001-2004) shows the same results.

A first attempt to explain this behaviour of the exposure correction factors from synoptic experience is the difference in air mass behaviour. In a northwesterly flow in the winter, most of the time a polar air mass is advected to the Netherlands. From origin, this air mass is cool and dry. With relatively warm sea surface temperatures compared to the cooler air mass, we will then generally find an unstable air mass over sea and coast, tending to become stable to neutral over land. In wintertime we may observe periods of shower activity, caused by instability (with increased gustiness), followed by clearing skies and less unstable time frames. Over land, the cooling air will cause a stable stratification of the lower part of the atmospheric boundary layer. Because the upper part of the boundary layer remains unstable and friction increases inland, gust

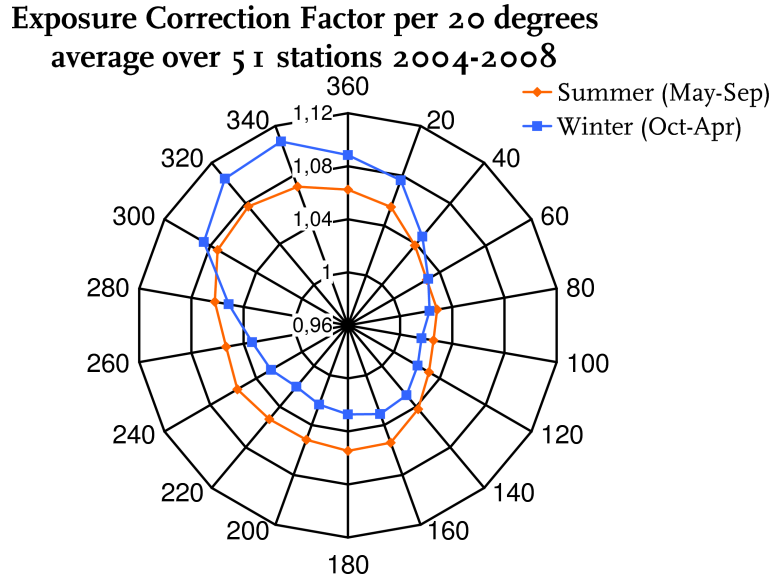


Figure 1.2.3: *Average of the exposure correction factors per wind direction sector of 51 stations 2004-2008, Summer period (May-September, orange) and Winter period (October-April, blue).*

factors will increase, due to occasional gusts with decreasing average wind speeds. An example of these strong wind variations (average and maximum wind speed) is shown in Figure 1.2.4. Increasing gust factors will give higher estimates of local roughness. Gustiness analysis can be used for gusts that develop due to the frictional effect of the surface and objects at the surface on the wind. For these gusts, the gust is proportional to the wind speed and the local roughness. When the turbulence is caused by strong surface heat fluxes (in spring and summer, usually at lower wind speeds, so naturally excluded from this analysis) or when the gusts are caused by outflow from deep convection, then the gusts are no longer proportional to the average wind speed (over longer periods) and the local roughness.

However, in HYDRA these effects were supposed to be infrequent enough to be cancelled out when taking the median of the gust factor distribution. Figure 1.2.2 suggests that those effects can occur frequently enough to influence the median. For communication purpose we will indicate this possible explanation as *air mass effect*.

The hypothesis in the concept of potential wind to have a neutral atmosphere in the lower $60$ metres when wind speeds are more than $5$ m/s during a period of an hour, might be questionable (*Holtslag*, 1984). We observed seasonal and regional dependencies in gustiness analysis, likely influenced by stability changes or non-stationary wind speed in polar air masses in northwesterly advection, and we suggest further research on this topic beyond this project.

## 1.3 Sensitivity for higher threshold of wind speed.

As illustrated in the previous section, the difference between summer and winter exposure correction factors for northwesterly wind directions is striking. For wind speeds of at least $5$ m/s, the assumption of a mixing layer of at least $60$ metres high with a neutral stability and logarithmic wind profile is assumed. We tested the influence of the wind speed threshold on the exposure correction factors. Using hourly data for a $10$-year period 1997-2007, exposure correction factors were calculated for wind speed thresholds of $5$, $9$ and $13$ m/s (see Figure 1.3.1). The figures show that by increasing wind speed thresholds, exposure correction factors change less than $3\%$, for summer and winter in the clockwise sector between northeast and west and about $3-6\%$ in the

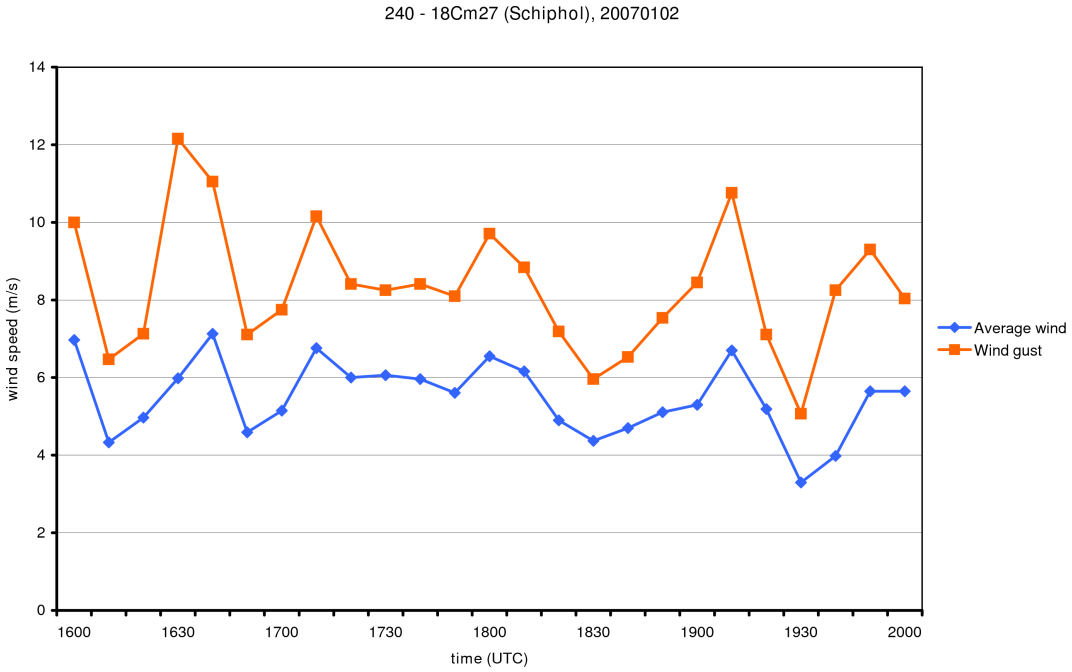


Figure 1.2.4: *Average wind speed and wind gust per* 10 *minutes for station* 240 *(Schiphol), location 18Cm27. Measurements from 20070102,* 16 − 20 *UTC. Main wind direction was* 310° *(northwest).*

remaining west to northeast sector. We also note that in the northeast to west sector, exposure correction factors in winter are a little lower than in summer. But for the sector west to northeast, exposure correction factors in winter are higher than in summer, consistent with Figure 1.2.4. We conclude that the directional and seasonal difference in the exposure correction factor in northwesterly directions is not solved by increasing wind speed thresholds.

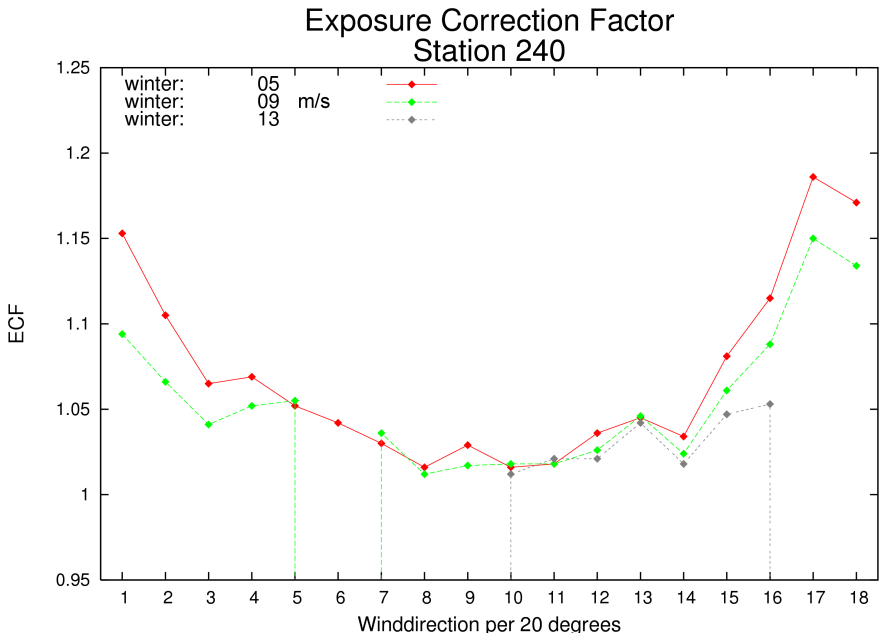


(a)

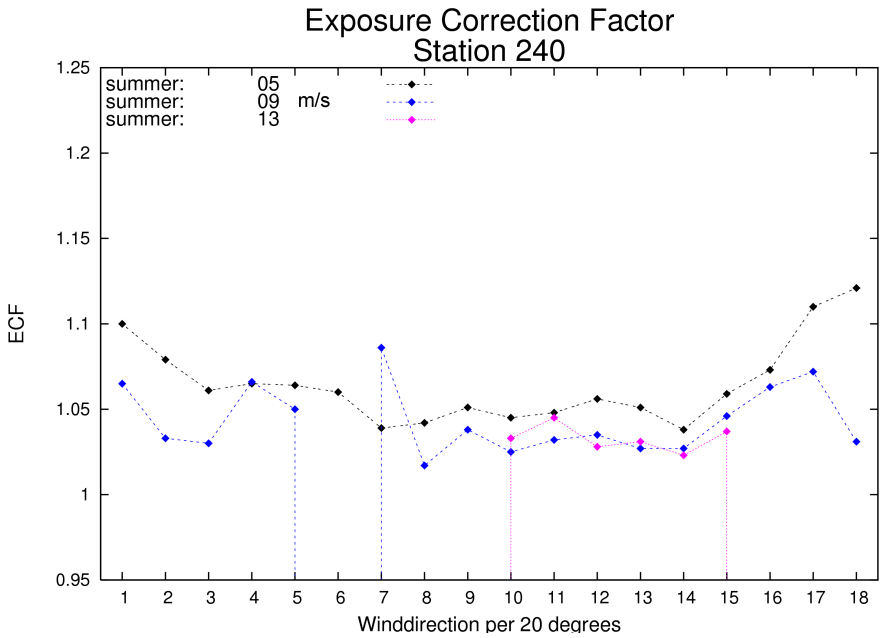


(b)

Figure 1.3.1: *Exposure correction factor for wind speeds thresholds of* 5, 9 *and* 13 *m/s, for station* 240 *(Schiphol), based on hourly data in the period 1997-2007. (a): winter period, (b): summer period. Note that lines drop when not enough data are available (less than* 10 *data points) for the given wind speed threshold and direction.*

# Chapter 2

# Estimating roughness

Key element in the concept of potential wind is the determination of the roughness length at the station location. Several methods to derive roughness have been developed. The roughness can be derived from the variations in wind speed. The most direct approach is calculating the standard deviation ($\sigma_{\mathrm{u}}$) from wind speed measurements. However, direct measurements of $\sigma_{\mathrm{u}}$ are only available from $1995$ onwards. Therefore, *Wieringa* (1993) and *Verkaik* (2000) used an (indirect) approach to estimate $\sigma_{\mathrm{u}}$ from the ratio wind gust over average wind, based on $1$ hour intervals (*gustiness analysis*).

An other approach is to derive roughness based on land use maps. The Dutch land use maps are referred to as LGN (*Landelijk Grondgebruiksbestand Nederland*). An algorithm can translate land use in the upstream sector of a measurement site to a roughness length. In the HYDRA project, such an algorithm was applied; due to time restrictions we briefly compare our result to the LGN derived roughness lengths from the HYDRA project.

## 2.1 Theoretical basis of gustiness analysis

Gustiness analysis is based on the relationship between the standard deviation ($\sigma_{\mathrm{u}}$) and the mean ($\overline{U}$) of the wind speed. Local roughness $z_0$ can be derived from $\sigma_{\mathrm{u}}$, using Equation 2.1 (*Verkaik*, 2000):

$$\left\langle \frac{\sigma_{\mathrm{u}}}{\overline{U}} \right\rangle = \frac{c\kappa}{\ln\left(\frac{z_{\mathrm{m}}}{z_0}\right)} \tag{2.1}$$

with $\overline{U}$ the average wind speed (m/s) and $c$ the dimensionless standard deviation for neutral wind (referred to as *scaling parameter*) and $\kappa$ the von Kármán constant (typically chosen as $0.4$). The brackets denote the median of the distribution.

The scaling parameter ($c$) scales with the friction velocity and is a function of stability and boundary layer height. A typical value for the neutral limit is $2.2$ (*Verkaik*, 2000). A value for $c$ of $2.5$, as used by *Wieringa and Rijkoort* (1983), will decrease potential wind about $2\%$ (*Verkaik*, 2000).

The standardized gust ($g$) relates the maximum wind gust ($U_{\max}$), the mean wind speed and the standard deviation of the wind (Equation 2.2):

$$g = \frac{\langle U_{\max} \rangle - \overline{U}}{\sigma_{\mathrm{u}}} \tag{2.2}$$

Now, local roughness can be derived from the wind gust and the mean wind speed using Equation 2.3:

$$\left\langle \frac{U_{\max}}{\overline{U}} \right\rangle = \left( 1 + \frac{gc\kappa}{\ln\left(\frac{z_{\mathrm{m}}}{z_0}\right)} \right) \tag{2.3}$$

## 2.2 Application of gustiness analysis to measurements

Now that we have introduced the theoretical framework, we turn our attention to the measurement chain. One factor to compensate for, is that the wind gust measured by the KNMI network is not an instantaneous wind speed, but a moving 3 seconds average with a sampling frequency of 4 Hz, so every 10 minutes, $\sigma_{\mathrm{u}}$ is calculated from 2400 wind speed samples. The filtering of the wind speed signal by the measuring chain will modify the shape of the spectrum, attenuating more strongly the higher frequencies and the apparent value of $\sigma_{\mathrm{u}}/\overline{U}$. We account for these effects by introducing a so-called *Attenuation factor* ($A$).

Introducing the attenuation factor, we rewrite Equation 2.1 to the following equation:

$$\left\langle \frac{\sigma_{\mathrm{u}}}{\overline{U}} \right\rangle = \frac{cA\kappa}{\ln\left(\frac{z_{\mathrm{m}}}{z_0}\right)} \tag{2.4}$$

with $\sigma_{\mathrm{u}}$ the standard deviation of a 3 s moving average wind speed (m/s) and $A$ the attenuation factor of the measurement chain.

Accordingly, Equation 2.3 becomes:

$$\left\langle \frac{U_{\max}}{\overline{U}} \right\rangle = \left(1 + \frac{gAc\kappa}{\ln\left(\frac{z_{\mathrm{m}}}{z_0}\right)}\right) \tag{2.5}$$

with $U_{\max}$ the maximum 3 s wind speed (wind gust) (m/s). The current time series of potential wind from Verkaik are based on Equation 2.5.

To prevent the domination of outliers and to have a more reliable estimate of median values, gustiness analysis or $\sigma_{\mathrm{u}}$ analysis should only be applied when 10 measurements or more are available. For stations with high roughness lengths (e.g. inland stations), this condition combined with a wind speed threshold of 5 m/s is sometimes not met in directions between northeast to southwest over east.

Note that besides the 3 s low pass filtering described by the attenuation factor, anemometers might show inaccuracies at very low wind speeds due to the discrete measuring system, and overspeeding effects due to the low response time of the anemometers. Currently, this is not accounted for.

### 2.2.1 Coefficients $A$ and $g$

The attenuation factor ($A$) is a function of some characteristics of the measurement chain, like the sample period, and wind speed. The attenuation factor as a function of wind speed for the KNMI measurement system is given in Appendix A. Typical values are in the order of 0.9 for an average wind speed of 6 m/s. The standardized gust is a function of measurement interval and wind speed. Typical values for an average wind speed of 6 m/s are in the order of 3.3 for an measurement interval of 1 hour and 2.7 for a 10 minute measurement interval (see Appendix A). The value for $c$ (in HYDRA taken as 2.2 (*Verkaik*, 2000)) is based on an integrated wind spectrum, measured at Cabauw. The Cabauw measurement site has relatively low local roughness. In rougher terrain the sensitivity of $c$ will increase (*Panofsky and Dutton*, 1984). The choice of the value of $c$ could be subject of further research as suggested in chapter 6 (Beljaars, personal communication).

## 2.3 Estimating roughness lengths

### 2.3.1 Land

An other approach is to estimate local roughness from land use and obstacles. By using standard roughness lengths for typical terrain types, as developed by *Davenport* (1960) and tested

and improved by *Wieringa* (1992), it is possible to estimate local roughness by on sight inspection. However, on sight terrain classification is a subjective way to estimate roughness lengths. In the HYDRA project *Verkaik* (1998-2005), some effort has been put into deriving local roughness lengths from land use maps. In principle, typical landscapes can be described by typical roughness lengths. Examples are given in *Wieringa* (1993). Using standard roughness lengths for typical land use classes, it is possible to use the land use maps to derive a roughness length in the upstream sector of the wind measurement location. If winds are to be estimated at any arbitrary location (rather than a measuring station), such land use classification maps are currently the only objective way to derive roughness information. However, results depend strongly on the quality and accuracy of the land use maps and the approach to integrate roughness classes to derive roughness lengths. Increasing the number of land use categories will increase the quality of the roughness length estimation. We will make a brief comparison with the roughness length data derived from land use maps, as produced in HYDRA (*Verkaik*, 2003). There, version 3 of the land use maps of the Netherlands was used (*LGN3*). Currently, much newer and more detailed land use maps are available (*LGN5*). No attempt has been made yet to derive local roughness lengths using this version.

### 2.3.2 Sea

Roughness lengths at sea are dependent of wave height and wave-atmosphere interactions. A relationship to describe sea roughness as a function of wind speed is developed by *Charnock* (1955):

$$z_0 = \frac{\beta C_{\mathrm{DN}} \overline{U}_{10}^2}{g} \tag{2.6}$$

with $\beta$ the Charnock constant, $\overline{U}_{10}$ the average $10$ minute wind speed, $g$ the gravitational accelaration ($9.8$ m/s$^2$) and $\mathrm{C_{DN}}$ the drag coefficient, determined using:

$$C_{\mathrm{DN}} = \left\{0.08\overline{U}_{10} + 0.9\right\} \cdot 10^{-3} \tag{2.7}$$

Typical values of $\beta$ used for the North Sea range from $0.017$ (*Verkaik*, 2003) to $0.032$ (*Benschop*, 1996). Using Equation 2.6, it can be found that $z_0$ at the North Sea will vary from $0.1$ mm for an average wind speed of $5$ m/s to $9.7$ mm for an average wind speed of $30$ m/s. *Wieringa* (1992) classified roughness lengths over sea for a free area of at least $1$ km$^2$ to be $0.2$ mm, independent of wave height. In HYDRA, a reference roughness length of 2 mm was chosen for wind measurement site over water (Zeeland, North Sea and Wadden Sea), see page 13 in *Verkaik* (2003) 114 in *Verkaik et al.* (2003c).

## 2.4 Calculating potential wind

When local roughness lengths are known, we can calculate the exposure correction factors using:

$$ECF = \frac{U_{\mathrm{p}}}{U_{\mathrm{m}}} = \frac{\ln z_{\mathrm{b}}/z_0 \ln z_{\mathrm{ref}}/z_{0,\mathrm{ref}}}{\ln z_{\mathrm{m}}/z_0 \ln z_{\mathrm{b}}/z_{0,\mathrm{ref}}} \tag{2.8}$$

with $z_{\mathrm{b}}$ the blending height (m), $z_{\mathrm{m}}$ the sensor height (m), $z_{\mathrm{ref}}$ the reference height ($10$ m) and $z_{0,\mathrm{ref}}$ the reference roughness length. The blending height is the height where it is assumed that the influence of each single roughness element on the vertical wind profile will not be recognizable individually and an overall stress profile will exist, representing the roughness of a larger area (*Wieringa*, 1986). For the landscape in the Netherlands, a typical value for $z_{\mathrm{b}}$ of $60$ m is chosen (*Wieringa and Rijkoort* (1983) and *Verkaik* (2006)). In HYDRA, the reference roughness length was chosen $3$ cm over land and $2$ mm over sea. However, for coastal stations, like Hoek van Holland or IJmuiden, this reference roughness length is not immediately clear. From a westerly direction, the wind is solely influenced by lower sea-roughness, while in the opposite direction

the wind is solely influenced by a higher land-roughness. In order to compare potential wind series, **we decided to use a reference roughness length for land of $3$ cm for *all* stations**, even for coastal stations or stations located at the North Sea.

This approach will not be problematic, as there is a very straightforward translation from exposure correction factors over sea to exposure corrections over land:

$$F = \frac{ECF_{\text{sea}}}{ECF_{\text{land}}} = \frac{\ln\left(\frac{z_{\text{ref}}}{z_{0,\text{sea}}}\right)\ln\left(\frac{z_{\text{b}}}{z_{0,\text{land}}}\right)}{\ln\left(\frac{z_{\text{b}}}{z_{0,\text{sea}}}\right)\ln\left(\frac{z_{\text{ref}}}{z_{0,\text{land}}}\right)} \tag{2.9}$$

using $z_{\text{ref}} = 10$ m, $z_{0,\text{sea}} = 2$ mm, $z_{\text{b}} = 60$ m and, $z_{0,\text{land}} = 3$ cm, gives $F = 1.0810$. This means that exposure correction factors, and thus potential wind speeds, with respect to sea are $1.0810$ times larger than exposure correction factors over land. In *Wieringa and Rijkoort* (1983), a reference roughness length of $z_{0,\text{sea}} = 0.2$ mm was chosen for sea stations (see page 67 of *Wieringa and Rijkoort* (1983)), giving $F = 1.1225$.

# Chapter 3

# Wind speed measurements

## 3.1 Wind speed measurements in the Netherlands

Wind speed is measured at many locations in the Netherlands. At the moment, there are approximately $44$ locations on shore or near the coast where wind speed is measured. Furthermore the KNMI receives wind data from approximately $5$ offshore locations, mainly oil platforms. At some locations, there are multiple sensors. For instance, on offshore locations, backup sensors exist and at airfields, sensors are located at different locations near runways. In the period 2003-2008 data from $109$ wind sensors are available. Detailed information about the wind measurement system, procedures and algorithms can be found in the *Handboek waarnemingen*, chapter 5 (*Royal Netherlands Meteorological Institute (KNMI)*, 2001).

## 3.2 Virtual stations

Some measurement sites have several wind speed and wind direction sensors. Sometimes they are located close to each other, to serve as a backup. For instance, on remote platforms at the North Sea, repair is difficult, and other sensors are used as a backup when the main sensor fails. In other cases, one location has several sensors to sample the spatial differences. This is mostly the case at airfields, were wind information is needed at different places along a runway. Station Schiphol ($240$), has $8$ wind measurement sites at the airfield itself, and $4$ on some distance of the airfield (used for fog advection monitoring). For all stations with more than one sensor, one sensor is chosen as main sensor. Whenever data from this sensor is unavailable, one of the other sensors is used to fill in the missing data. However, it is not registered from which sensor the data originally came. In practice, it means that the wind measurements for multi-sensor locations like airports, will come from one of the sensors, without the possibility to track the measurement to an individual location. These type of stations, were multiple sensors exist, is referred to as *virtual station*. The principle of virtual stations might interfere with gustiness analysis or $\sigma_{\mathrm{u}}$ analysis, although the influence is expected to be small. This assumption is based on comparison of $10$ minute data from multiple sensors at specific measurement sites.

## 3.3 Height corrections

Not all sensors are located at the same height. Especially for stations at the coast and North Sea, sensor heights may deviate from the reference level of $10$ m. This makes direct comparison difficult. Therefore, the KNMI has introduced methods to transform the measured wind speed to a wind speed representative for a height of $10$m. Because this height correction plays an important role, we will briefly discuss the history of those corrections. We distinguish between wind measurement sites at platforms at the North Sea and sites over land which are not at a height of $10$m.

Table 3.3.1: *Height correction factors for both mean wind speed and wind gust for stations with a sensor height unequal to the WMO-standard of* 10*m. To retrieve the original sensor data, the* 10 *m-derived wind data should be multiplied by the factors listed in the table.*

| station number | station name | sensor height (m) | corrected since | corrected till | factor $U_{\mathrm{mean}}$ | factor $U_{\mathrm{max}}$ |
|---|---|---|---|---|---|---|
| 225 | IJmuiden | 18.5 | 19940111 | 19950711 | 1.025 | 1.025 |
| 225 | IJmuiden | 18.5 | 19950712 | now | 1.070 | 1.060 |
| 239 | F3-FB-1 | 59.2 | 19940111 | 19950711 | 1.260 | 1.260 |
| 239 | F3-FB-1 | 59.2 | 19950712 | now | 1.200 | 1.160 |
| 252 | K13 | 73.8 | 19940111 | 19950711 | 1.298 | 1.298 |
| 252 | K13 | 73.8 | 19950712 | now | 1.230 | 1.180 |
| 253 | AUK-ALPHA | 103.3 | 19940111 | 19950711 | 1.355 | 1.355 |
| 253 | AUK-ALPHA | 103.3 | 19950712 | now | 1.270 | 1.210 |
| 254 | Meetpost Noordwijk | 27.6 | 19940111 | 19950711 | 1.142 | 1.142 |
| 254 | Meetpost Noordwijk | 27.6 | 19950712 | now | 1.120 | 1.090 |
| 255 | North Cormorant | 101.3 | 19940111 | 19950711 | 1.355 | 1.355 |
| 255 | North Cormorant | 101.3 | 19950712 | now | 1.270 | 1.210 |
| 260 | De Bilt | 20.0 | 19960503 | now | 1.079 | 1.063 |
| 270 | Leeuwarden | 6.0 | 19710423 | 19711207 | 0.890 | 1.000 |
| 285 | Huibertgat | 18.0 | 19950712 | now | 1.070 | 1.050 |
| 308 | Cadzand | 17.0 | 19960503 | now | 1.060 | 1.050 |
| 310 | Vlissingen | 27.0 | 19971002 | now | 1.079 | 1.063 |
| 311 | Hoofdplaat | 16.5 | 19970201 | now | 1.060 | 1.045 |
| 312 | Oosterschelde | 16.5 | 19960503 | now | 1.060 | 1.045 |
| 313 | Vlakte v.d. Raan | 16.5 | 19970201 | now | 1.060 | 1.045 |
| 315 | Hansweert | 16.0 | 19960503 | now | 1.055 | 1.040 |
| 316 | Schaar | 16.5 | 19960503 | now | 1.060 | 1.045 |
| 320 | Lichteiland Goeree | 38.3 | 19940111 | 19950711 | 1.120 | 1.120 |
| 320 | Lichteiland Goeree | 38.3 | 19950712 | now | 1.150 | 1.120 |
| 321 | Europlatform | 29.1 | 19940111 | 19950711 | 1.148 | 1.148 |
| 321 | Europlatform | 29.1 | 19950712 | now | 1.120 | 1.100 |
| 324 | Stavenisse | 16.5 | 19971001 | now | 1.060 | 1.045 |
| 330 | Hoek van Holland | 15.0 | 19940111 | 19950711 | 1.055 | 1.055 |
| 330 | Hoek van Holland | 15.0 | 19950712 | now | 1.045 | 1.040 |
| 331 | Tholen | 16.5 | 19960503 | now | 1.060 | 1.045 |

Table 3.3.1 presents an overview of height correction factors for all stations with deviating sensor heights.

### 3.3.1 Platforms at the North Sea

Data from platforms at the North Sea are stored from 19940111 onwards. A height correction was applied to those stations, to transform the measured wind into a wind representative for a height of 10 m. However, this correction factor was found to be too crude and a new correction method was developed by *Benschop* (1996), referred to as *Benschop correction*. The Benschop correction for the average wind speed is based on a logarithmic wind profile with neutral stability and a typical sea roughness of 0.16 cm[1]. Wind gusts are transformed with a slightly different approach, result-

[1]This value for the roughness length was determined by applying the Charnock relationship (Equation 2.6) with properties typical for a water basin like the North Sea in a rough sea and a normative wind speed of 15 m/s at a height of 10 m.

ing in slightly smaller factors. The Benschop correction was applied on all data from platforms at the North Sea from 19950712 onwards. By inverting this correction, the original sensor data can be retrieved.

### 3.3.2 Wind posts over land

Many wind measurement sites onshore meet the WMO standard. However, some stations at the coast measure at a different height: Vlissingen (310), Hoek van Holland (330), IJmuiden (225), Terschelling-Brandaris (250). The wind measurement height at De Bilt (260) has changed many times. From 1916 to 1961, wind speeds were measured at approximately 37 m. Then, the measurement height was changed to 10 m. From 19930626, the height of the wind sensor changed to 20 m, in order to compensate for the high roughness environment in De Bilt. With an estimated vertical displacement height of about 10 m, it would be more representative for a wind speed of 10 m in a WMO-reference landscape.

After the introduction and application of the Benschop factor in 1996, it was also applied on land stations with a measuring height other than 10 m. Before that moment, no correction was applied over land. Note that the data stored for De Bilt are height corrected values, corrected with an in fact unrealistic roughness length found over sea.

To conclude: before the introduction of the Benschop factor, the wind speed records over land in the database represent the wind speed measured at sensor height. For data measured after the introduction of the Benschop factor, we can retrieve the original sensor data by inverting the correction. Per September 1st, 2009, the Benschop correction will not be applied anymore on wind posts over land. From that date onwards, the wind speed stored in the climatological database of the KNMI will represent the values at sensor height again.

### 3.3.3 Height corrections and exposure correction factors

The definition of the exposure correction factor in this study relates the sensor values to a wind speed at 10 m reference height wind. This means that for stations not measuring at 10 m, part of the exposure correction factor is in fact a height correction. By using omnidirectional local roughness, we can estimate the part of the exposure correction factor correcting for deviations from reference roughness length, using:

$$ECF_{\mathrm{r}} = \frac{\ln\left(\frac{z_{\mathrm{ref}}}{z_{0,\mathrm{omni}}}\right)}{\ln\left(\frac{z_{\mathrm{m}}}{z_{0,\mathrm{omni}}}\right)} ECF \tag{3.1}$$

with $ECF_{\mathrm{r}}$ the part of the exposure correction factor estimated to correct for local roughness only and $z_{0,\mathrm{omni}}$ the omnidirectional local roughness length, based on $\sigma_{\mathrm{u}}$ analysis.

## 3.4 Data availability

For station De Bilt (260), wind speed measurements have started in 1904. Also for some other stations, early data are available. However, during the HYDRA project, metadata of these measurements have been investigated extensively and it was concluded that all data before 1961 cannot be used for constructing potential wind series. Therefore, only series from 1961 onwards were delivered by Verkaik in the HYDRA project. Apart from only some stations which have longer series, hourly data of mean wind speed and wind gust is available in the database from 1971 onwards. Figure 3.4.1 represents graphically the availability of hourly wind speed measurements for all stations. From 1995, 10 minute interval data are available for some stations. In this 10 minute data, $\sigma_{\mathrm{u}}$ is also recorded for some stations. However, these data have not been used in this study for various reasons. From 2003, 10 minute data and $\sigma_{\mathrm{u}}$ is recorded on an operational basis for almost all stations. Figure 3.4.2 shows in two tables the number of 10 minute records

available for both mean wind speed and $\sigma_u$. In Figure 3.4.3 the several wind measurements sites in the Netherlands and part of the North Sea with location name and number are presented.

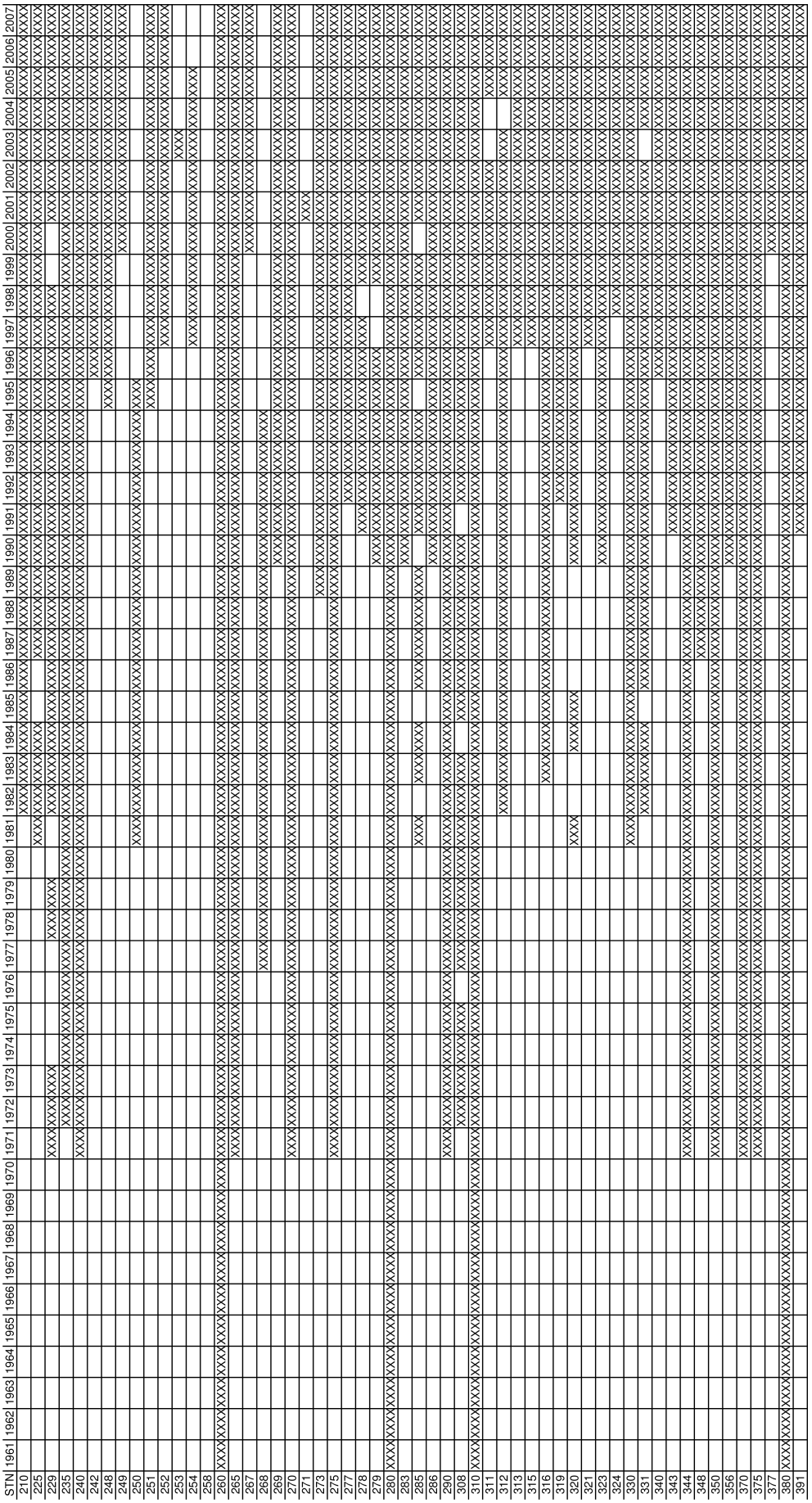


Figure 3.4.1: *Years with at least* 90% *of the time valid measurements of mean wind speed and wind gusts in* 1 *hour intervals.*

| stn_lcd | 2003 | 2004 | 2005 | 2006 | 2007 | 2008 |
|---|---|---|---|---|---|---|
| 204_KV | 0 | 0 | 0 | 0 | 1995 | 0 |
| 204_KV1 | 0 | 0 | 0 | 0 | 1993 | 0 |
| 209_1 | 36593 | 51849 | 51231 | 51810 | 52104 | 40350 |
| 210_obs | 39560 | 52491 | 52527 | 52506 | 52544 | 40460 |
| 225_a | 39499 | 52329 | 52398 | 52106 | 52475 | 40354 |
| 229_a | 37767 | 51951 | 52392 | 52399 | 50112 | 40339 |
| 235_obs | 39593 | 52214 | 52510 | 52442 | 52010 | 40453 |
| 239_a | 37353 | 52488 | 51477 | 51374 | 22526 | 0 |
| 239_b | 37353 | 52501 | 51475 | 51391 | 15022 | 0 |
| 240_18Cm | 39542 | 52555 | 52552 | 52458 | 52525 | 40464 |
| 240_18Ct | 39452 | 52512 | 52454 | 52409 | 52520 | 40444 |
| 240_18Rtw | 39451 | 52551 | 52552 | 52458 | 52525 | 40458 |
| 240_22t | 39492 | 52548 | 52469 | 52480 | 52489 | 40461 |
| 240_36Cdf | 39040 | 52476 | 52525 | 52000 | 51308 | 40428 |
| 240_36Ct | 39128 | 52515 | 52505 | 51728 | 52520 | 40457 |
| 240_36Lt | 39482 | 52551 | 52410 | 52500 | 52546 | 40449 |
| 240_36Rt0 | 39459 | 52367 | 52482 | 52473 | 52342 | 40459 |
| 240_ISAD | 39282 | 52521 | 52407 | 52503 | 52524 | 40081 |
| 240_ISMU | 39351 | 52239 | 52499 | 52399 | 52518 | 40449 |
| 240_ISNK | 38857 | 52538 | 52493 | 52499 | 52453 | 40451 |
| 240_ISNV | 38684 | 52288 | 51808 | 52447 | 52549 | 40444 |
| 242_a | 0 | 4040 | 51913 | 51553 | 50594 | 37766 |
| 242_obs | 0 | 4140 | 50118 | 51550 | 52123 | 39600 |
| 242_wind | 0 | 4040 | 51918 | 51567 | 50594 | 37766 |
| 248_a | 39534 | 52516 | 52445 | 52285 | 51580 | 38647 |
| 249_a | 39549 | 52236 | 52484 | 52322 | 52526 | 40451 |
| 251_a | 39582 | 52266 | 52532 | 52478 | 52529 | 40432 |
| 252_0 | 38965 | 51410 | 49605 | 47535 | 52105 | 39544 |
| 252_1 | 38893 | 51123 | 50406 | 49165 | 52100 | 39540 |
| 252_2 | 34017 | 51374 | 44404 | 40015 | 31132 | 23953 |
| 253_0 | 38204 | 6741 | 151 | 146 | 0 | 0 |
| 253_1 | 38436 | 6784 | 152 | 147 | 0 | 0 |
| 253_2 | 38457 | 6783 | 0 | 0 | 0 | 0 |
| 254_0 | 39123 | 51005 | 51927 | 26534 | 0 | 0 |
| 254_1 | 29517 | 50013 | 52057 | 26585 | 0 | 0 |
| 254_2 | 37460 | 43022 | 52037 | 26588 | 0 | 0 |
| 255_0 | 39184 | 17554 | 151 | 151 | 0 | 594 |
| 255_1 | 39281 | 17615 | 152 | 152 | 0 | 603 |
| 258_a | 0 | 0 | 0 | 33219 | 43871 | 38518 |
| 260_a | 39566 | 52346 | 52482 | 52470 | 52496 | 40371 |
| 261_a | 37988 | 51266 | 50649 | 52023 | 52291 | 39743 |
| 261_e | 0 | 0 | 0 | 0 | 0 | 0 |
| 261_g | 0 | 0 | 0 | 0 | 0 | 0 |
| 265_09t | 0 | 0 | 33138 | 52018 | 52300 | 40398 |
| 265_27t | 0 | 0 | 33145 | 51934 | 52254 | 40414 |
| 265_a | 0 | 0 | 30898 | 51942 | 52290 | 40434 |
| 265_obs09 | 0 | 0 | 32484 | 51996 | 52292 | 40436 |
| 267_a | 39512 | 52381 | 52549 | 52161 | 52503 | 40459 |
| 269_23t | 39570 | 52539 | 52436 | 52233 | 52498 | 40462 |
| 270_06t | 0 | 7344 | 45395 | 52120 | 52523 | 36279 |
| 270_24t | 0 | 7450 | 51792 | 52082 | 51791 | 40364 |
| 270_a | 0 | 7485 | 52278 | 52114 | 52210 | 40367 |
| 270_obs06 | 0 | 7485 | 52278 | 52114 | 52210 | 40367 |
| 273_a | 39551 | 52448 | 52528 | 52249 | 51776 | 40450 |
| 275_20t | 0 | 7348 | 52402 | 52364 | 51901 | 40396 |
| 275_a | 39549 | 44768 | 52182 | 52402 | 51952 | 40429 |
| 275_obs02 | 0 | 7459 | 52190 | 52420 | 51950 | 40431 |
| 277_a | 39055 | 52397 | 52101 | 52413 | 52513 | 40452 |
| 278_a | 39007 | 52270 | 52527 | 52262 | 52520 | 40230 |
| 279_a | 39561 | 52174 | 52542 | 52444 | 52532 | 40437 |
| 280_23t | 39572 | 52480 | 52512 | 52459 | 52548 | 40461 |
| 283_a | 39404 | 52467 | 52227 | 52275 | 52438 | 40302 |
| 285_a | 39011 | 48293 | 51758 | 52017 | 51415 | 39766 |
| 286_a | 39550 | 52279 | 52524 | 51905 | 52464 | 40321 |
| 290_06t | 0 | 0 | 36695 | 52290 | 51100 | 34710 |
| 290_24t | 0 | 0 | 36603 | 52449 | 52486 | 35792 |
| 290_a | 0 | 0 | 33058 | 52451 | 52510 | 39992 |
| 290_obs06 | 0 | 0 | 34925 | 52467 | 52509 | 39995 |
| 308_a | 38514 | 51871 | 51841 | 51181 | 49305 | 37612 |
| 310_a | 39582 | 52405 | 52542 | 52492 | 52517 | 40449 |
| 311_a | 28890 | 23251 | 51747 | 47365 | 51691 | 34058 |
| 312_a | 39243 | 16984 | 52124 | 52261 | 52400 | 40193 |
| 315_a | 39366 | 52094 | 52190 | 52190 | 52347 | 40203 |
| 316_a | 39326 | 52277 | 48717 | 52305 | 50996 | 39676 |
| 319_a | 39571 | 52445 | 52483 | 52255 | 52540 | 40160 |
| 320_0 | 39213 | 51641 | 52225 | 52263 | 52141 | 40254 |
| 320_1 | 39139 | 51350 | 52212 | 52247 | 52134 | 40252 |
| 320_2 | 39191 | 51606 | 52224 | 50734 | 52139 | 40254 |
| 321_0 | 39070 | 51408 | 52148 | 52218 | 52211 | 40254 |
| 321_1 | 36099 | 50987 | 52140 | 52206 | 52198 | 40245 |
| 321_2 | 38658 | 51333 | 51900 | 52217 | 51707 | 40134 |
| 323_a | 39371 | 52173 | 52494 | 51625 | 52422 | 40268 |
| 330_a | 39383 | 51837 | 52057 | 52435 | 52504 | 40380 |
| 331_a | 30153 | 51122 | 50520 | 51869 | 52283 | 39973 |
| 340_07t | 0 | 31038 | 52320 | 52371 | 52454 | 40463 |
| 340_25t | 0 | 31348 | 52194 | 49451 | 45599 | 40441 |
| 340_a | 0 | 31365 | 52178 | 52304 | 52217 | 40455 |
| 340_obs07 | 0 | 31227 | 52178 | 52304 | 52218 | 40455 |
| 343_a | 39532 | 52543 | 52525 | 52294 | 52523 | 40456 |
| 344_06t | 39284 | 52527 | 52402 | 52193 | 52534 | 40462 |
| 344_24t | 39493 | 52489 | 52553 | 52470 | 52450 | 40457 |
| 348_a | 39578 | 52296 | 52474 | 52443 | 52264 | 40393 |
| 350_10t | 0 | 7351 | 52061 | 52148 | 52517 | 38927 |
| 350_28t | 0 | 7413 | 52280 | 52406 | 52521 | 40430 |
| 350_a | 38731 | 45214 | 52487 | 52314 | 52520 | 40284 |
| 350_obs10 | 0 | 7388 | 52487 | 52314 | 52520 | 40284 |
| 356_a | 38672 | 52031 | 52020 | 52470 | 52415 | 40393 |
| 370_04t | 0 | 7454 | 52403 | 52423 | 52511 | 40439 |
| 370_22t | 0 | 7390 | 52313 | 52430 | 52316 | 40051 |
| 370_a | 0 | 7455 | 52485 | 52399 | 52503 | 40436 |
| 370_obs04 | 0 | 7455 | 52485 | 52399 | 52503 | 40436 |
| 375_06Lt | 0 | 7129 | 52356 | 52105 | 52320 | 40427 |
| 375_24Rt | 0 | 7455 | 52286 | 51620 | 52350 | 36335 |
| 375_a | 0 | 7469 | 52314 | 50827 | 52250 | 40413 |
| 375_obs06 | 0 | 7469 | 52320 | 50838 | 52253 | 40413 |
| 377_a | 39565 | 52524 | 52485 | 52024 | 52514 | 38686 |
| 380_04t | 5467 | 52363 | 52478 | 52319 | 52546 | 40457 |
| 380_22t | 39545 | 52407 | 52417 | 52370 | 52389 | 40313 |
| 391_a | 39465 | 52336 | 52349 | 52321 | 52432 | 40463 |

| stn_lcd | 2003 | 2004 | 2005 | 2006 | 2007 | 2008 |
|---|---|---|---|---|---|---|
| 204_KV | 0 | 0 | 0 | 0 | 1995 | 0 |
| 204_KV1 | 0 | 0 | 0 | 0 | 1993 | 0 |
| 209_1 | 0 | 0 | 0 | 0 | 0 | 0 |
| 210_obs | 39560 | 52489 | 52527 | 52506 | 52544 | 40460 |
| 225_a | 39499 | 52329 | 52398 | 52106 | 52475 | 40354 |
| 229_a | 37767 | 51951 | 52392 | 52399 | 50112 | 40339 |
| 235_obs | 39539 | 52210 | 52510 | 52442 | 52010 | 40453 |
| 239_a | 37353 | 52488 | 51477 | 51374 | 22526 | 0 |
| 239_b | 37353 | 52501 | 51475 | 51391 | 15022 | 0 |
| 240_18Cm | 39463 | 52553 | 52552 | 52458 | 52525 | 40464 |
| 240_18Ct | 39452 | 52512 | 52454 | 52409 | 52520 | 40444 |
| 240_18Rtw | 39451 | 52551 | 52552 | 52458 | 52525 | 40458 |
| 240_22t | 39492 | 52548 | 52469 | 52480 | 52489 | 40461 |
| 240_36Cdf | 39040 | 52476 | 52525 | 52000 | 51308 | 40428 |
| 240_36Ct | 39128 | 52515 | 52505 | 51728 | 52520 | 40457 |
| 240_36Lt | 39482 | 52551 | 52410 | 52500 | 52546 | 40449 |
| 240_36Rt0 | 39459 | 52367 | 52482 | 52473 | 52342 | 40459 |
| 240_ISAD | 39282 | 52521 | 52407 | 52503 | 52524 | 40081 |
| 240_ISMU | 39351 | 52239 | 52499 | 52399 | 52518 | 40449 |
| 240_ISNK | 38857 | 52538 | 52493 | 52499 | 52453 | 40451 |
| 240_ISNV | 38684 | 52288 | 51808 | 52447 | 52549 | 40444 |
| 242_a | 0 | 4040 | 51913 | 51553 | 50594 | 37766 |
| 242_obs | 0 | 4040 | 50117 | 51550 | 52123 | 39600 |
| 242_wind | 0 | 4040 | 51918 | 51567 | 50594 | 37766 |
| 248_a | 39534 | 52516 | 52445 | 52285 | 51580 | 38647 |
| 249_a | 39549 | 52236 | 52484 | 52322 | 52526 | 40451 |
| 251_a | 39582 | 52266 | 52532 | 52478 | 52529 | 40432 |
| 252_0 | 0 | 0 | 0 | 0 | 0 | 0 |
| 252_1 | 0 | 0 | 0 | 0 | 0 | 0 |
| 252_2 | 0 | 0 | 0 | 0 | 0 | 0 |
| 253_0 | 0 | 0 | 0 | 0 | 0 | 0 |
| 253_1 | 0 | 0 | 0 | 0 | 0 | 0 |
| 253_2 | 0 | 0 | 0 | 0 | 0 | 0 |
| 254_0 | 0 | 0 | 0 | 0 | 0 | 0 |
| 254_1 | 0 | 0 | 0 | 0 | 0 | 0 |
| 254_2 | 0 | 0 | 0 | 0 | 0 | 0 |
| 255_0 | 0 | 0 | 0 | 0 | 0 | 0 |
| 255_1 | 0 | 0 | 0 | 0 | 0 | 0 |
| 258_a | 0 | 0 | 0 | 33219 | 43871 | 38518 |
| 260_a | 39566 | 52346 | 52482 | 52470 | 52496 | 40371 |
| 261_a | 37988 | 51266 | 50649 | 52023 | 52291 | 39743 |
| 261_e | 0 | 0 | 0 | 0 | 0 | 0 |
| 261_g | 0 | 0 | 0 | 0 | 0 | 0 |
| 265_09t | 0 | 0 | 33138 | 52018 | 52300 | 40398 |
| 265_27t | 0 | 0 | 33145 | 51934 | 52254 | 40414 |
| 265_a | 0 | 0 | 30898 | 51942 | 52290 | 40434 |
| 265_obs09 | 0 | 0 | 32483 | 51996 | 52292 | 40436 |
| 267_a | 39512 | 52381 | 52549 | 52161 | 52503 | 40459 |
| 269_23t | 39570 | 52537 | 52436 | 52233 | 52498 | 40462 |
| 270_06t | 0 | 7344 | 45395 | 52120 | 52523 | 36279 |
| 270_24t | 0 | 7450 | 51792 | 52082 | 51791 | 40364 |
| 270_a | 0 | 7485 | 52277 | 52114 | 52210 | 40367 |
| 270_obs06 | 0 | 7485 | 52277 | 52114 | 52210 | 40367 |
| 273_a | 39551 | 52448 | 52528 | 52249 | 51776 | 40450 |
| 275_20t | 0 | 7348 | 52402 | 52364 | 51901 | 40396 |
| 275_a | 39549 | 44768 | 52182 | 52402 | 51952 | 40429 |
| 275_obs02 | 0 | 7459 | 52189 | 52420 | 51950 | 40431 |
| 277_a | 39055 | 52397 | 52101 | 52413 | 52513 | 40452 |
| 278_a | 39007 | 52270 | 52527 | 52262 | 52520 | 40230 |
| 279_a | 39561 | 52174 | 52542 | 52444 | 52532 | 40437 |
| 280_23t | 39572 | 52479 | 52512 | 52459 | 52548 | 40461 |
| 283_a | 39404 | 52467 | 52227 | 52275 | 52438 | 40302 |
| 285_a | 39011 | 48293 | 51758 | 52017 | 51415 | 39766 |
| 286_a | 39550 | 52279 | 52524 | 51905 | 52464 | 40321 |
| 290_06t | 0 | 0 | 36695 | 52290 | 51100 | 34710 |
| 290_24t | 0 | 0 | 36603 | 52449 | 52486 | 35792 |
| 290_a | 0 | 0 | 33058 | 52451 | 52510 | 39992 |
| 290_obs06 | 0 | 0 | 34925 | 52467 | 52509 | 39995 |
| 308_a | 0 | 0 | 0 | 0 | 0 | 0 |
| 310_a | 39582 | 52405 | 52542 | 52492 | 52517 | 40449 |
| 311_a | 0 | 0 | 0 | 0 | 0 | 0 |
| 312_a | 0 | 0 | 0 | 0 | 0 | 0 |
| 315_a | 0 | 0 | 0 | 0 | 0 | 0 |
| 316_a | 0 | 0 | 0 | 0 | 0 | 0 |
| 319_a | 39571 | 52445 | 52483 | 52255 | 52540 | 40160 |
| 320_0 | 0 | 0 | 0 | 0 | 0 | 0 |
| 320_1 | 0 | 0 | 0 | 0 | 0 | 0 |
| 320_2 | 0 | 0 | 0 | 0 | 0 | 0 |
| 321_0 | 0 | 0 | 0 | 0 | 0 | 0 |
| 321_1 | 0 | 0 | 0 | 0 | 0 | 0 |
| 321_2 | 0 | 0 | 0 | 0 | 0 | 0 |
| 323_a | 39371 | 52173 | 52494 | 51625 | 52422 | 40268 |
| 330_a | 39383 | 51837 | 52057 | 52435 | 52504 | 40380 |
| 331_a | 0 | 0 | 0 | 0 | 0 | 0 |
| 340_07t | 0 | 31038 | 52320 | 52371 | 52454 | 40463 |
| 340_25t | 0 | 31348 | 52194 | 49451 | 45599 | 40441 |
| 340_a | 0 | 31365 | 52176 | 52304 | 52217 | 40455 |
| 340_obs07 | 0 | 31227 | 52176 | 52304 | 52218 | 40455 |
| 343_a | 39532 | 52543 | 52525 | 52294 | 52523 | 40456 |
| 344_06t | 39284 | 52522 | 52402 | 52193 | 52534 | 40462 |
| 344_24t | 39493 | 52489 | 52553 | 52470 | 52450 | 40457 |
| 348_a | 39578 | 52296 | 52474 | 52443 | 52264 | 40393 |
| 350_10t | 0 | 7351 | 52061 | 52148 | 52517 | 38927 |
| 350_28t | 0 | 7413 | 52280 | 52406 | 52521 | 40430 |
| 350_a | 38731 | 45214 | 52464 | 52314 | 52520 | 40284 |
| 350_obs10 | 0 | 7388 | 52464 | 52314 | 52520 | 40284 |
| 356_a | 38672 | 52031 | 52020 | 52470 | 52415 | 40393 |
| 370_04t | 0 | 7454 | 52403 | 52423 | 52511 | 40439 |
| 370_22t | 0 | 7390 | 52313 | 52430 | 52316 | 40051 |
| 370_a | 0 | 7455 | 52485 | 52399 | 52503 | 40436 |
| 370_obs04 | 0 | 7455 | 52485 | 52399 | 52503 | 40436 |
| 375_06Lt | 0 | 7129 | 52356 | 52105 | 52320 | 40427 |
| 375_24Rt | 0 | 7455 | 52286 | 51620 | 52350 | 36335 |
| 375_a | 0 | 7469 | 52314 | 50827 | 52250 | 40413 |
| 375_obs06 | 0 | 7469 | 52320 | 50838 | 52253 | 40413 |
| 377_a | 39565 | 52524 | 52485 | 52024 | 52514 | 38686 |
| 380_04t | 5467 | 52363 | 52478 | 52319 | 52546 | 40457 |
| 380_22t | 39545 | 52403 | 52417 | 52370 | 52389 | 40313 |
| 391_a | 39465 | 52336 | 52349 | 52321 | 52432 | 40463 |

Figure 3.4.2: *Number of* 10 *minute intervals with data for mean wind speed and wind gust (left) and additionally* $\sigma_u$ *(right). The first column denotes the station number, followed by location name (specific sensor location).*


Figure 3.4.3: *Station numbers and names of wind measurement sites in the Netherlands and part of the North Sea. Not shown are remote platforms K14-FA-1C (204), F3-FB-1 (239), North Cormorant (255) and AUK-ALFA (253).*

# Chapter 4

# Comparison of exposure correction factors from gustiness analysis and $\sigma_u$-analysis

## 4.1 Local roughness lengths

For most stations, we calculated roughness lengths based on both gustiness analysis for $1$ hour periods and $10$ minute periods. This was done for the periods for which $10$ minute data were available (see Figure 3.4.2). Only $10$ minute intervals with a mean wind speed of at least $5$ m/s or more were taken into account. The $1$ hour data was aggregated whenever all $6$ consecutive $10$ minute periods have a mean wind speed of at least $5$ m/s. See Appendix B for rose plots for the individual stations. We will discuss some interesting stations.

### 4.1.1 Soesterberg

Figure 4.1.1 shows a rose plot of exposure correction factors for station Soesterberg (265), wind post *obs09t*, derived by gustiness analysis of $1$ hour, $10$ minutes and $\sigma_u$ analysis. This particular wind post is located at the touch down point of a west to east runway. The plot shows that exposure corrections based on $1$ hour gustiness analysis are larger than for $10$ minute gustiness or $\sigma_u$ analysis. Gustiness $10$ minute and $\sigma_u$ analysis are in good agreement, although in general, $\sigma_u$ gives slightly smaller roughness lengths.

### 4.1.2 Hoek van Holland

Figure 4.1.3 shows a rose plot of exposure correction factors for station Hoek van Holland (330), derived by gustiness analysis of $1$ hour, $10$ minutes and $\sigma_u$ analysis after applying a height correction based on the omnidirectional local roughness length (Equation 3.1). At Hoek van Holland wind speed is measured $15$ m above the surface. Figure 4.1.4 shows that in the southwest direction, a large industrial area is visible, which is reflected in the rose plot of the exposure correction factors.

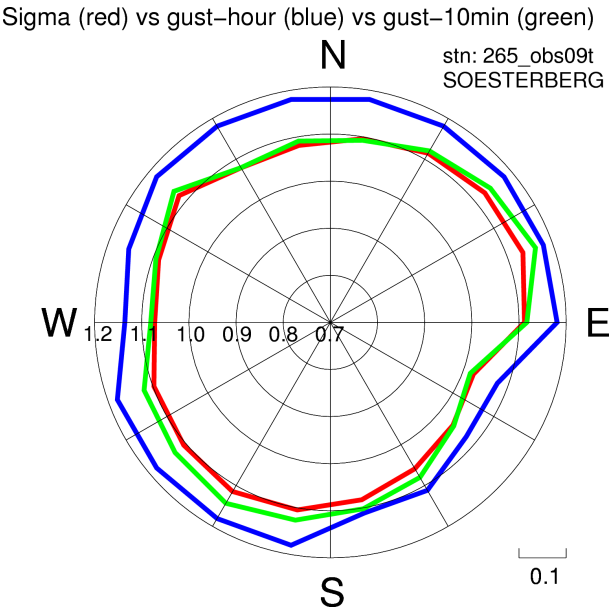


Figure 4.1.1: *Rose plot of exposure correction factors for station Soesterberg (265), based on* 1 *hour gustiness (blue),* 10 *minute gustiness (green) and* $\sigma_u$ *analysis (red).*


Figure 4.1.2: *Aerial view of the surroundings of station Soesterberg (265). Source: Google Maps.*

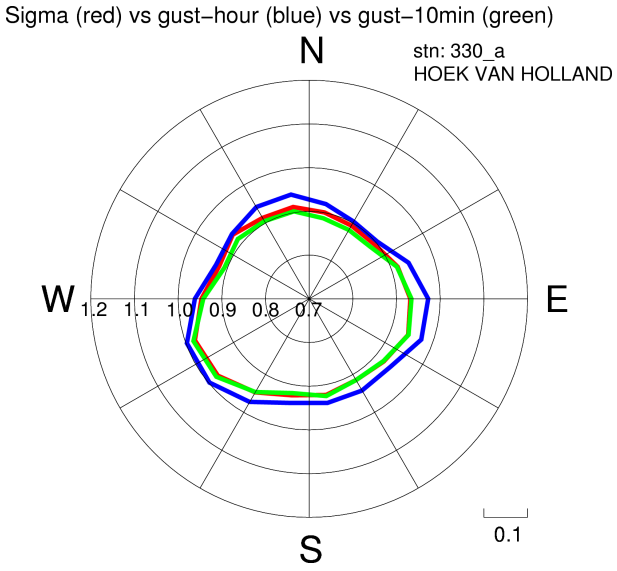


Figure 4.1.3: *Rose plot of exposure correction factors for station Hoek van Holland (330), based on* 1 *hour gustiness (blue),* 10 *minute gustiness (green) and* $\sigma_u$ *analysis (red).*

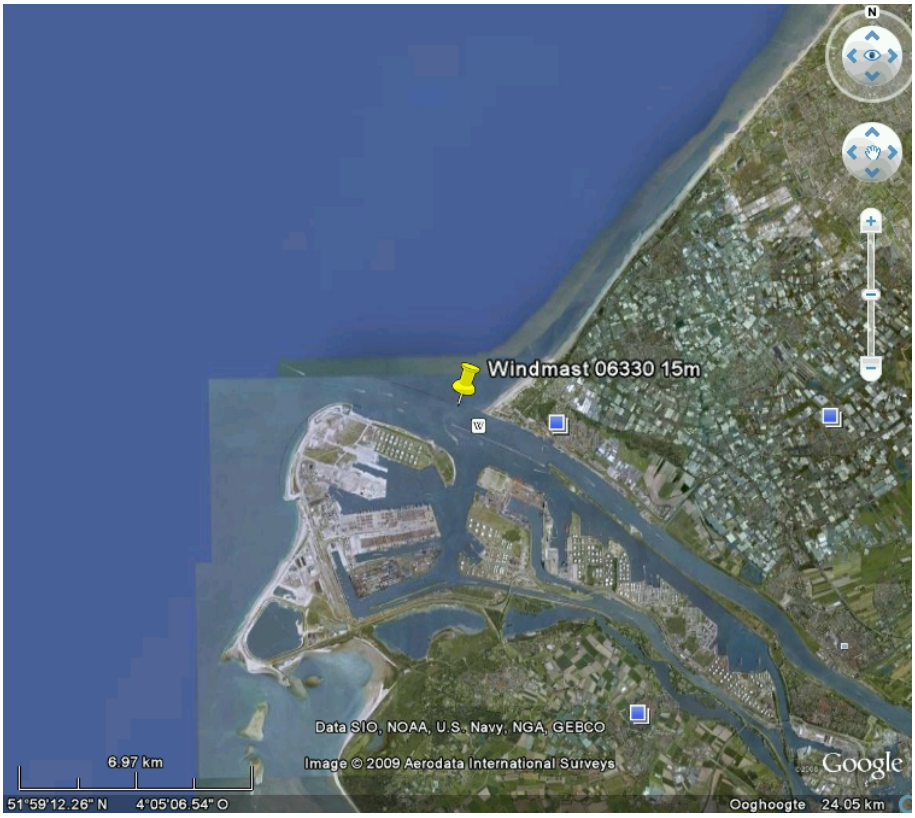


Figure 4.1.4: *Aerial view of the surroundings of station Hoek van Holland (330). Source: Google Maps.*

### 4.1.3 Schiphol

Figure 4.1.5 shows a rose plot of exposure correction factors for station Schiphol (240), derived by gustiness analysis of 1 hour, 10 minutes and $\sigma_u$ analysis. At Schiphol, wind speed is measured at reference height (10 m), so the exposure correction factors correct only for deviations of local roughness length from reference roughness length. In most directions, Schiphol represent reference roughness quite well, as the exposure correction factors are close to 1.0 ($1.0 - 1.05$). In the southsouthwest and northnortheast direction, the exposure correction factors are smaller than 1.0, as the smooth surface of runways will give roughness lengths lower than 3 cm. In the southeast direction, some stronger deviations occur. In the southeast direction these deviations are mainly caused by buildings of Schiphol-Oost.

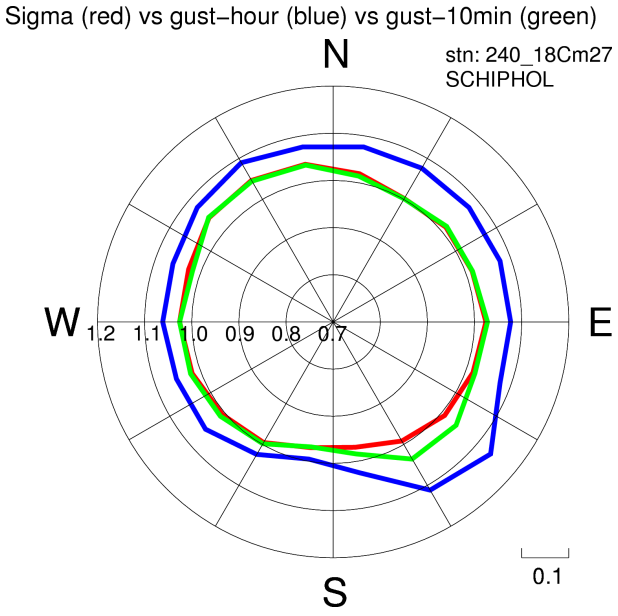


Figure 4.1.5: *Rose plot of exposure correction factors for station Schiphol (240), based on 1 hour gustiness (blue), 10 minute gustiness (green) and $\sigma_u$ analysis (red).*

### 4.1.4 All stations

To average out all individual local effects, we averaged the exposure correction factors of all land and coastal stations per sector (see Figure 4.1.7). For all directions, we find the exposure correction factors based on 1 hour gustiness analysis to be highest. The difference between the other analysis methods is up to 3% in the northwest sector. 10 minute gustiness analysis and 10 minute $\sigma_u$ analysis yield similar results, although 10 minute gustiness analysis shows larger exposure correction factors in the south sector.

We observe a clear signal of relatively low exposure correction factors in the south west and high exposure correction factors in the north west. Although one might expect a round shaped distribution, we find an oval shape. An explanation might be that many measurement sites are located at airports. Most runways are orientated in the climatologically most frequent wind directions with high wind speeds (southwest-northeast and west-east), which might introduce a bias. Figure 4.1.8 shows a rose plot of exposure correction factors for all airports. We see that the oval shape has become more pronounced, which means that we can indeed explain part of the shape by the airfields bias. When we only look at land stations, excluding air fields and coastal stations, we find a more round shape, as shown in Figure 4.1.9. However, we can still see a signal in the northwest direction, as stated earlier most likely caused by the *air mass effect*.

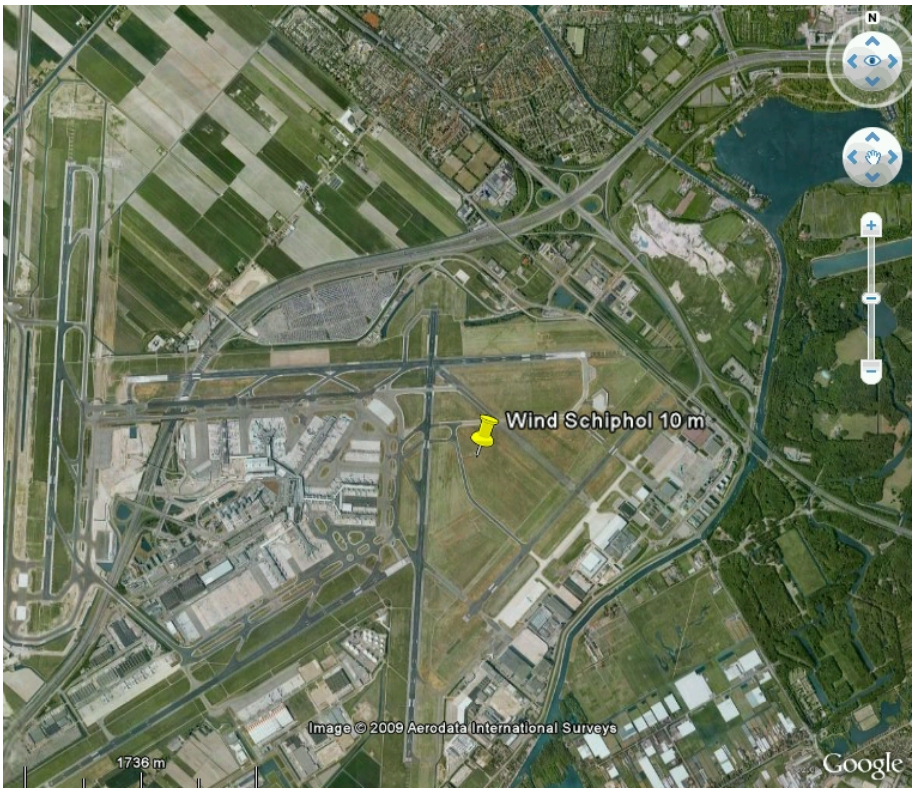


Figure 4.1.6: *Aerial view of the surroundings of the main measurement site at Schiphol* (240)*. Source: Google Maps.*

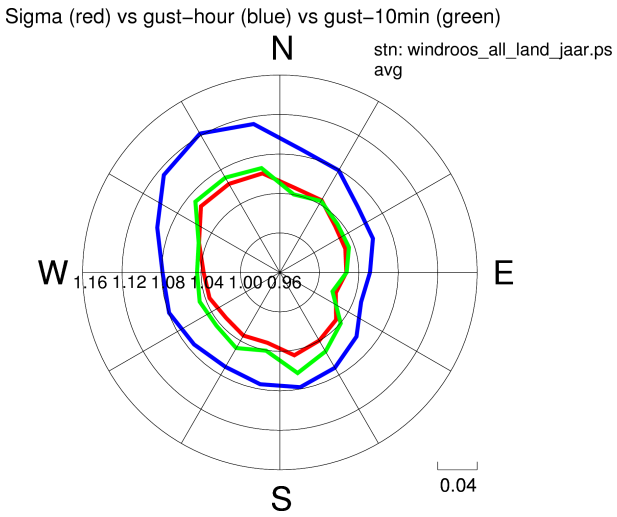


Figure 4.1.7: *Rose plot of the mean of exposure correction factors for all land and coastal stations, based on* 1 *hour gustiness (blue),* 10 *minute gustiness (green) and* $\sigma_u$ *analysis (red).*

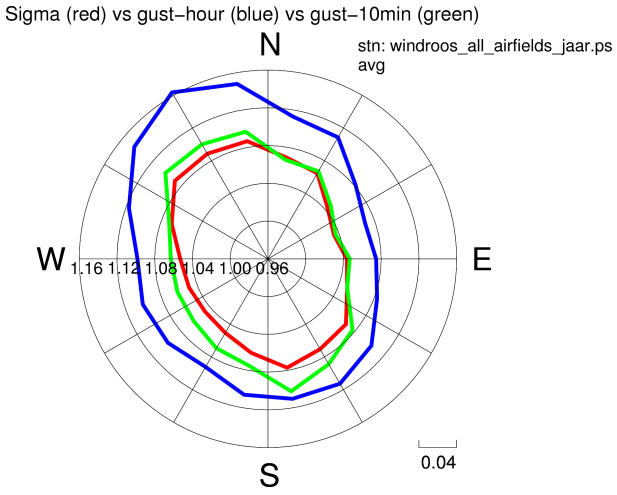


Figure 4.1.8: *Rose plot of the mean of exposure correction factors for all airfields, based on* 1 *hour gustiness (blue),* 10 *minute gustiness (green) and* $\sigma_u$ *analysis (red).*

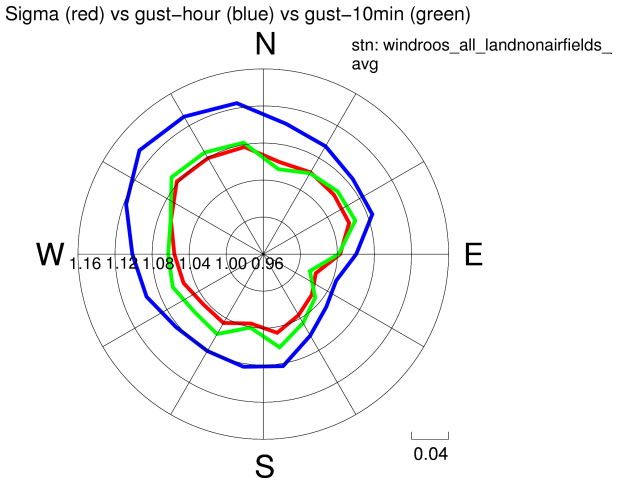


Figure 4.1.9: *Rose plot of the mean of exposure correction factors for all land stations, without airfields and coastal stations (Vlissingen, Hoek van Holland, IJmuiden, Vlieland) based on* 1 *hour gustiness (blue),* 10 *minute gustiness (green) and* $\sigma_u$ *analysis (red).*

## 4.2 Seasonal variations

In the previous sections it was described that the *air mass effect* for the northwesterly flow was reduced by using $\sigma_u$ analysis. Another test for the $\sigma_u$ analysis is the seasonal variation of the exposure correction factors. We therefore investigated the differences between summer (April-October) and winter (November-March). As explained in the introduction, the *air mass effect* is expected to be mainly present in winter season, when cold air is advected over relatively warm sea water. Figure 4.2.1 shows the exposure correction factors for both 1 hour and 10 minutes gustiness analysis, for both summer and winter. In the southerly sectors, we see that the correction factors are smaller in winter than in summer. This is not unphysical, as one might expect that roughness decreases in winter due to trees loosing their leaves and less crops on agricultural land. However, especially in the northwest sector, exposure correction factors tend to be higher in winter than in summer. We think this is a demonstration of *air mass effect* with northwesterly flow in the winter. Interestingly, the effect decreases when going from a 1 hour period to a 10 minute period.

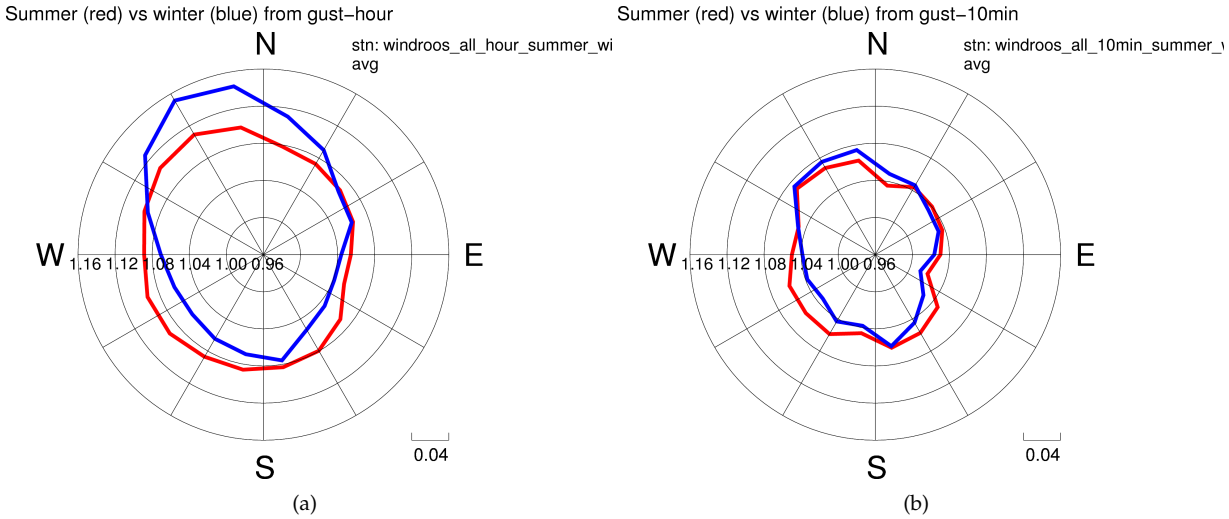


Figure 4.2.1: *Rose plot of the mean of exposure correction factors for all land stations based on (a):* 1 *hour and (b):* 10 *minutes gustiness analysis for summer (red) and winter (blue).*

When we analyze the exposure correction factors derived from $\sigma_u$ analysis, we see that exposure correction factors are smaller in winter than in summer for all directions (see Figure 4.2.2). The *air mass effect* in the north westerly direction is not directly detectable. This is an other indication that using $\sigma_u$ is producing more reliable results.

## 4.3 Roughness lengths from land use maps

We translated the roughness lengths found by *Verkaik* (2003) to exposure correction factors, using Equation 1.1. In Appendix B, rose plots of individual stations are shown. Figure 4.3.1 shows the mean rose plot for all stations in the Appendix. When we compare the rose plots based on wind speed measurements to the rose plot based on land use maps, we see that the relatively low roughness in southwest direction is both visible in the factors derived from wind speed measurements as from land use maps. We therefore conclude that this is a terrain feature, which is probably related to the fact that many measurement sites are located at airfields (see section 4.1.4). The high roughness found in the measurements in the northwesterly directions is not found in the land use maps, supporting our idea that this is a stability issue. The plot derived

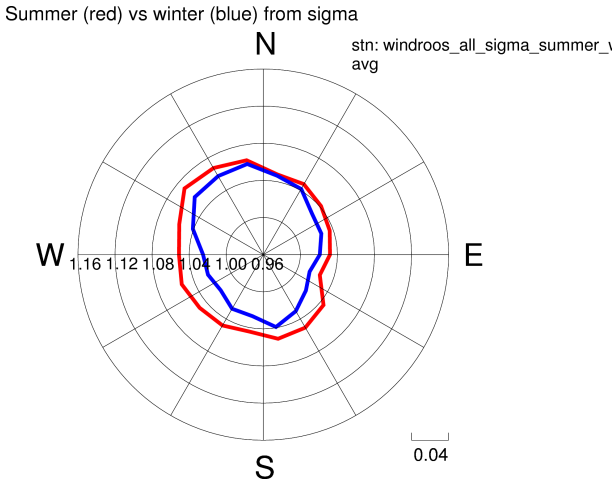


Figure 4.2.2: *Rose plot of the mean of exposure correction factors for all land and coastal stations based on $\sigma_u$ analysis for summer (red) and winter (blue).*

from land use maps shows a higher roughness in the north to northeast sector, which is not seen so pronounced in the measurements. Currently, we do not have an explanation for this.

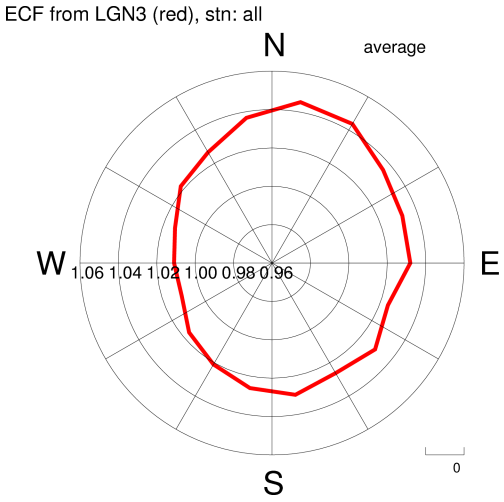


Figure 4.3.1: *Rose plot of the mean of exposure correction factors for all land stations, derived from land use maps.*

## 4.4 Spatial distribution of exposure correction factors

Figure 4.4.1 shows the spatial distribution of omnidirectional exposure correction factors at the measurement sites, derived from wind measurements (1 hour gustiness analysis and $\sigma_u$ analysis). By definition, local roughness lengths, and thus exposure correction factors, are a property of a specific location and therefore, spatial distribution of exposure correction factors at a low resolution will give a meaningless field. Moreover, the Netherlands Royal Meteorological Institute (KNMI) will preferably choose an open area representing WMO-standards when choosing a new measurement site. From this point of view, a spatial gradient in exposure correction factors is not expected. However, Figure 4.4.1 shows a gradient in both 1 hour gustiness analysis and $\sigma_u$ analysis, with the gradient being stronger in the gustiness analysis. In fact, the very local open land at the measurement site will still feel this difference in land use, as gusts are not produced very locally, but over a larger area influencing the whole boundary layer. Therefore roughness element as far as a few kilometres away can still influence the local roughness derived from the gustiness analysis.

When we compare these results with the spatial distribution of exposure correction factors at measurement sites calculated from land use maps (Figure 4.4.2), we find a gradient as well. This is an indication that local roughness at the measurement sites is increasing inland. Apparently, in spite of all the efforts by the KNMI, the required field for wind measurements (open grass land with a typical roughness length of 3 cm) is easier found closer to the coast than inland. Compared to the gradient from 1 hour gustiness analysis, the gradient from $\sigma_u$ analysis is weaker, and in absolute sense more in agreement with the gradient found in the land use maps. In Appendix C, directional maps are shown.

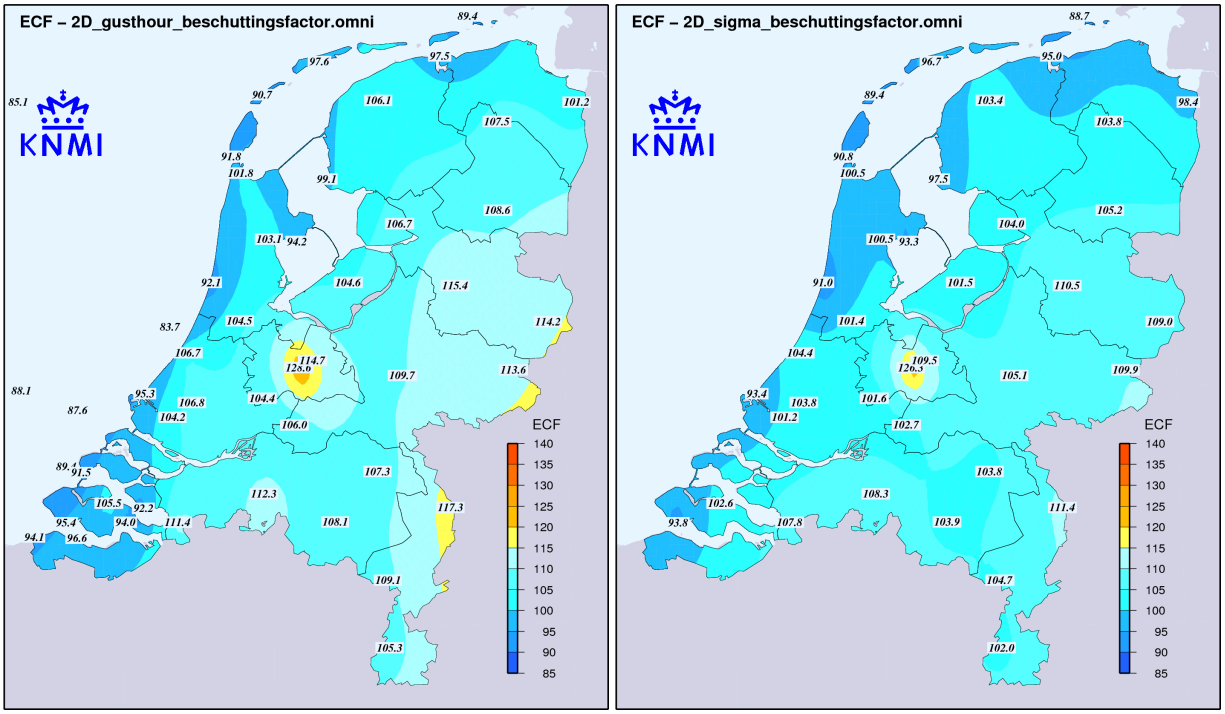


(a) (b)

Figure 4.4.1: *Spatial distribution of local roughness at the measurement sites, expressed as exposure correction factors, derived from (a): 1 hour gustiness analysis and (b): $\sigma_u$ analysis. Exposure correction factors have been averaged over all wind direction sectors. For stations measuring at a hight not equal to 10 m, exposure correction factors are corrected using Equation 3.1.*

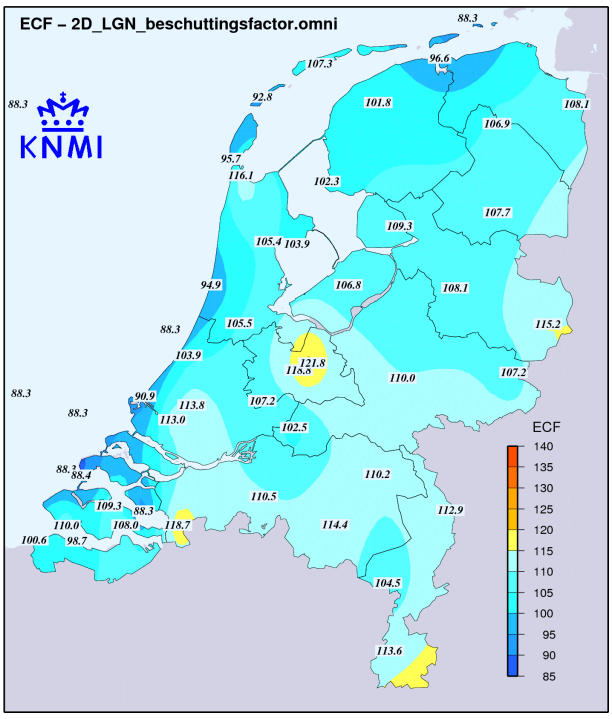


Figure 4.4.2: *Spatial distribution of local roughness at the measurement sites, expressed as exposure correction factors, derived from land use maps. Exposure correction factors have been averaged over all wind direction sectors. Note that this figure does not show the spatial distribution of local roughness over the Netherlands (as does for instance Figure 4.4 in Wieringa and Rijkoort (1983)), but just the spatial distribution of local roughness at the measurement sites.*

## 4.5 Linking the analysis methods

Because of the only very recent availability of $\sigma_u$ measurements, a method was developed to correct exposure correction factors based on 1 hour gustiness analysis. We investigated whether we could find a statistical relationship between exposure correction factors based on 1 hour gustiness analysis and $\sigma_u$ analysis. Figure 4.5.1 shows the relation between both methods of calculating exposure correction factors. It shows that 1 hour gustiness analysis gives significant higher exposure correction factors than $\sigma_u$ analysis, especially when roughness lengths (and thus exposure correction factors) increase. Appendix D shows the relationship in a directional perspective. As can be seen, the relationship is quite strong and therefore, we suggest to use a directional fit of the relationship between the two methods and to translate exposure correction factors based on 1 hour gustiness analysis to factors based on $\sigma$ analysis. This relationship can then be applied on historical time series. As fitting equation, we used:

$$ECF_{\sigma_u} = aECF^{b}_{g,1hr} \tag{4.1}$$

with $a$ and $b$ fit coefficients, $ECF_{\sigma_u}$ and $ECF_{g,1hr}$ exposure correction factors for respectively $\sigma_u$ and 1 hour gustiness analysis. Table 4.5.1 shows the coefficients after fitting. We can see that separating to wind direction is interesting, as the fit coefficients show some variations over the sectors. Table 4.5.2 shows the fit coefficients, separated for the winter and summer period. We see some differences in fit coefficients for summer and winter. As can be seen, variations in coefficients between summer and winter are small compared to the overall effect of the fit. Because of the seasonal variations found in gustiness analysis, we decided to use the seasonal fit

coefficients when correcting exposure correction factors, although for many stations no seasonal separation is made in the historical measurement series.

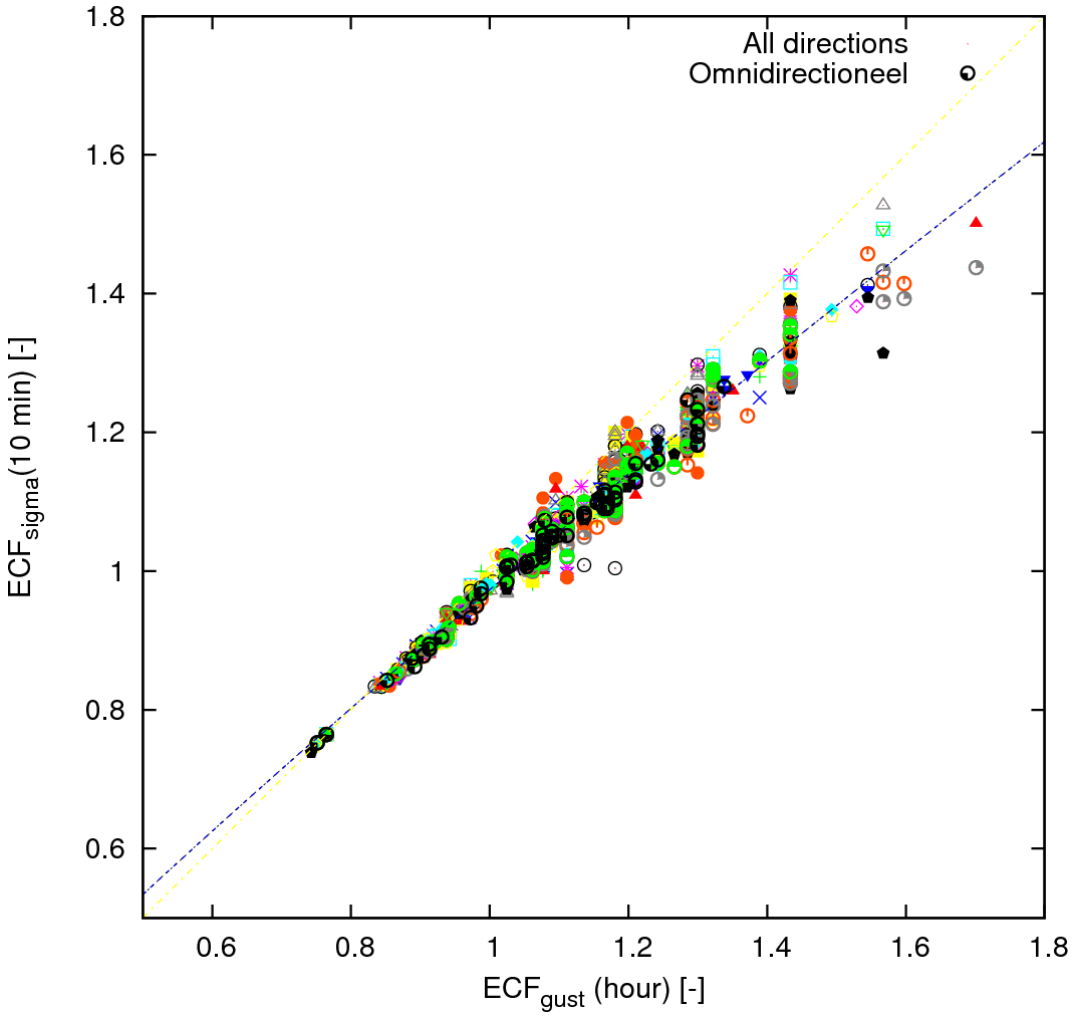


Figure 4.5.1: *Omnidirectional relation between exposure correction factors from gustiness analysis and* $\sigma_u$ *analysis for* 109 *wind sites in the period 2003-2008. Each dot represents an exposure correction factor for a wind direction sector for a station; each colour dot represents a* 20 *degree wind direction sector. The blue line denotes a fit, based on all directions and stations together.*

Table 4.5.1: *Directional fitting of exposure correction factors based on* 1 *hour gustiness analysis and* $\sigma_u$ *analysis on* 109 *wind sensors, following Equation 4.1. DD denotes wind direction. The error estimates are asymptotic standard errors.*

| DD | a (year) | b (year) |
|---|---|---|
| 20 | 0.973 +/- 0.003 | 0.889 +/- 0.016 |
| 40 | 0.976 +/- 0.003 | 0.882 +/- 0.018 |
| 60 | 0.974 +/- 0.003 | 0.929 +/- 0.017 |
| 80 | 0.977 +/- 0.002 | 0.946 +/- 0.016 |
| 100 | 0.977 +/- 0.003 | 0.907 +/- 0.019 |
| 120 | 0.979 +/- 0.003 | 0.907 +/- 0.021 |
| 140 | 0.977 +/- 0.004 | 0.876 +/- 0.025 |
| 160 | 0.974 +/- 0.003 | 0.949 +/- 0.019 |
| 180 | 0.972 +/- 0.002 | 0.844 +/- 0.012 |
| 200 | 0.971 +/- 0.002 | 0.893 +/- 0.010 |
| 220 | 0.968 +/- 0.001 | 0.879 +/- 0.009 |
| 240 | 0.970 +/- 0.002 | 0.851 +/- 0.011 |
| 260 | 0.972 +/- 0.002 | 0.849 +/- 0.010 |
| 280 | 0.969 +/- 0.002 | 0.853 +/- 0.010 |
| 300 | 0.972 +/- 0.003 | 0.832 +/- 0.015 |
| 320 | 0.961 +/- 0.003 | 0.851 +/- 0.014 |
| 340 | 0.970 +/- 0.003 | 0.822 +/- 0.015 |
| 360 | 0.970 +/- 0.003 | 0.883 +/- 0.017 |

Table 4.5.2: *Directional fitting of exposure correction factors based on* 1 *hour gustiness analysis and* $\sigma_u$ *analysis on* 109 *wind sensors, following Equation 4.1, separated into winter (November-March) and summer (April-October). The error estimates are asymptotic standard errors.*

| DD | a (winter) | b (winter) | DD | a (summer) | b (summer) |
|---|---|---|---|---|---|
| 20 | 0.964 +/- 0.001 | 0.852 +/- 0.007 | 20 | 0.983 +/- 0.001 | 0.823 +/- 0.008 |
| 40 | 0.970 +/- 0.001 | 0.896 +/- 0.006 | 40 | 0.982 +/- 0.001 | 0.896 +/- 0.008 |
| 60 | 0.972 +/- 0.001 | 0.913 +/- 0.007 | 60 | 0.980 +/- 0.001 | 0.926 +/- 0.007 |
| 80 | 0.976 +/- 0.001 | 0.900 +/- 0.007 | 80 | 0.981 +/- 0.001 | 0.905 +/- 0.007 |
| 100 | 0.975 +/- 0.001 | 0.845 +/- 0.007 | 100 | 0.979 +/- 0.001 | 0.890 +/- 0.007 |
| 120 | 0.975 +/- 0.001 | 0.864 +/- 0.009 | 120 | 0.980 +/- 0.001 | 0.875 +/- 0.007 |
| 140 | 0.972 +/- 0.001 | 0.859 +/- 0.008 | 140 | 0.980 +/- 0.002 | 0.803 +/- 0.010 |
| 160 | 0.970 +/- 0.001 | 0.843 +/- 0.006 | 160 | 0.976 +/- 0.001 | 0.803 +/- 0.009 |
| 180 | 0.968 +/- 0.001 | 0.850 +/- 0.005 | 180 | 0.969 +/- 0.001 | 0.843 +/- 0.006 |
| 200 | 0.971 +/- 0.001 | 0.849 +/- 0.003 | 200 | 0.971 +/- 0.001 | 0.860 +/- 0.005 |
| 220 | 0.967 +/- 0.001 | 0.868 +/- 0.004 | 220 | 0.972 +/- 0.001 | 0.838 +/- 0.004 |
| 240 | 0.968 +/- 0.001 | 0.862 +/- 0.004 | 240 | 0.975 +/- 0.001 | 0.852 +/- 0.005 |
| 260 | 0.966 +/- 0.001 | 0.857 +/- 0.004 | 260 | 0.979 +/- 0.001 | 0.841 +/- 0.006 |
| 280 | 0.965 +/- 0.001 | 0.860 +/- 0.004 | 280 | 0.977 +/- 0.001 | 0.874 +/- 0.008 |
| 300 | 0.958 +/- 0.001 | 0.834 +/- 0.005 | 300 | 0.982 +/- 0.001 | 0.869 +/- 0.006 |
| 320 | 0.946 +/- 0.002 | 0.813 +/- 0.007 | 320 | 0.979 +/- 0.001 | 0.857 +/- 0.007 |
| 340 | 0.944 +/- 0.002 | 0.859 +/- 0.009 | 340 | 0.982 +/- 0.001 | 0.852 +/- 0.007 |
| 360 | 0.957 +/- 0.001 | 0.864 +/- 0.007 | 360 | 0.984 +/- 0.001 | 0.808 +/- 0.008 |

## 4.6 Conclusion

Reducing the period from 1 hour to 10 minutes in the gustiness analysis showed a strong improvement of the consistency of exposure correction factors. Comparing the performance of the gustiness analysis versus the $\sigma_u$ analysis, showed even more improvement, by showing a more robust, round shape, with less wiggles than the gustiness analysis.

An elegant method for improving HYDRA time series of potential wind was developed: by applying the fitted relationship between exposure correction factors calculated from 1 hour gustiness analysis, we will be able to approximate historical exposure correction factors with those based on $\sigma_u$ analysis. Because of the seasonal dependency found in the exposure correction factors, we used the season dependent fits.

# Chapter 5

# Extreme wind

Now, differences between gustiness and $\sigma_u$-analysis will be discussed in relation to extreme winds with return periods longer than the length of the measurement series. We will compare both peak over threshold methods (which were used in HYDRA, e.g., *Verkaik et al.* (2003c) and *Verkaik et al.* (2003a)), and Gumbel analysis, as described in for instance *Brink and Können* (2008). We will refer to results using exposure correction factors based on 1 hour gustiness analysis as *old*. Results achieved by applying the directional fit (see section 4.5), will be referred to as *new*.

## 5.1 Extreme wind speeds from gustiness and $\sigma_u$-analysis

Figure 5.1.1 shows the 2000 highest peaks of hourly mean wind speed for the potential wind series using the fit between exposure correction factors based on 1 hour gustiness analysis and $\sigma_u$ analysis, for stations Hoek van Holland (330) versus Soesterberg (265). It illustrates the effect of correcting the potential wind series. As can be seen, the curve of Soesterberg has become less steep, with a reduction of approximately 5%. The curve of Hoek van Holland shows almost no visible change. This is caused by the effect that the $\sigma_u$ analysis differed most from 1 hour gustiness analysis for inland stations with higher exposure correction factors. Compared to the *old* potential wind series, a possible intersection has moved outside of the measurement series, meaning that choosing an appropriate extreme value distribution is of significant importance.

## 5.2 Extreme wind from Rijkoort-Weibull model

The Rijkoort-Weibull model (*Rijkoort*, 1983) was developed to calculate return levels of hourly mean wind speeds with high return periods (up to 10.000 years) at several stations in the Netherlands (see Figure 5.2.1 and *Rijkoort and Wieringa* (1983)). During the HYDRA project, it turned out that the Rijkoort-Weibull model could not be reconstructed. Furthermore, it appeared to have a number of shortcomings with the consequence that the return levels for hourly mean values of wind speed derived from this model were unreliable (*Smits*, 2003). The extreme wind maps published by *Wieringa and Rijkoort* (1983) were not only based on statistical results, but also on expert judgment. For instance, wind speeds in the Rhine valley south from the *Utrechtse Heuvelrug*, from Rotterdam, via Cabauw and Herweijnen to Deelen, are known to be higher than surrounding areas. This is an explanation for Deelen having relatively high wind speeds compared to other inland stations. Furthermore, the Rijkoort-Weibull model excluded coastal stations, that have complex sea-land transitions, and only used those stations to check the results (Wieringa, personal communication).

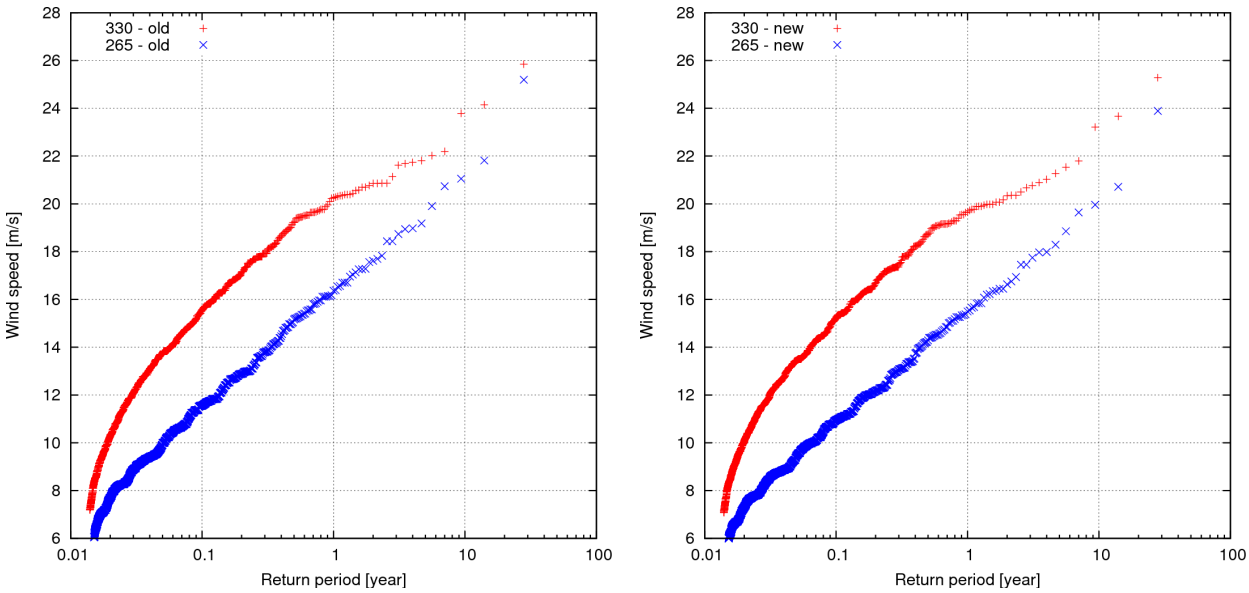


(a) (b)

Figure 5.1.1: *Return level plots for the extreme wind speeds in Hoek van Holland and Soesterberg, based on the* 2000 *highest peaks of hourly mean potential wind speed. (a): old, (b): new. On the x-axis, the return period is shown, on the y-axis, peaks of hourly mean wind speed (m/s) are shown. Period shown: January* 1981 - *December* 2008. *Plot position used:* $\frac{n}{2000+1}$

## 5.3 Extrapolating extreme wind from gustiness- and $\sigma_u$-analysis

To give an impression of the effects of the $\sigma_u$ fit to the exposure correction factors on extreme winds and how it compares to the Rijkoort-Weibull results, a relatively simple extreme wind analysis was carried out by Gumbel fitting to yearly maxima of hourly mean wind speed to the power of $k$, with $k$ being the Weibull shape parameter. By doing so, the data converges to a Gumbel distribution faster (*Palutikof et al.*, 1999). $k$ is approximately $2$ in coastal regions and $1.6$ inland. We used $k = 2$ for all stations, thereby slightly overestimating extreme wind speeds above land. Figures 5.3.1, 5.3.2 and 5.3.3 show the annual maxima of measured and potential hourly mean wind speed for respectively station Hoek van Holland $(330)$, Soesterberg $(265)$ and Schiphol $(240)$ in a Gumbel plot, using the plot position $\frac{n}{N+1}$. Gumbel fits to $U^2$ are also shown. It can be seen that using a Gumbel fit of wind speed to a certain power is more appropriate than using ordinary Gumbel fit.

Spatial distributions of $1000$ year return values were also investigated. Therefore, only stations having at least $90\%$ availability of hourly mean wind speed records in each year for the period $1993 - 2007$ were selected. Figure 3.4.1 shows the data availability of all stations. Figure 5.3.4 shows the hourly mean potential wind speed for a return period of $1000$ years. Both the old and new results show results comparable to *Wieringa and Rijkoort* (1983) (Figure 5.2.1), as far as spatial distribution is concerned: both show a northwest to southeast gradient in the order of $8$ m/s and relatively high wind speeds in the Rhine valley and Deelen. Surprisingly, the highest potential wind speeds are not found at the coast or at the North Sea, but at Schiphol. Note that in the linear Gumbel fit by *Wieringa and Rijkoort* (1983) (Figure 5.2.1), Schiphol also shows a local maximum. Currently we do not have an explanation for this. However, the results from *Wieringa and Rijkoort* (1983) also show signs of a curvature problem: the $1000$ year wind speed in Deelen is higher than for Vlissingen, Hoek van Holland and IJmuiden.

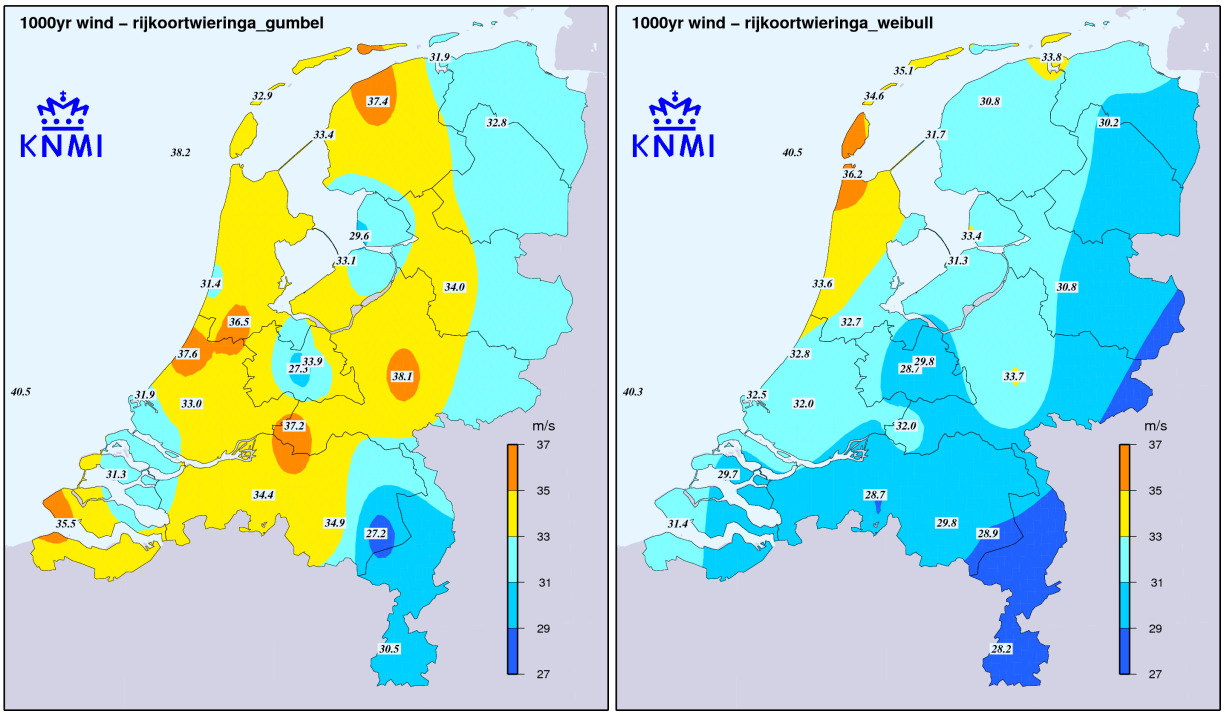


(a) (b)

Figure 5.2.1: *Reproduction of hourly mean potential wind speeds for a return period of* 1000 *years by using (a): linear Gumbel extrapolation of individual station measurement series and (b): the Rijkoort-Weibull model (right) from Figures 5.20 and 5.21 in Wieringa and Rijkoort (1983), based on the measurement period 1962-1976. Due to the automatic interpolation algorithm, expert judgement could not be incorporated in these reproductions.*

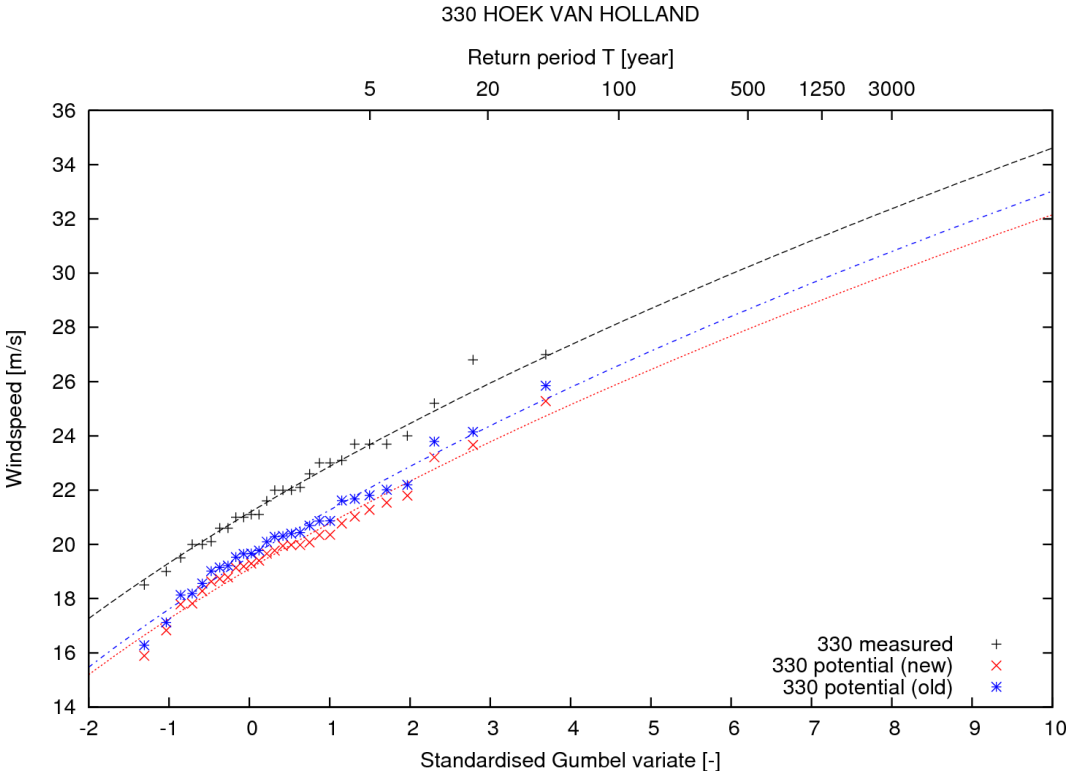


Figure 5.3.1: *Gumbel plot of omnidirectional yearly maxima of hourly mean wind speed, for measured wind, old and new potential wind at station Hoek van Holland* (330)*. All available years having at least* 90% *availability of hourly mean wind speed records are plotted (period* 1981-2008*).*

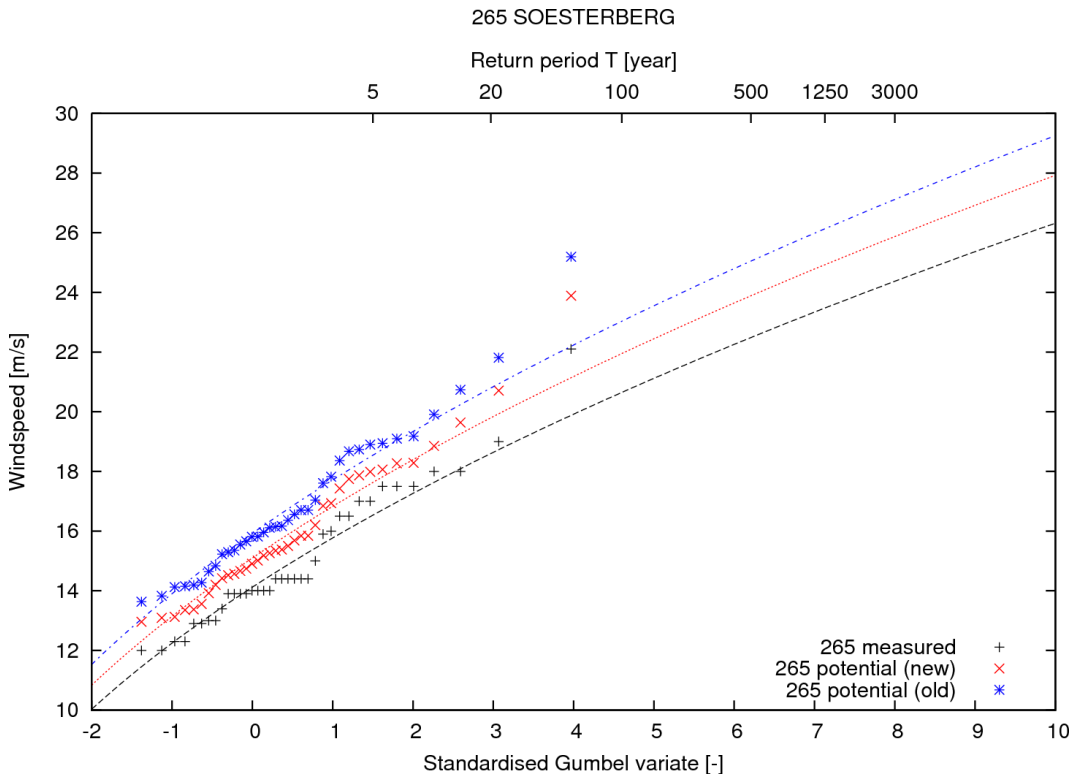


Figure 5.3.2: *Gumbel plot of omnidirectional yearly maxima of hourly mean wind speed, for measured wind, old and new potential wind at station Soesterberg* (265)*. All available years having at least* 90% *availability of hourly mean wind speed records are plotted (period* 1971-2008*). Note that the deviation of the highest measured wind speed from the Gumbel fit does not automatically imply that the Gumbel model used does not describe the observations. The probability of finding the highest observations to be higher than the Gumbel fit is higher than finding the Gumbel fit to be higher than the highest observations (Brink and Können, 2008).*

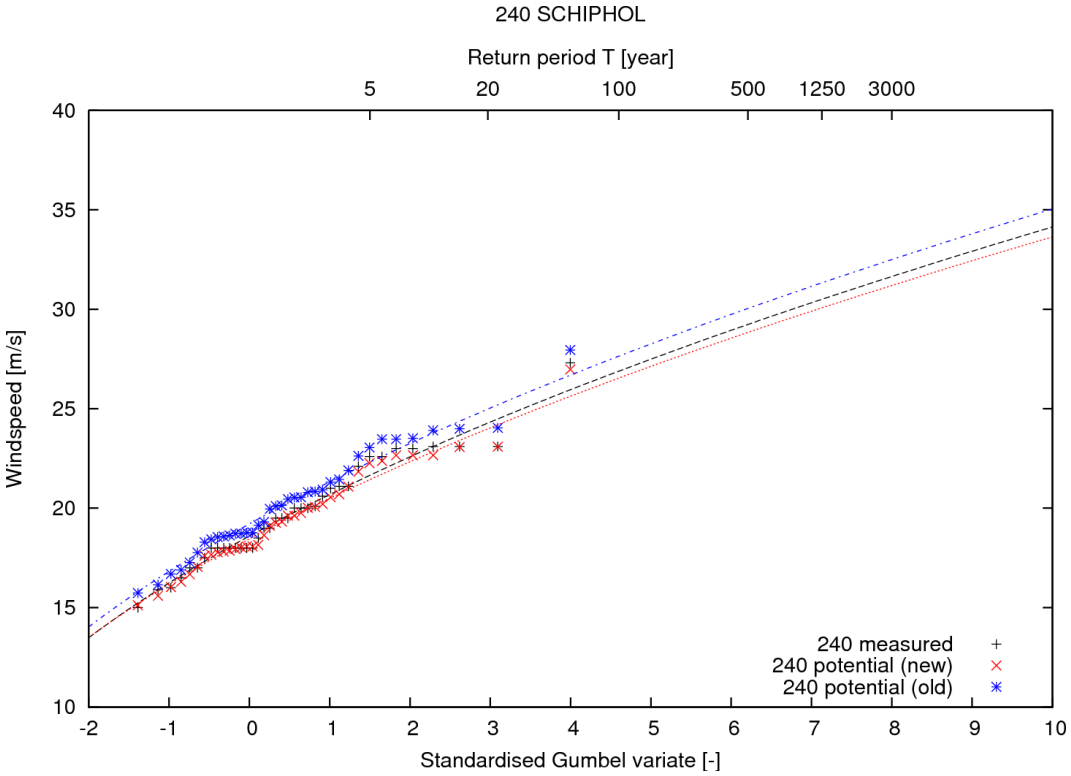


Figure 5.3.3: *Gumbel plot of omnidirectional yearly maxima of hourly mean wind speed, for measured wind, old and new potential wind at station Schiphol* (240). *All available years having at least* 90% *availability of hourly mean wind speed records are plotted (period* 1971-2008*).*

In general, results based on potential wind have lower extreme wind speeds for a specific return period than the Rijkoort-Weibull model. This could be caused by the fact that the period for which the Rijkoort-Weibull model is shown is 1962-1976, while the results based on potential wind are determined on the period 1981-2008. However, the difference in statistical distribution will also play a significant role. Therefore, direct comparison is difficult.

Directional extremes for return periods of 1000 years were calculated as well (see Appendix E). It confirms that yearly maximum hourly wind speeds are mostly coming from directions between southwest and northwest. Directional maps can be used to determine a range of extreme winds for specific regions (like Lake IJssel or Wadden Sea), taking into account specific circumstances in stresses on water defence systems.

Comparing both maps (*old* and *new*) of Figure 5.3.4 reveals the effect of applying the fit between exposure correction factors derived from 1 hour gustiness analysis and $\sigma_u$ analysis: inland stations got a stronger reduction in local roughness than coastal stations (illustrated by Figure 4.5.1), resulting in a stronger reduction of extreme potential winds. For instance, the 1000 year potential wind for IJmuiden decreases only 0.3 m/s (about 1%), while Schiphol has a reduction of 1 m/s (about 3%). Further inland, the reduction is in the order of 1.2 m/s (about 5%). Whether the curvature problem disappeared should become clear in the statistical analysis, although we notice that the intersection point will move to longer return periods.

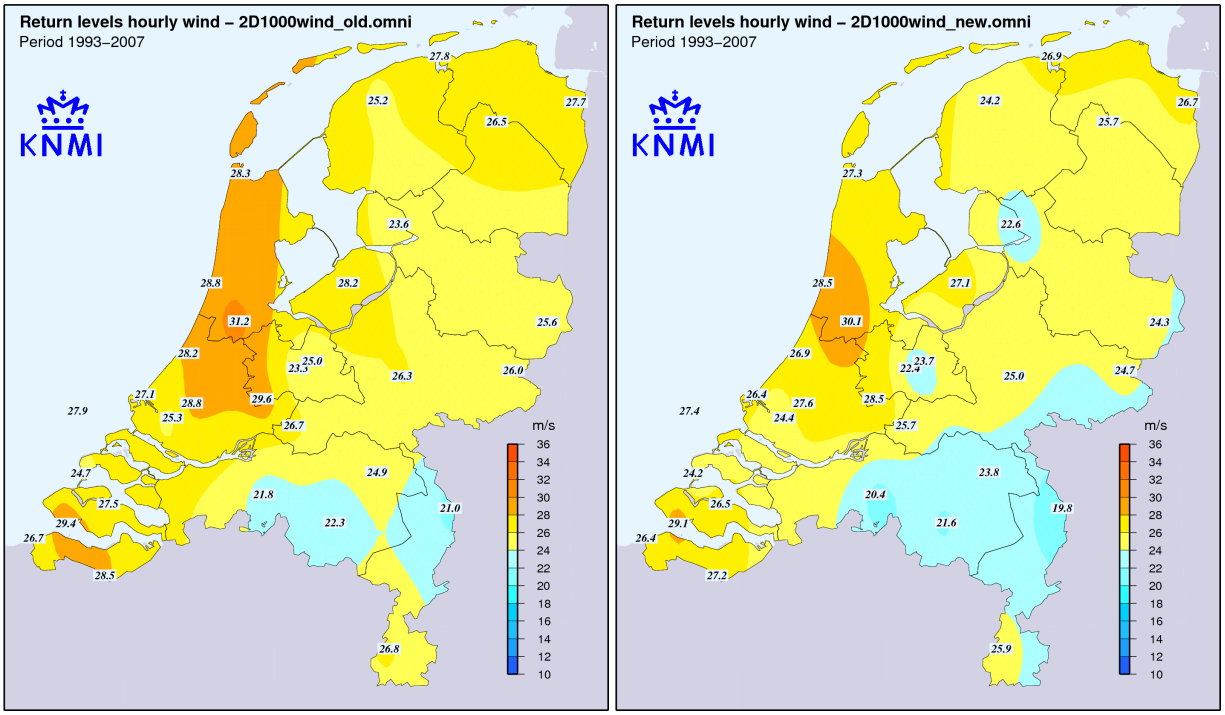


(a) (b)

Figure 5.3.4: *Hourly mean potential wind speeds for a return period of* 1000 *years, determined with a Gumbel fit to yearly maxima of hourly mean potential wind speed squared. (a): using exposure correction factors as determined in the HYDRA project. (b): using exposure correction factors calculated using the fit relationship between* 1 *hour gustiness analysis and* $\sigma_u$ *analysis. Potential wind speeds are based on a reference roughness length of* 3 *cm.*

## 5.4 Conclusion

New exposure correction factors have produced potential wind series that show a reduction up to $5\%$ of potential wind speed over land and little change near the coast. The effect on previously applied extreme wind statistics is a slight reduction in the curvature problem.

Comparing the results from the Rijkoort-Weibull model and the improved potential wind series, we can conclude that both share many features. Using a special Gumbel extrapolation, a logical spatial gradient in extreme wind is found. The spatial gradient is, in general, comparable to the non-reconstructable results from the Rijkoort-Weibull model. However, the present Gumbel extrapolations (both with old and new exposure corrections) yield $10$-$30\%$ lower wind extremes than the Rijkoort-Weibull model. This is probably caused by the different measurement period the extreme value analysis is applied on, and the choice of the extreme value distribution.

We conclude that the results from the HYDRA project can therefore be considered to be a refinement of *Wieringa and Rijkoort* (1983), giving the possibility to make use of the longer measurement period and new wind measurement sites currently available. Whether the curvature problem has disappeared should become clear in further statistical analyses as foreseen in the next phase of the SBW Wind project. The present results suggest that the curvature problem decreases, i.e. the crossing point moves to longer return periods. However, following the present Gumbel extrapolation, the curvature problem is still present in extremes with return times of $1000$ years; the extremes of the stations Rotterdam, Schiphol and Cabauw are still higher than the extremes of some nearby coastal and sea stations.

# Chapter 6

# Discussion

## 6.1 Conclusions

When the HYDRA project was finished, the potential wind series that were produced showed some unexpected behaviour. Especially the fact that the calculated extremes over land were sometimes higher than over sea (a phenomenon referred to as *curvature problem*) gave rise to doubts whether potential wind time series are useful for extreme wind statistics.

### Objective of this study

The objective of this study is to introduce a new technique for evaluating exposure correction factors for the KNMI time series of hourly wind, based on the relatively modern 10 minute data sets, and evaluate its effect, including its effect on previously applied extreme value analysis.

### Towards improved exposure correction factors

Recently, it was found that seasonal and directional variations in exposure correction factors derived from gustiness analysis could be part of this problem. It was suggested that atmospheric conditions (stability) could influence the turbulent exchange of momentum in such a way that the assumptions for gustiness analysis were questionable, especially unsteady conditions in north-westerly flows with polar air masses. Reducing the measurement interval from 1 hour to 10 minutes for the gustiness analysis improved the consistency of the exposure correction factors. Directly using the recently available $\sigma_u$ measurements gives an even better improvement of the results, because the sensitivity of the correction factors to the *air mass effect* decreased.

- The default technique is to calculate exposure correction factors by using gustiness analysis during 1-hour time intervals. Since 2003, exposure correction factors can also be evaluated from 10-minute data, using gustiness analysis. Since 2003, also standard deviation of the wind signal can be used. The latter option is considered to be the most accurate.
- Exposure correction factors for land stations are typically larger than those of sea and coastal stations. Wind directions with shelter were demonstrated to have relatively large exposure correction factors
- A pronounced feature shown in the averaged exposure correction factors for the Netherlands is relatively low values for south-westerly and north-easterly winds. This is caused by the many airports and airfields that are part of the measurement network, having smooth runways in the most frequent wind direction.
- Directional and seasonal analysis of the exposure correction factors demonstrated that for land stations and during the winter season with northwesterly winds, exposure correction

factors from 1-hour-gustiness analysis are systematically higher than exposure correction factors from the other techniques. A plausible explanation is the non stationary behaviour of the wind speed within the time frame of 1 hour, and the directional differences in air mass.

- Exposure correction factors based on the standard deviation of the wind speed were correlated with those based on the 1-hour-gustiness analysis using a power fit. The resulting fit was of good quality, thereby allowing for the estimation of improved exposure correction factors for the whole measuring period (and not only for years after 2003). This will improve the consistency of the potential wind series, as the more consistent characteristics from $\sigma_u$ analysis can be applied on the historical series.

### Extreme wind statistics

Using simple extreme value statistics, estimations of the 1000 year return values were given. Return values based on potential wind series show good spatial resemblance with *Wieringa and Rijkoort* (1983). It has become likely that using the power fit, the curvature problem will appear only at longer return periods than before. Furthermore, using potential wind series allows to make use of the increasing amount of available wind measurements locations and extensions of already existing series. This makes a refinement of extreme wind statistics for the Netherlands possible.

- The new corrections yield 1-5% reduction in the 1000 year return values, with the largest reductions inland.
- Results using a special Gumbel extrapolation were compared with results by *Wieringa and Rijkoort* (1983). The spatial patterns are qualitatively comparable, but the differences in 1000 year return values, are large: the new extreme winds are 10-30% lower than the 1983 Rijkoort-Weibull model. This is probably due to differences in the measurement period and the applied extreme value model. Following the used Gumbel extrapolation, the curvature problem is still present in the new 1000 year return values of wind extremes as the extremes for Schiphol, Cabauw and Rotterdam are higher than those for the coast and North Sea, although the new exposure corrections have produced a slight reduction in the curvature problem.

## 6.2 Outlook and recommendations

The results presented in this report can be used to construct improved time series of potential wind for future extreme wind research by applying the proposed power fit. We now have come to a point that the choice of extreme value model becomes of more importance. The refinement of the power fit, to approximate exposure correction factors based on $\sigma_u$ analysis should be applied on historical records to improve the quality of the potential wind data series.

However, more research is needed to come to a better understanding of the relationship between the wind speed measurements, the synoptic situation and the local and regional landscape. For instance, we sense strong indications that the underlying theory is sensitive for stability assumptions under specific conditions like season, region and air mass. Another question is the relationship between roughness lengths derived from land use maps and roughness lengths derived from wind speed measurements. We have seen that some features found using land use maps are well represented in the measurements, giving an indication that there is a good correlation between both methods. However, other features found in measurements cannot be traced back to features on land use maps. This might partly be caused by the *air mass effect* or partly by the algorithm to translate land use classes to roughness lengths.

Finally, the question arises whether extreme winds in independent data sets also indicate signs of the curvature problem, and how this relates to the neutral wind profile, the scaling factor

and *air mass effect*. Indications for this are found in studies over open water areas like Lake IJssel (*Bottema*, 2007).

## Recommendations

This study has produced a method of deriving exposure correction factors, such that the curvature problem decreased. The applied exposure correction no longer seems to be the main cause of the curvature problem.

Rather, following the previously applied extreme value analysis, the curvature problem seems to be a real phenomenon, which is not understood however. A systematic analysis of the curvature problem is important.

In relation to the exposure factors, the following is recommended:

- Gustiness analysis might be improved for periods where the $\sigma_u$ data is not yet available, by excluding the hours with observations that clearly show a too large gustiness. From the $\sigma_u$ analysis these conditions probably can be determined, giving a recipe for the use of the available long time series of observations that are available in the Netherlands.
- Detailed case studies of storms might give insight in the interaction between air mass and surface roughness. This is important, as also in measurements of individual events, wind above land sometimes is higher than above water (*Bottema*, 2007).
- The effect of the stability and short-lived convective enhancement of the background flow is not limited to the north-westerly flows. Also during large-scale storm conditions this effect can be seen as short periods, usually 10 minutes, of strong average winds accompanied by the strongest gusts. In this way also the gust factor during the strong wind events will be overestimated. It probably also is one of the reasons why the 10-minute gustiness analysis is much closer to the $\sigma_u$ analysis.

The following actions are recommended to get some further understanding of the curvature problem:

- As we found a possible relation with air mass and wind direction, it is possible that by looking at omnidirectional extremes, different distributions are mixed. Therefore, we suggest looking at a directional approach in extreme wind statistics, and verify whether the curvature problem also exists for non-polar air masses and south-westerly winds (which the results of *Bottema* (2007) seem to suggest).
- By applying the extreme value analysis, it is also important to investigate the assumption that the measurement sites are independent. It is known that storms can have preferred tracks. It would be interesting to investigate the effect of storm tracks, the size of storm fields on the spatial distribution of extreme wind? (Note that Figure 4.7 of *Wieringa and Rijkoort* (1983) suggests an average northwest-southeast decrease in wind speed that is related to weather systems and not to roughness effects).
- The relation between extreme value trend of the air pressure gradient (and the geostrophic wind) and the trends in surface winds could be researched. If they are dissimilar, some phenomenon in the lowest layers of the atmosphere (boundary layer) must play a role.
- An other interesting source of data is the measurement site of Cabauw, where a 200 m wind post is located. Analyzing these data, more insight can be found in the extrapolation of the near-surface wind speed to a wind speed higher in the atmospheric boundary layer, and the robustness of statistical extrapolation methods.
- Coastal stations might have their own exposure problems which currently are not addressed: the sea surface roughness may not obey the Charnock relation when the waves break due to either shallow water or extreme wind forcing, the jetty on which the wind

mast is located may give flow distortion, and the height of the observation above the water may be systematically lower in strong wind conditions due to the storm surge.

# References


Benschop, H. (1996), Windsnelheidsmetingen op zeestations en kuststations: herleiding warden windsnelheid naar 10-meter niveau, *KNMI Publication*, (TR-188).

Bottema, M. (2007), *Measured wind-wave climatology Lake IJssel (NL), 2007.020*, 278 pp., RWS RIZA.

Brink, H. v. d., and G. Können (2008), The statistical distribution of meteorological outliers, *Geophysical Research letters*, *35*.

Charnock, H. (1955), Wind stress on a water surface, *The Quarterly Journal of the Royal Meteorological Society*, *81*, 639–640.

Davenport, A. (1960), Rationale for Determining Design Wind Velocities, *Journal of the Structural Division of the American Society of Civil Engineering*, *86*, 39–68.

Holtslag, A. (1984), Estimates of diabatic wind speed profiles from near surface weather observations., *Boundary-layer Meteorology*, (29), 225–250.

KNMI and Deltares wind modeling team (2008), Extreme wind statistics for the Netherlands., *Plan of approach*.

Palutikof, J., B. Brabson, D. Lister, and S. Adcock (1999), A review of methods to calculate extreme wind speeds, *Meteorological Applications*, *6*, 119–132.

Panofsky, H., and J. Dutton (1984), *Atmospheric Turbulence, Models and Methods for Engineering Applications*, 396 p. pp., John Wiley and Sons.

Rijkoort, P. (1983), A Compound Weibull Model For The Description Of Surface Wind Velocity Distributions, *KNMI Publication (Wetenschappelijk Rapport)*, (WR 83-13).

Rijkoort, P., and J. Wieringa (1983), Extreme wind speeds by compound Weibull analysis of exposure-corrected data, *Journal of Wind Engineering and Industrial Aerodynamics*, (13).

Royal Netherlands Meteorological Institute (KNMI) (2001), *Handboek waarnemingen*, http://www.knmi.nl/samenw/hawa/.

Smits, A. (2003), HYDRA Phase report 5: Analysis of the Rijkoort-Weibull model.

Taminiau, C. (2004), *Wind(extremen) in het IJsselmeergebied*, RIZA werkdocument 2004.138x, 60 pp., RWS RIZA.

Tennekes, H. (1973), The logarithmic wind profile, *Journal of the Atmospheric Sciences*, *30*, 234–238.

Verkaik, J. (1998-2005), HYDRA-project.

Verkaik, J. (2000), Evaluation of Two Gustiness Models for Exposure Correction Calculations., *Journal of Applied Meteorology*, *39*(9), 1613–1626.

Verkaik, J. (2003), HYDRA Phase report 11 and 12: A method for the geographical interpolation of wind speed over heterogeneous terrain.

Verkaik, J. (2006), On wind and roughness over land., Ph.D. thesis.

Verkaik, J., A. Smits, and J. Ettema (2003a), HYDRA Phase report 15: Wind statistics of the Netherlands including the coastal zone.

Verkaik, J., A. Smits, and J. Ettema (2003b), HYDRA Phase report 16: Naar een nieuwe extreme waardenstatistiek van de wind in Nederland.

Verkaik, J., A. Smits, and J. Ettema (2003c), HYDRA Phase report 9: Wind Climate Assessment of the Netherlands 2003: Extreme value analysis and spatial interpolation methods for the determination of extreme return levels of wind speed.

Wieringa, J. (1986), Roughness-dependent geographical interpolation of surface wind speed averages., *Quarterly Journal of the Royal Meteorological Society*, (112), 867–889.

Wieringa, J. (1992), Updating the Davenport roughness classification, *Journal of Wind Engineering and Industrial Aerodynamics*, *41*, 357–368.

Wieringa, J. (1993), Representative roughness parameters for homogeneous terrain, *Boundary-Layer Meteorology*, *63*, 323–363.

Wieringa, J., and P. Rijkoort (1983), *Windklimaat van Nederland*, Koninklijk Nederlands Meteorologisch Instituut (KNMI).

# Appendix A

# Coefficients $A$ and $g$

Coefficients for $A$ and $g$ are shown for a measurement period of $1$ hour (Table A.0.1) and $10$ minutes (Table A.0.2). Coefficients are calculated following *Verkaik* (2000).

Table A.0.1: *Wind speed dependence of the coefficients $A$ (Attenuation) and $g$ (normalized gust) for a measurement period of* 1 *hour.*

| $U$ | $A$ | $g$ | $Ag$ |
|---|---|---|---|
| 1 | 0.917 | 3.014 | 2.76 |
| 2 | 0.923 | 3.163 | 2.92 |
| 3 | 0.919 | 3.231 | 2.97 |
| 4 | 0.914 | 3.270 | 2.99 |
| 5 | 0.908 | 3.297 | 2.99 |
| 6 | 0.902 | 3.317 | 2.99 |
| 7 | 0.896 | 3.332 | 2.99 |
| 8 | 0.890 | 3.344 | 2.98 |
| 9 | 0.885 | 3.356 | 2.97 |
| 10 | 0.880 | 3.366 | 2.96 |
| 11 | 0.875 | 3.376 | 2.96 |
| 12 | 0.871 | 3.383 | 2.95 |
| 13 | 0.866 | 3.389 | 2.94 |
| 14 | 0.862 | 3.399 | 2.93 |
| 15 | 0.858 | 3.402 | 2.92 |
| 16 | 0.854 | 3.407 | 2.91 |
| 17 | 0.851 | 3.413 | 2.90 |
| 18 | 0.847 | 3.420 | 2.90 |
| 19 | 0.844 | 3.423 | 2.89 |
| 20 | 0.840 | 3.435 | 2.89 |
| 21 | 0.837 | 3.444 | 2.88 |
| 22 | 0.834 | 3.435 | 2.86 |
| 23 | 0.831 | 3.440 | 2.86 |
| 24 | 0.828 | 3.443 | 2.85 |
| 25 | 0.825 | 3.446 | 2.84 |
| 26 | 0.822 | 3.447 | 2.83 |
| 27 | 0.819 | 3.452 | 2.83 |
| 28 | 0.817 | 3.455 | 2.82 |
| 29 | 0.814 | 3.471 | 2.83 |
| 30 | 0.812 | 3.480 | 2.82 |
| 31 | 0.809 | 3.464 | 2.80 |
| 32 | 0.807 | 3.468 | 2.80 |
| 33 | 0.804 | 3.469 | 2.79 |
| 34 | 0.802 | 3.471 | 2.78 |
| 35 | 0.799 | 3.480 | 2.78 |

Table A.0.2: *Wind speed dependence of the coefficients $A$ (Attenuation) and $g$ (normalized gust) for a measurement period of* 10 *minutes.*

| $U$ | $A$ | $g$ | $Ag$ |
|---|---|---|---|
| 1 | 0.824 | 2.397 | 1.97 |
| 2 | 0.866 | 2.563 | 2.22 |
| 3 | 0.878 | 2.639 | 2.32 |
| 4 | 0.882 | 2.684 | 2.37 |
| 5 | 0.881 | 2.714 | 2.39 |
| 6 | 0.879 | 2.737 | 2.41 |
| 7 | 0.876 | 2.754 | 2.41 |
| 8 | 0.873 | 2.768 | 2.42 |
| 9 | 0.869 | 2.782 | 2.42 |
| 10 | 0.866 | 2.792 | 2.42 |
| 11 | 0.862 | 2.804 | 2.42 |
| 12 | 0.859 | 2.812 | 2.41 |
| 13 | 0.855 | 2.819 | 2.41 |
| 14 | 0.852 | 2.831 | 2.41 |
| 15 | 0.848 | 2.835 | 2.40 |
| 16 | 0.845 | 2.839 | 2.40 |
| 17 | 0.842 | 2.847 | 2.40 |
| 18 | 0.839 | 2.854 | 2.39 |
| 19 | 0.836 | 2.858 | 2.39 |
| 20 | 0.833 | 2.873 | 2.39 |
| 21 | 0.830 | 2.883 | 2.39 |
| 22 | 0.827 | 2.872 | 2.37 |
| 23 | 0.824 | 2.878 | 2.37 |
| 24 | 0.821 | 2.881 | 2.37 |
| 25 | 0.819 | 2.885 | 2.36 |
| 26 | 0.816 | 2.886 | 2.35 |
| 27 | 0.813 | 2.892 | 2.35 |
| 28 | 0.811 | 2.896 | 2.35 |
| 29 | 0.809 | 2.915 | 2.36 |
| 30 | 0.806 | 2.926 | 2.36 |
| 31 | 0.804 | 2.907 | 2.34 |
| 32 | 0.801 | 2.910 | 2.33 |
| 33 | 0.799 | 2.913 | 2.33 |
| 34 | 0.797 | 2.915 | 2.32 |
| 35 | 0.795 | 2.925 | 2.32 |

# Appendix B

# Exposure correction factors: rose plots

## B.1 Yearly plots

Figures B.1.1, B.1.2 and B.1.3 show rose plots of exposure correction factors for various stations for both 1 hour and 10 minute gustiness analysis and $\sigma_u$ analysis.

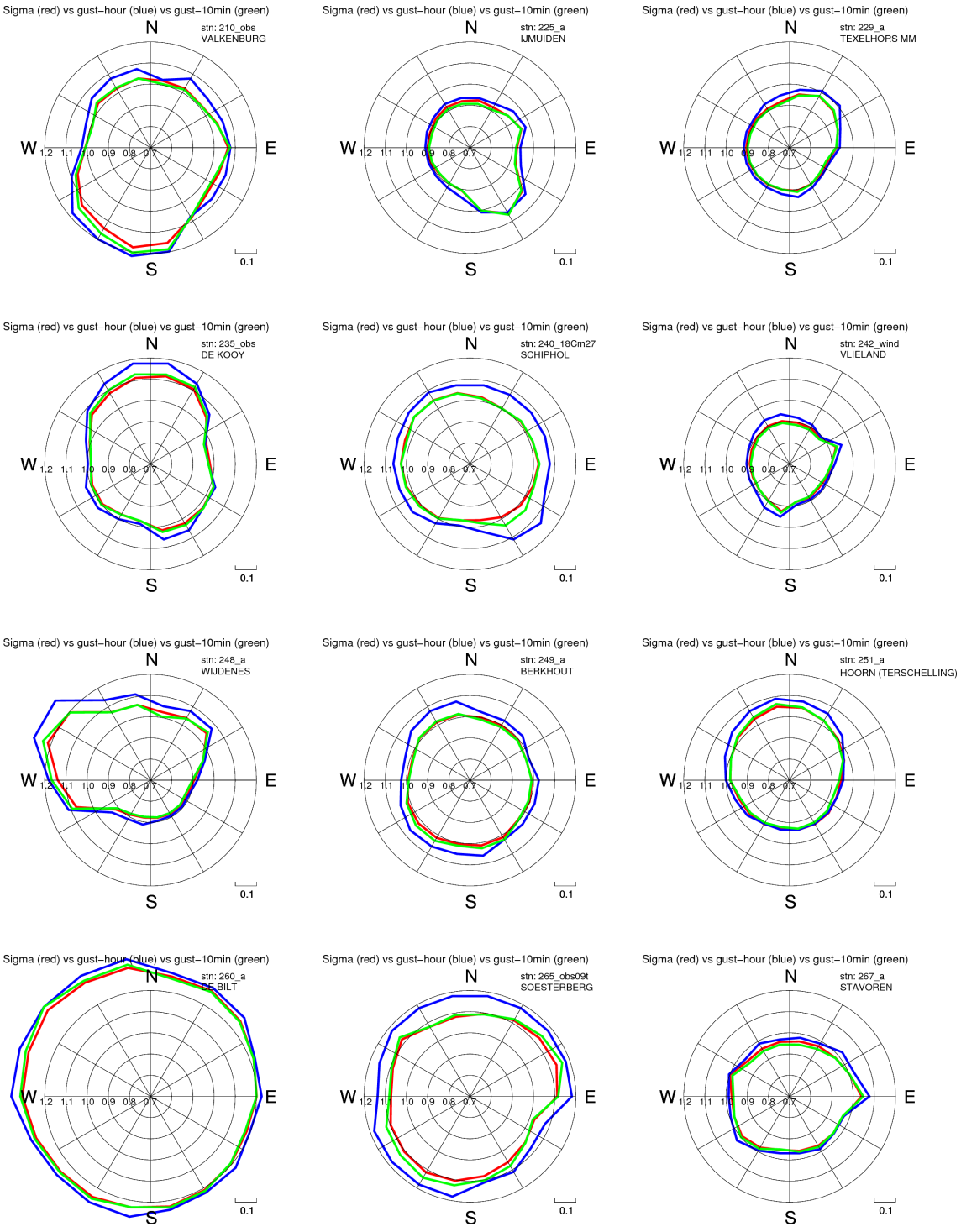


Figure B.1.1: *Rose plot of exposure correction factors for various stations, based on* 1 *hour gustiness (blue),* 10 *minute gustiness (green) and* $\sigma_u$ *analysis (red). In case the sensor height deviates from* 10 *m, the exposure correction factors have been adjusted, assuming a logarithmic wind profile with a roughness length derived from omnidirectional* $\sigma_u$ *analysis (see Section 3.3.3).*

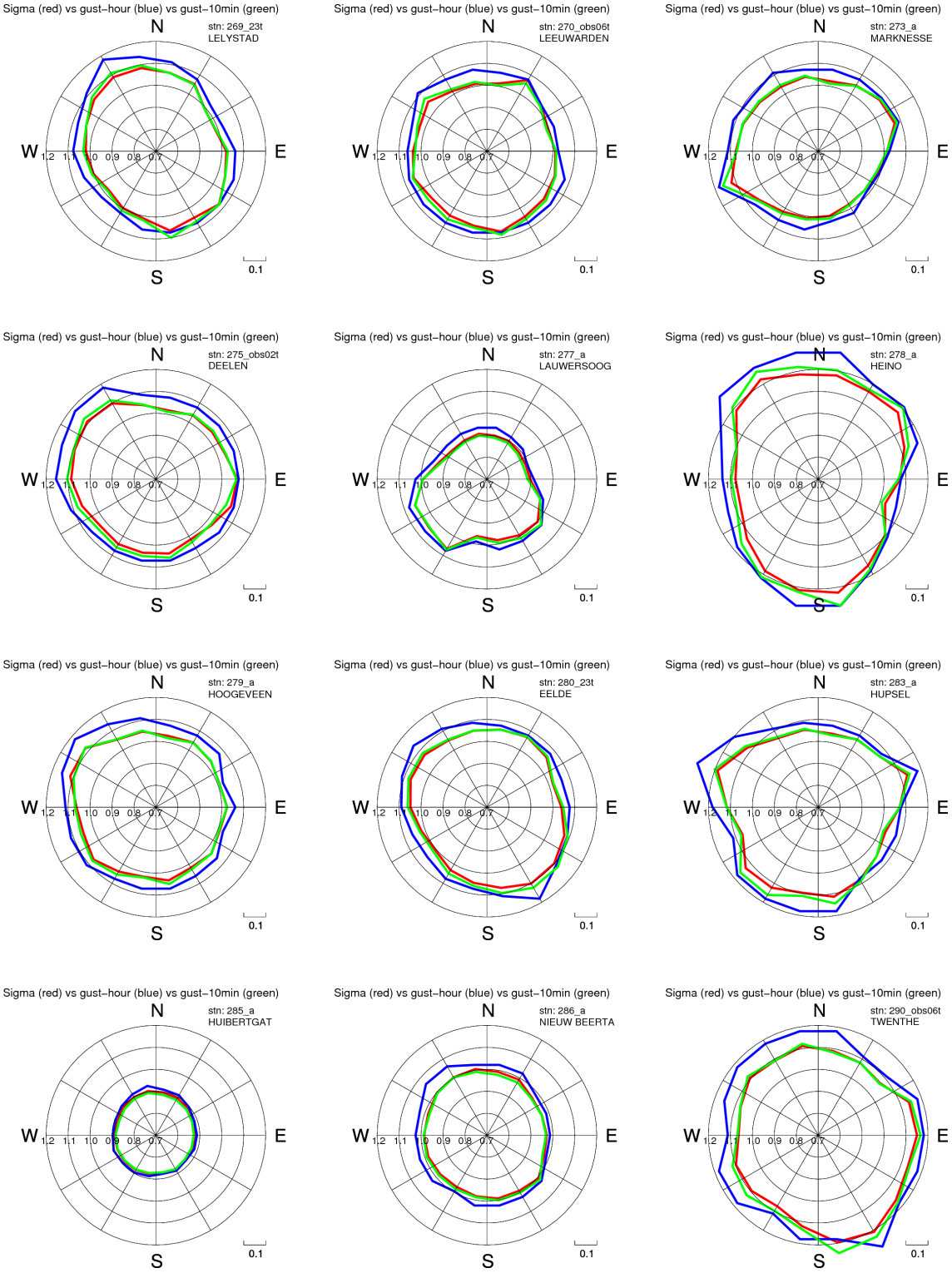


Figure B.1.2: *Rose plot of exposure correction factors for various stations, based on* 1 *hour gustiness (blue),* 10 *minute gustiness (green) and* $\sigma_u$ *analysis (red). In case the sensor height deviates from* 10 *m, the exposure correction factors have been adjusted, assuming a logarithmic wind profile with a roughness length derived from omnidirectional* $\sigma_u$ *analysis (see Section 3.3.3). Lines connected to the centre of the plot indicate data shortage for calculating exposure correction factors (less than* 10 *measurements).*

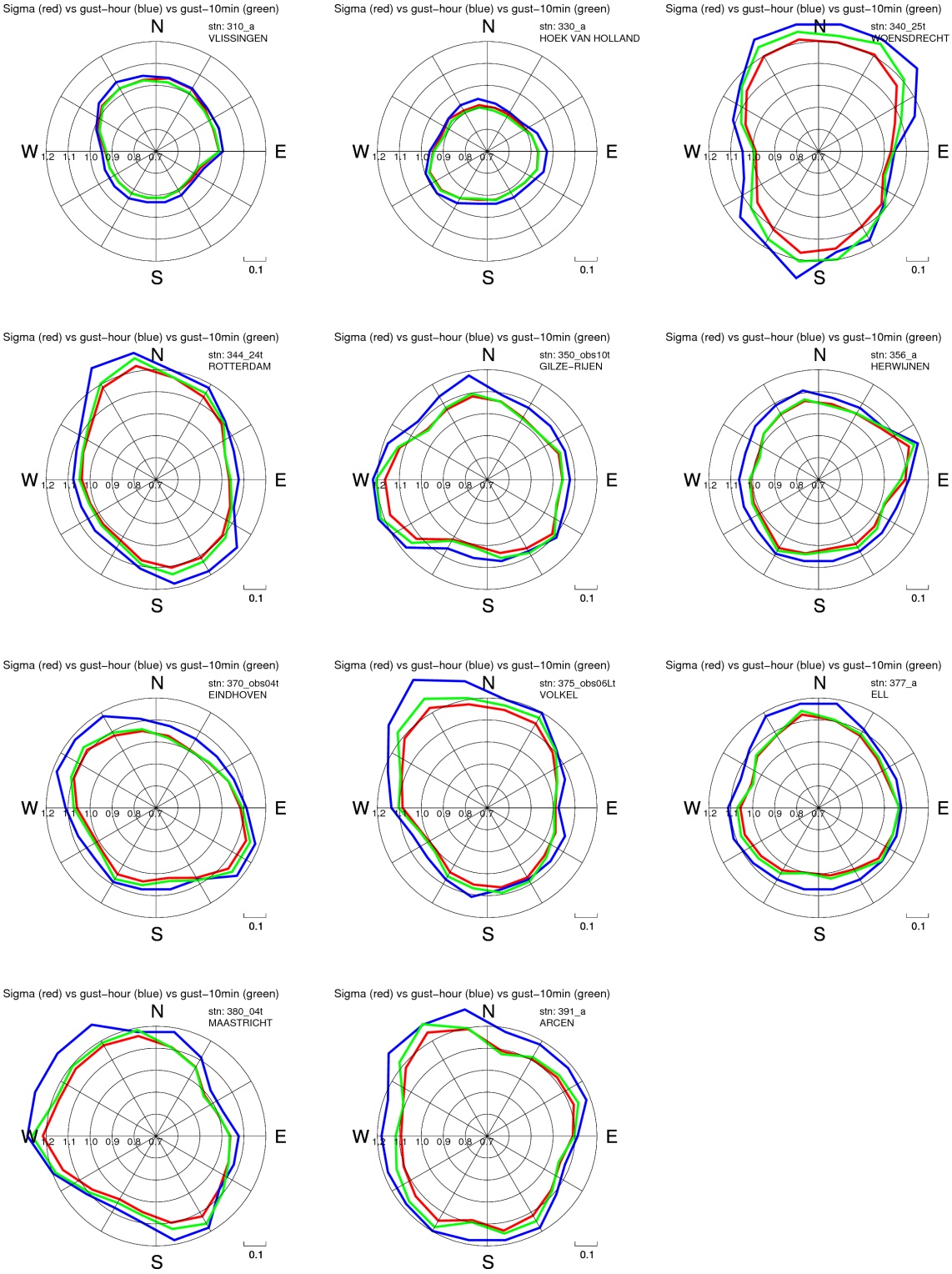


Figure B.1.3: *Rose plot of exposure correction factors for various stations, based on* 1 *hour gustiness (blue),* 10 *minute gustiness (green) and* $\sigma_u$ *analysis (red). In case the sensor height deviates from* 10 *m, the exposure correction factors have been adjusted, assuming a logarithmic wind profile with a roughness length derived from omnidirectional* $\sigma_u$ *analysis (see Section 3.3.3). Lines connected to the centre of the plot indicate data shortage for calculating exposure correction factors (less than* 10 *measurements).*

## B.2 Seasonal plots

Figures B.2.1, B.2.2 and B.2.3 show rose plots of exposure correction factors for various stations for 1 hour gustiness analysis, separated into summer (April-October) and winter (November-March).

Figures B.2.4, B.2.5 and B.2.6 show rose plots of exposure correction factors for various stations for 10 minute gustiness analysis, separated into summer (April-October) and winter (November-March).

Figures B.2.7, B.2.8 and B.2.9 show rose plots of exposure correction factors for various stations for $\sigma_u$ hour gustiness analysis, separated into summer (April-October) and winter (November-March).

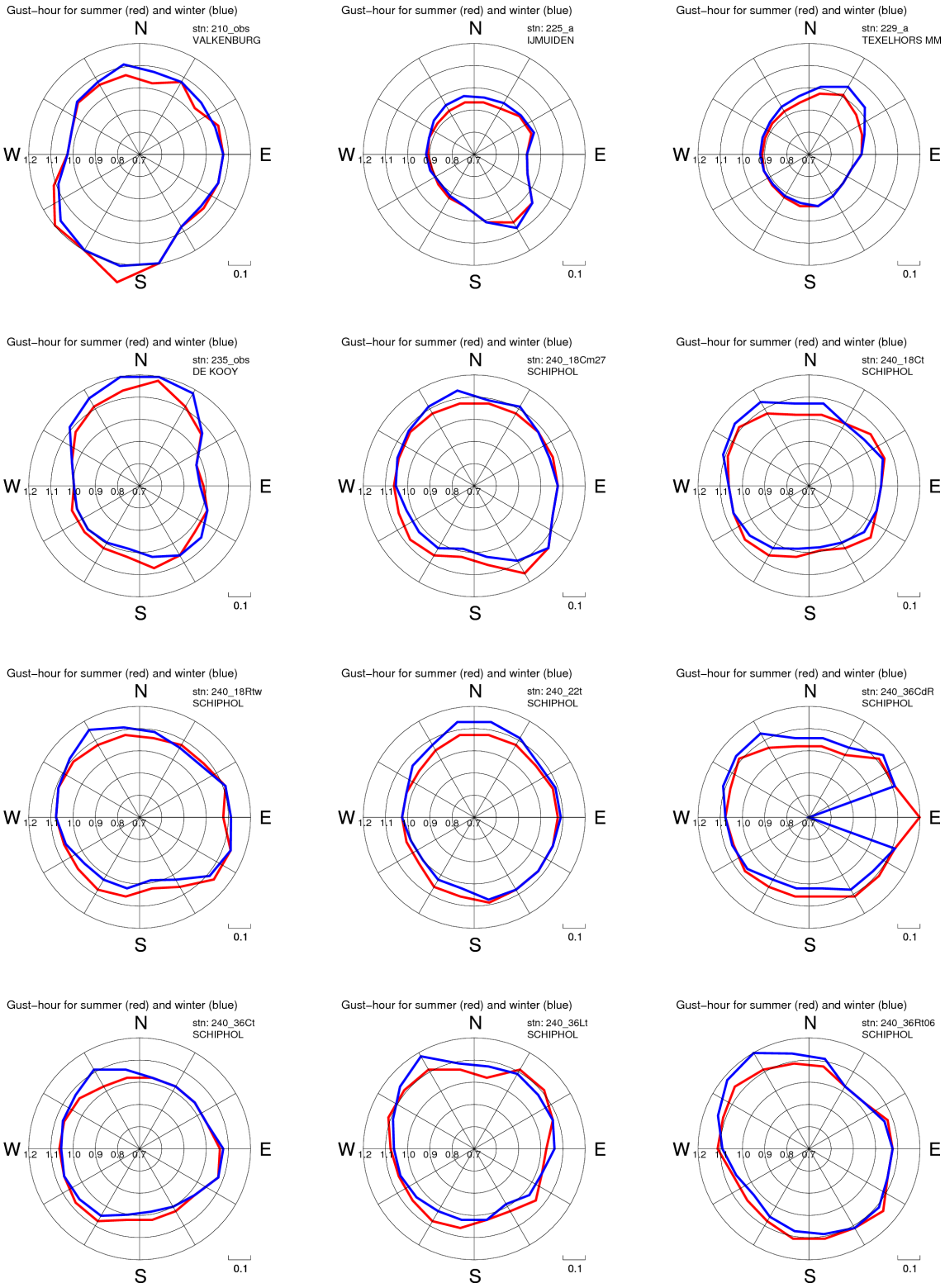


Figure B.2.1: *Rose plot of exposure correction factors for various stations, based on* 1 *hour gustiness analysis, separated into summer (red) and winter (blue). In case the sensor height deviates from* 10 *m, the exposure correction factors have been adjusted, assuming a logarithmic wind profile with a roughness length derived from omnidirectional* $\sigma_u$ *analysis (see Section 3.3.3).*

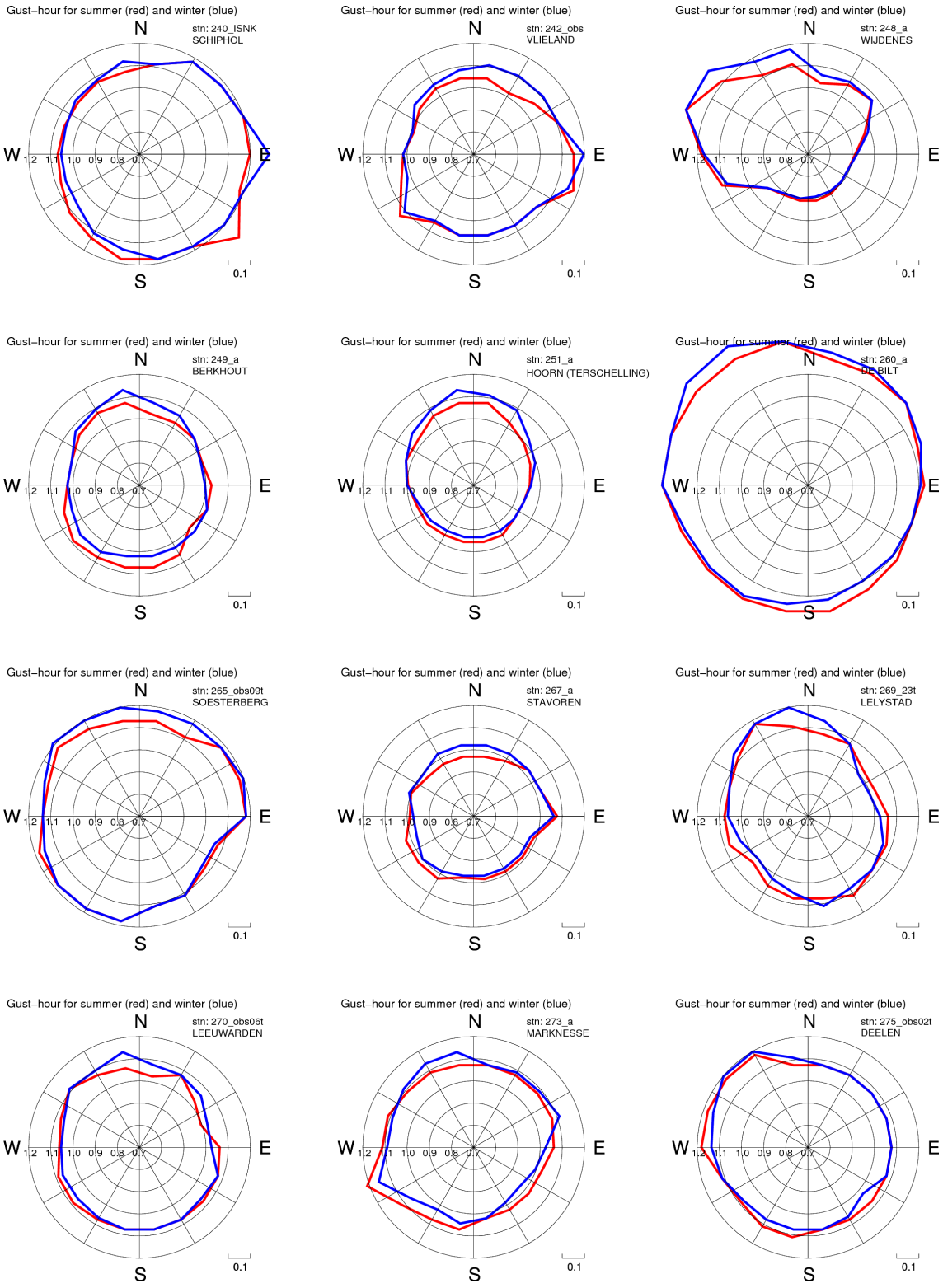


Figure B.2.2: *Rose plot of exposure correction factors for various stations, based on* 1 *hour gustiness analysis, separated into summer (red) and winter (blue). In case the sensor height deviates from* 10 *m, the exposure correction factors have been adjusted, assuming a logarithmic wind profile with a roughness length derived from omnidirectional* $\sigma_u$ *analysis (see Section 3.3.3). Lines connected to the centre of the plot indicate data shortage for calculating exposure correction factors (less than* 10 *measurements).*

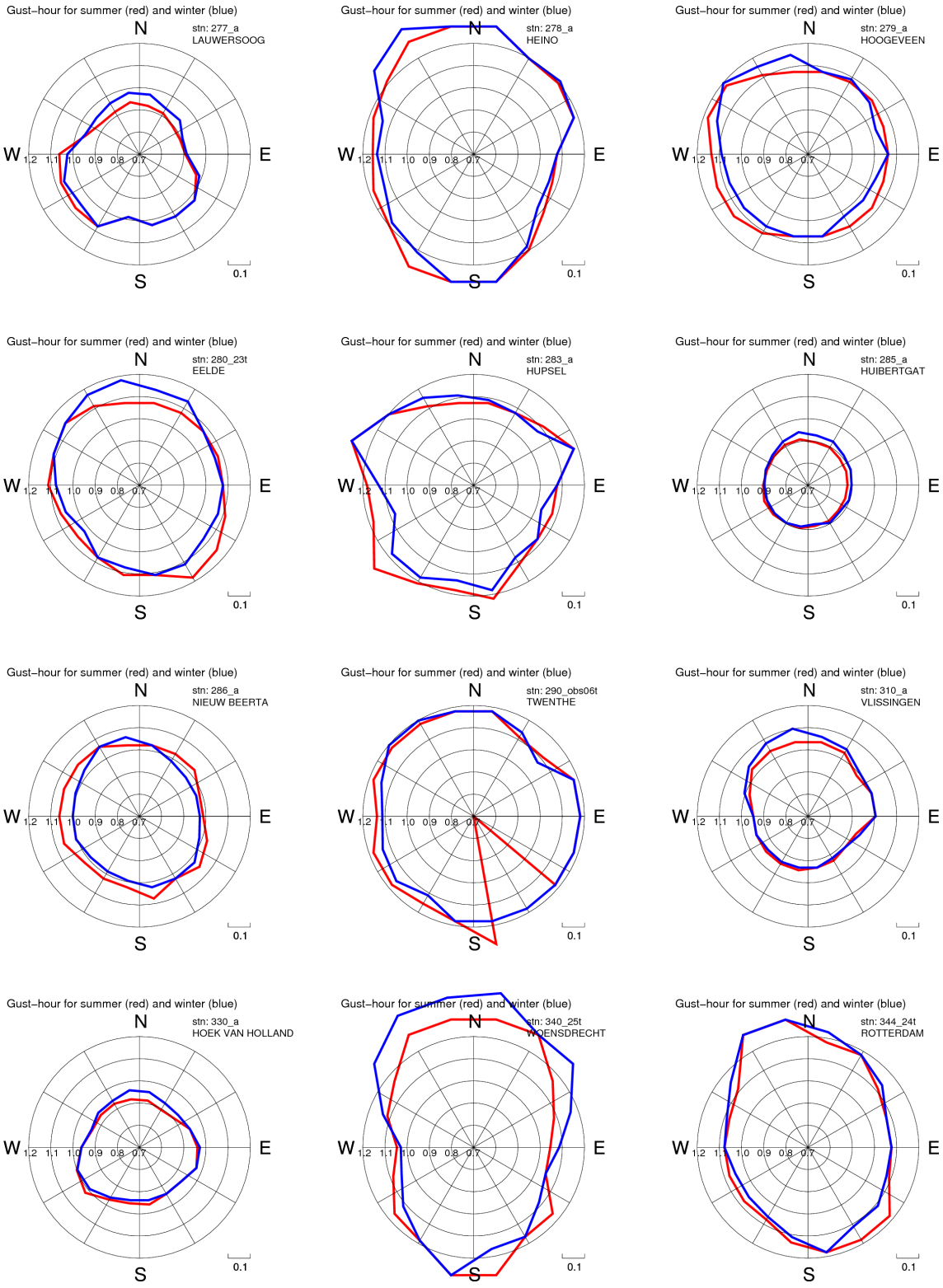


Figure B.2.3: *Rose plot of exposure correction factors for various stations, based on* 1 *hour gustiness analysis, separated into summer (red) and winter (blue). In case the sensor height deviates from* 10 *m, the exposure correction factors have been adjusted, assuming a logarithmic wind profile with a roughness length derived from omnidirectional* $\sigma_u$ *analysis (see Section 3.3.3). Lines connected to the centre of the plot indicate data shortage for calculating exposure correction factors (less than* 10 *measurements).*

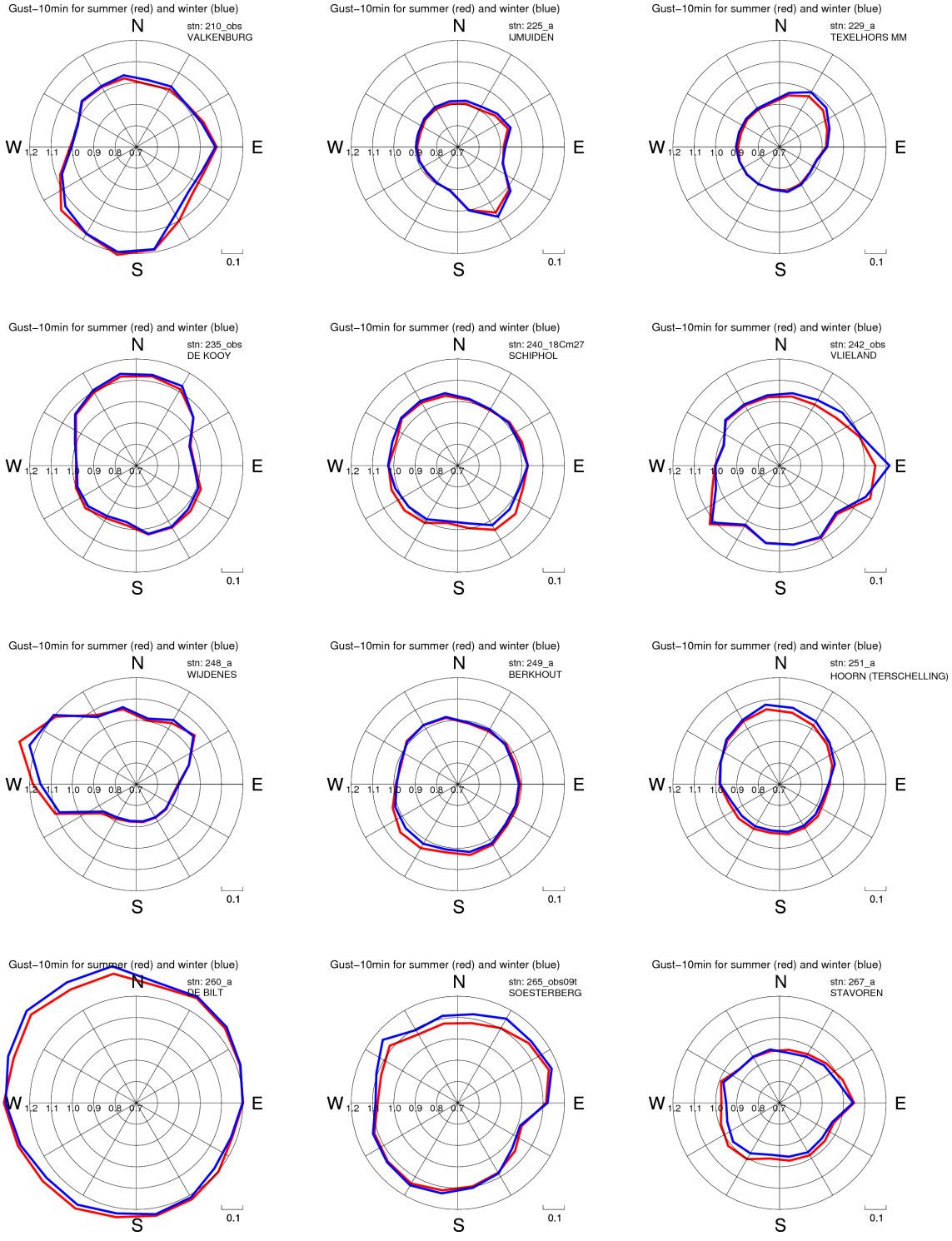


Figure B.2.4: *Rose plot of exposure correction factors for various stations, based on* 10 *minute gustiness analysis, separated into summer (red) and winter (blue). In case the sensor height deviates from* 10 *m, the exposure correction factors have been adjusted, assuming a logarithmic wind profile with a roughness length derived from omnidirectional* $\sigma_u$ *analysis (see Section 3.3.3).*

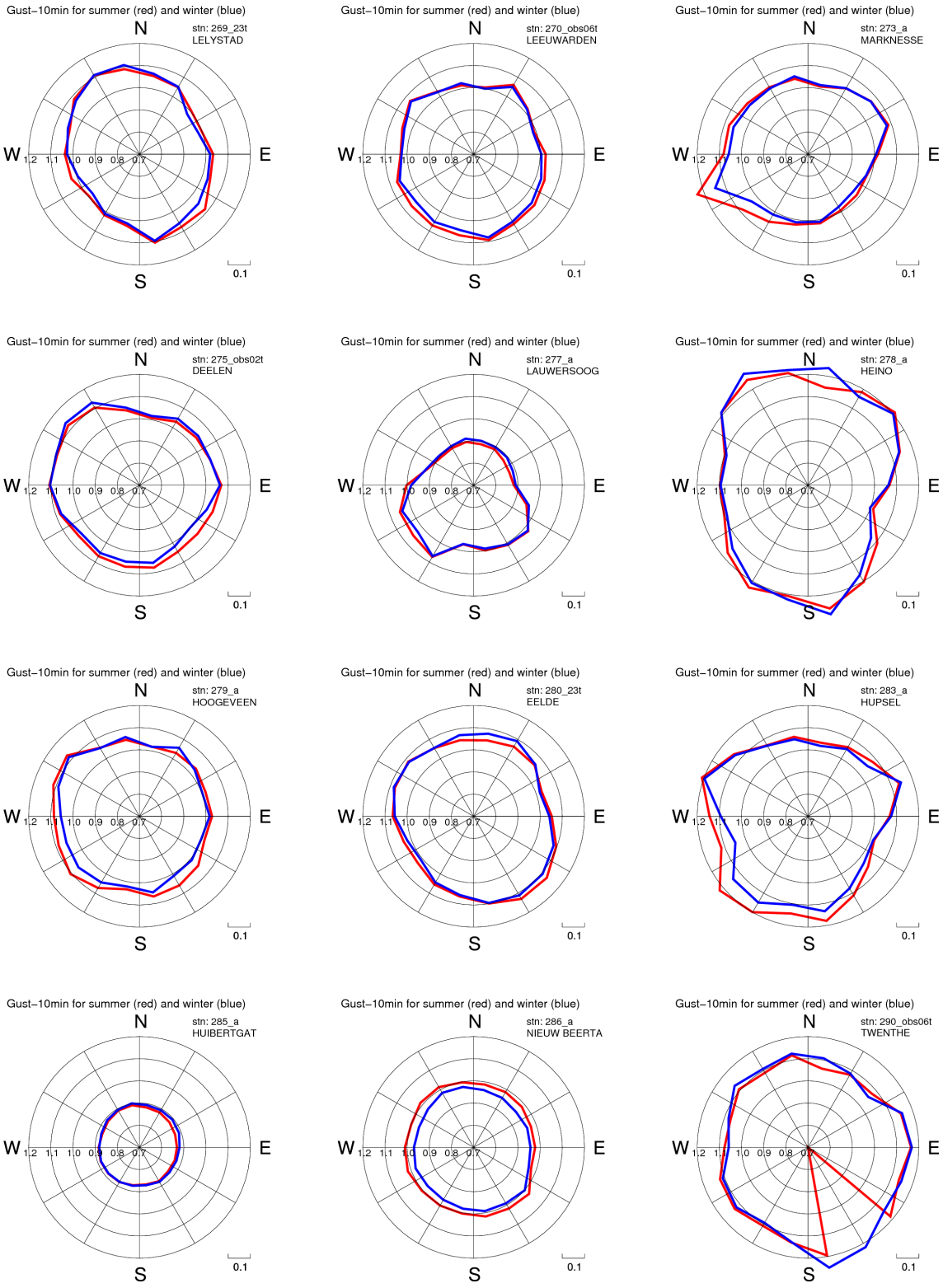


Figure B.2.5: *Rose plot of exposure correction factors for various stations, based on* 10 *minute gustiness analysis, separated into summer (red) and winter (blue). In case the sensor height deviates from* 10 *m, the exposure correction factors have been adjusted, assuming a logarithmic wind profile with a roughness length derived from omnidirectional* $\sigma_u$ *analysis (see Section 3.3.3). Lines connected to the centre of the plot indicate data shortage for calculating exposure correction factors (less than* 10 *measurements).*

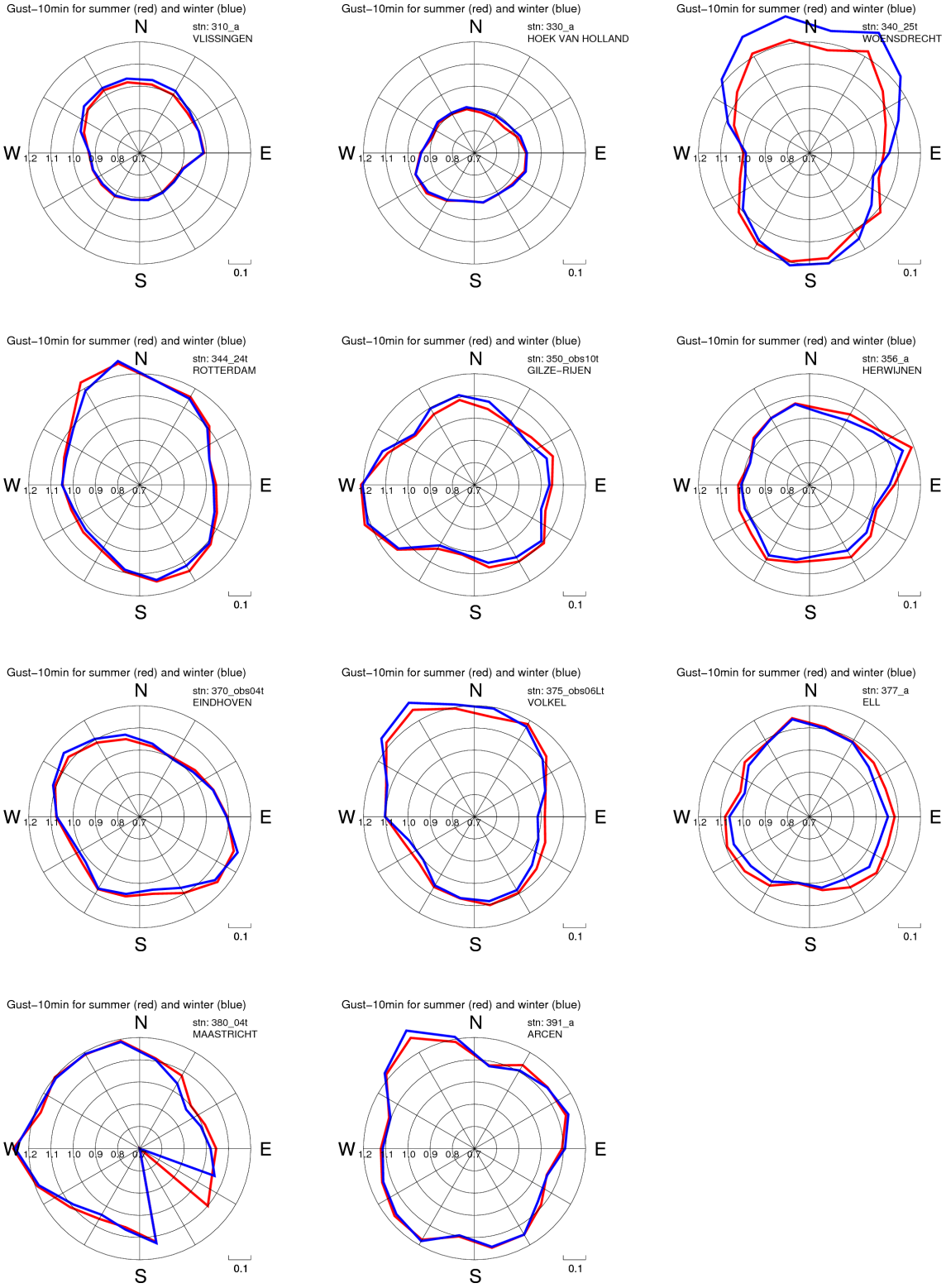


Figure B.2.6: *Rose plot of exposure correction factors for various stations, based on* 10 *minute gustiness analysis, separated into summer (red) and winter (blue). In case the sensor height deviates from* 10 *m, the exposure correction factors have been adjusted, assuming a logarithmic wind profile with a roughness length derived from omnidirectional* $\sigma_u$ *analysis (see Section 3.3.3). Lines connected to the centre of the plot indicate data shortage for calculating exposure correction factors (less than* 10 *measurements).*

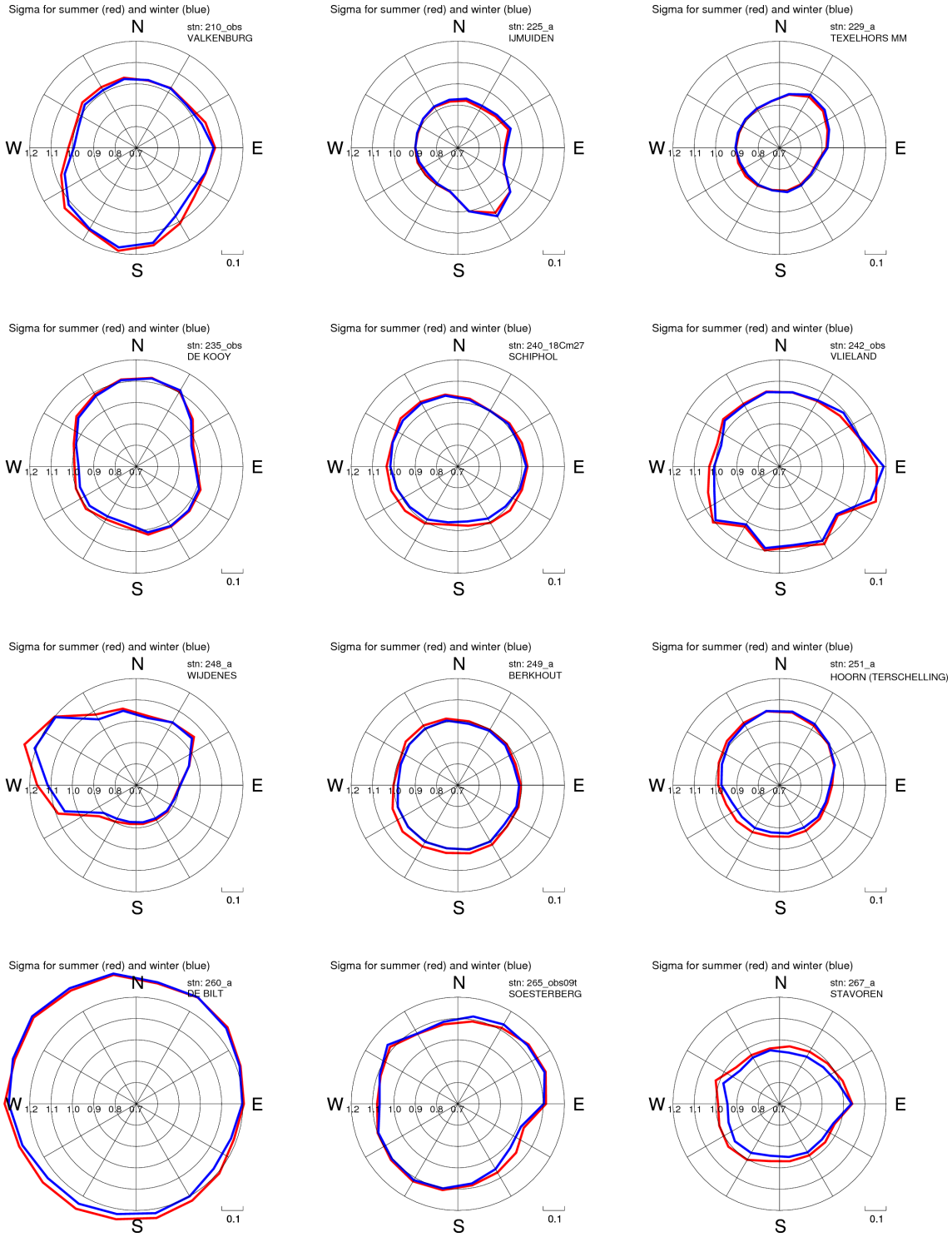


Figure B.2.7: *Rose plot of exposure correction factors for various stations, based on $\sigma_u$ analysis, separated into summer (red) and winter (blue). In case the sensor height deviates from 10 m, the exposure correction factors have been adjusted, assuming a logarithmic wind profile with a roughness length derived from omnidirectional $\sigma_u$ analysis (see Section 3.3.3).*

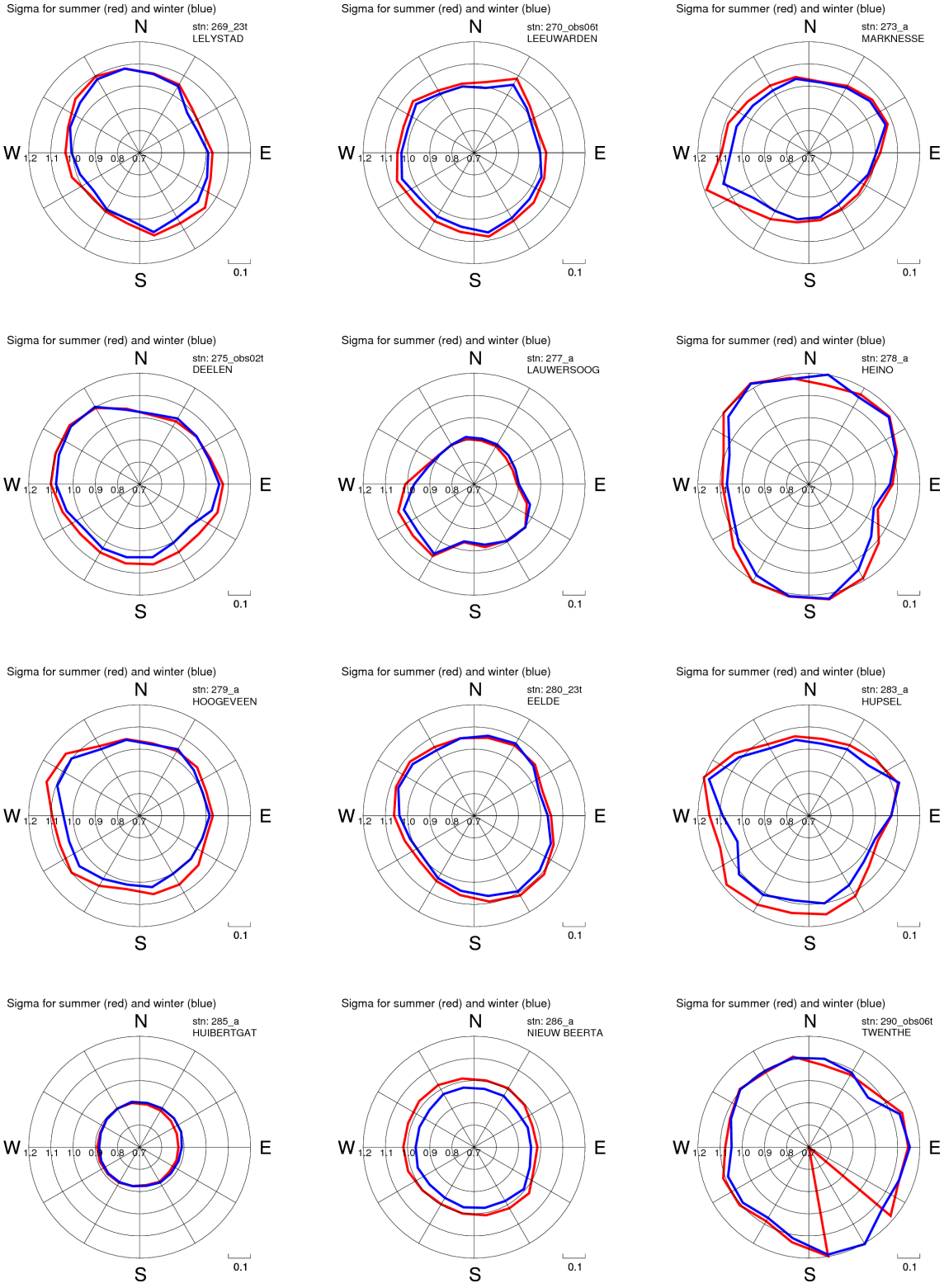


Figure B.2.8: *Rose plot of exposure correction factors for various stations, based on $\sigma_u$ analysis, separated into summer (red) and winter (blue). In case the sensor height deviates from 10 m, the exposure correction factors have been adjusted, assuming a logarithmic wind profile with a roughness length derived from omnidirectional $\sigma_u$ analysis (see Section 3.3.3). Lines connected to the centre of the plot indicate data shortage for calculating exposure correction factors (less than 10 measurements).*

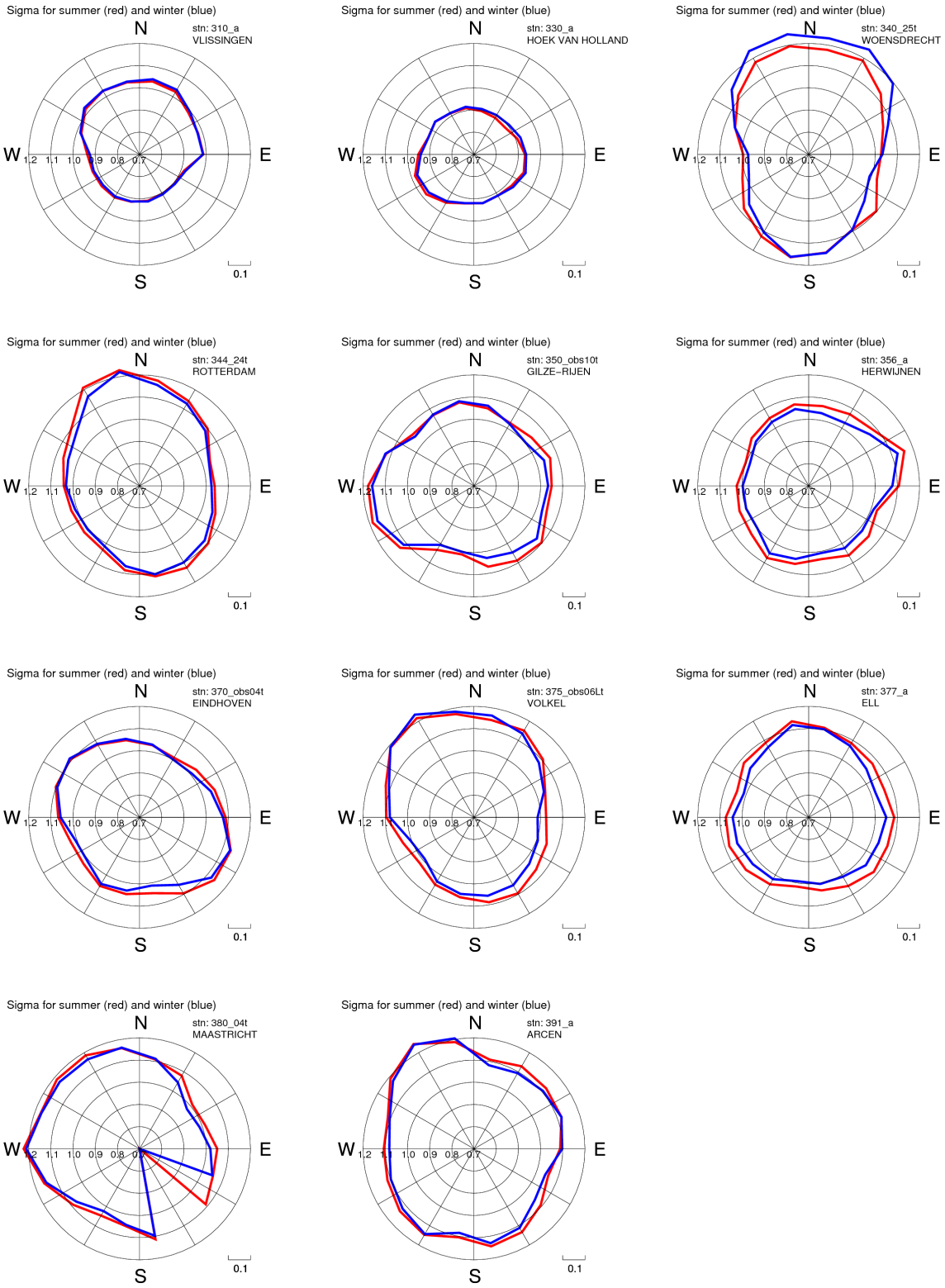


Figure B.2.9: *Rose plot of exposure correction factors for various stations, based on $\sigma_u$ analysis, separated into summer (red) and winter (blue). In case the sensor height deviates from* 10 *m, the exposure correction factors have been adjusted, assuming a logarithmic wind profile with a roughness length derived from omnidirectional $\sigma_u$ analysis (see Section 3.3.3). Lines connected to the centre of the plot indicate data shortage for calculating exposure correction factors (less than* 10 *measurements).*

## B.3 Plots derived from land use maps

Figures B.3.1, B.3.2 and B.3.3 show rose plots of exposure correction factors for various stations based on land use maps (*LGN*). Note that these figures do not show the spatial distribution of local roughness over the Netherlands (as does for instance Figure 4.4 in *Wieringa and Rijkoort* (1983)), but just the spatial distribution of local roughness at the measurement sites. Data replotted from HYDRA. For description, see *Verkaik* (2003).

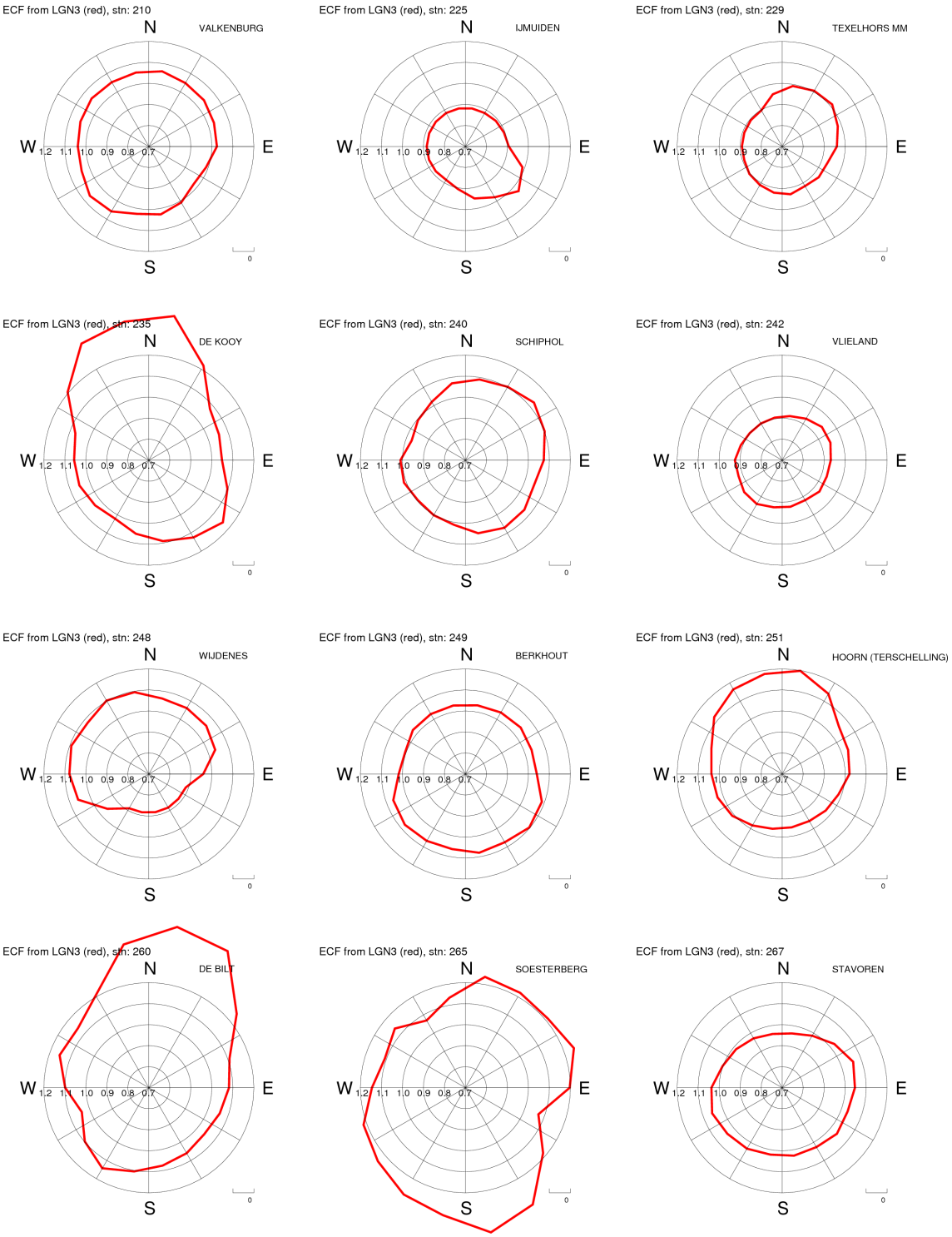


Figure B.3.1: *Rose plot of exposure correction factors for various stations, based on land use maps (LGN).*

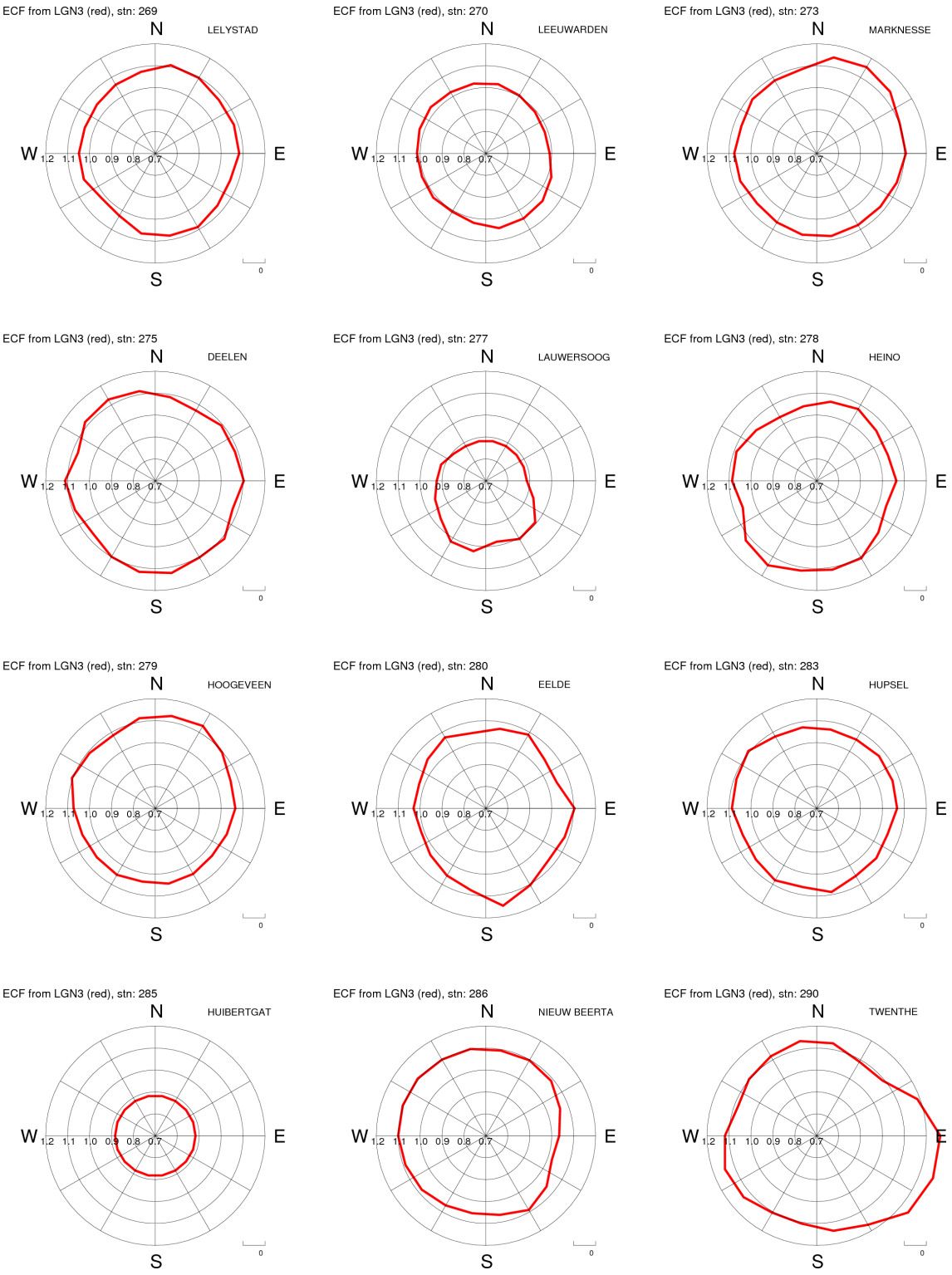


Figure B.3.2: *Rose plot of exposure correction factors for various stations, based on land use maps (LGN).*

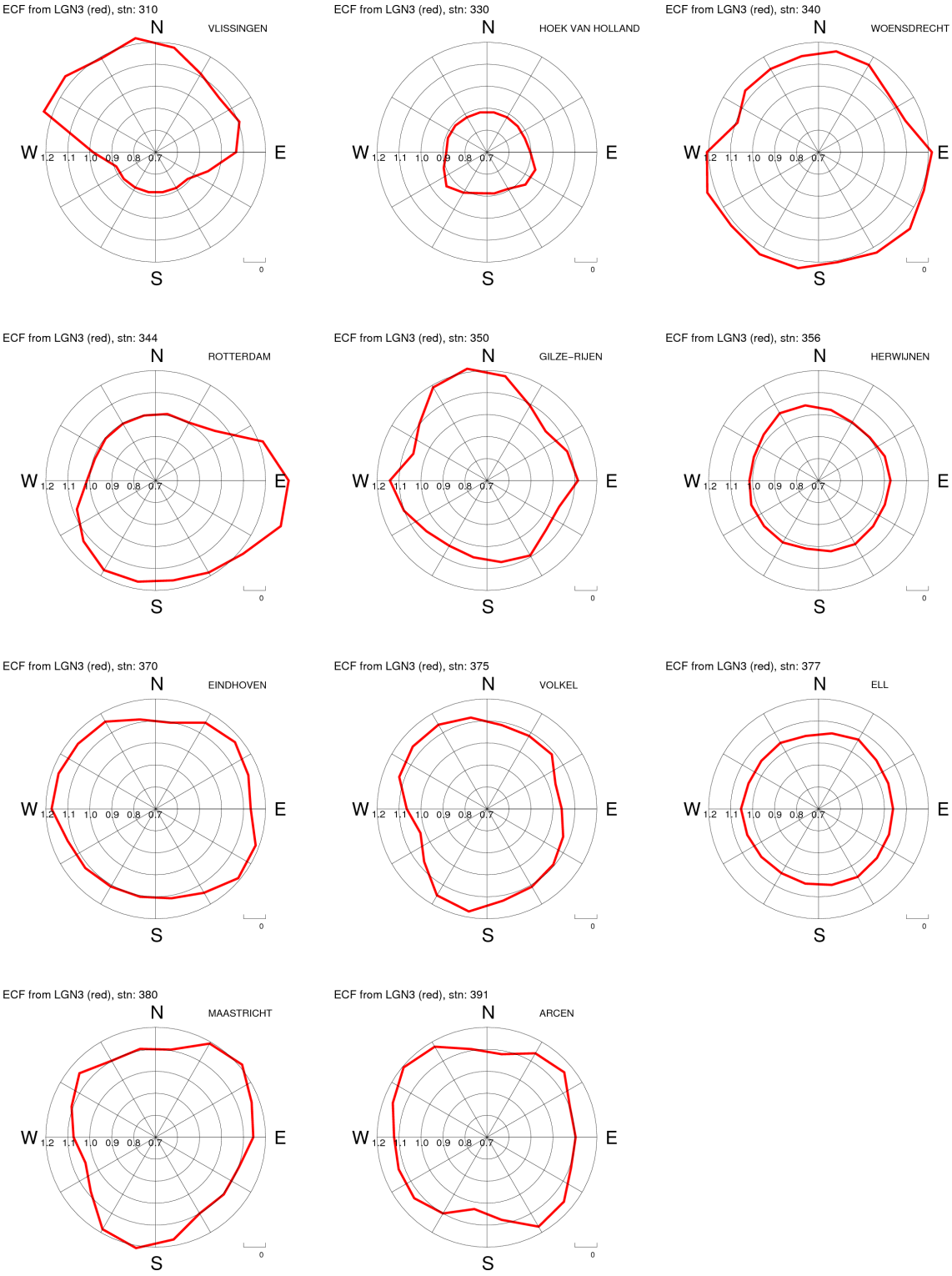


Figure B.3.3: *Rose plot of exposure correction factors for various stations, based on land use maps (LGN).*

# Appendix C

# Directional exposure correction factors

## C.1 Land use maps

Figures C.1.1, C.1.2, C.1.3, C.1.4 and C.1.5 show the spatial distribution exposure correction factors per wind direction sector. Exposure correction factors are calculated based on land use maps.

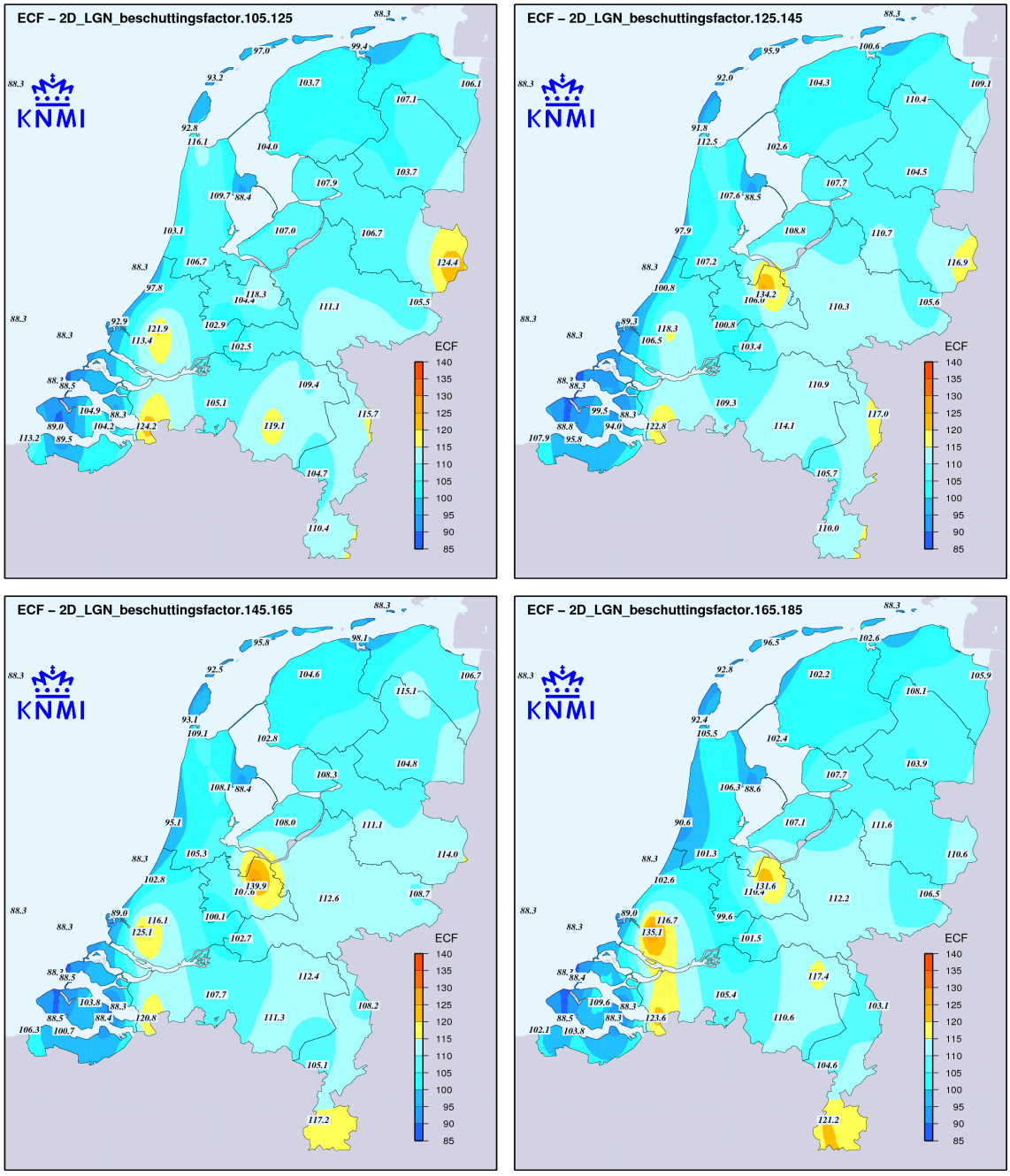


Figure C.1.1: *Directional exposure correction factors, based on land use maps. The wind direction sectors are denoted at the top line of each figure.*

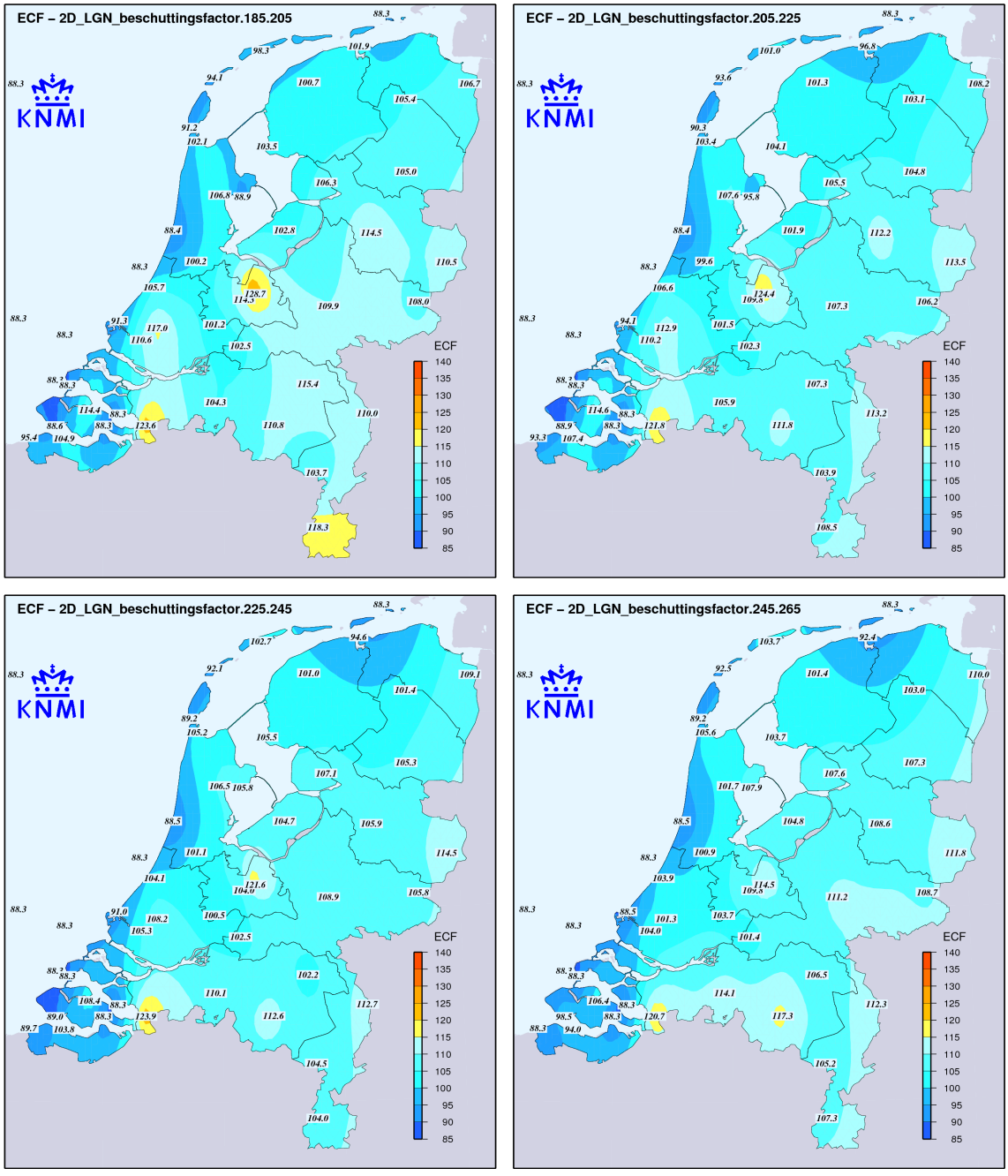


Figure C.1.2: *Directional exposure correction factors, based on land use maps. The wind direction sectors are denoted at the top line of each figure.*

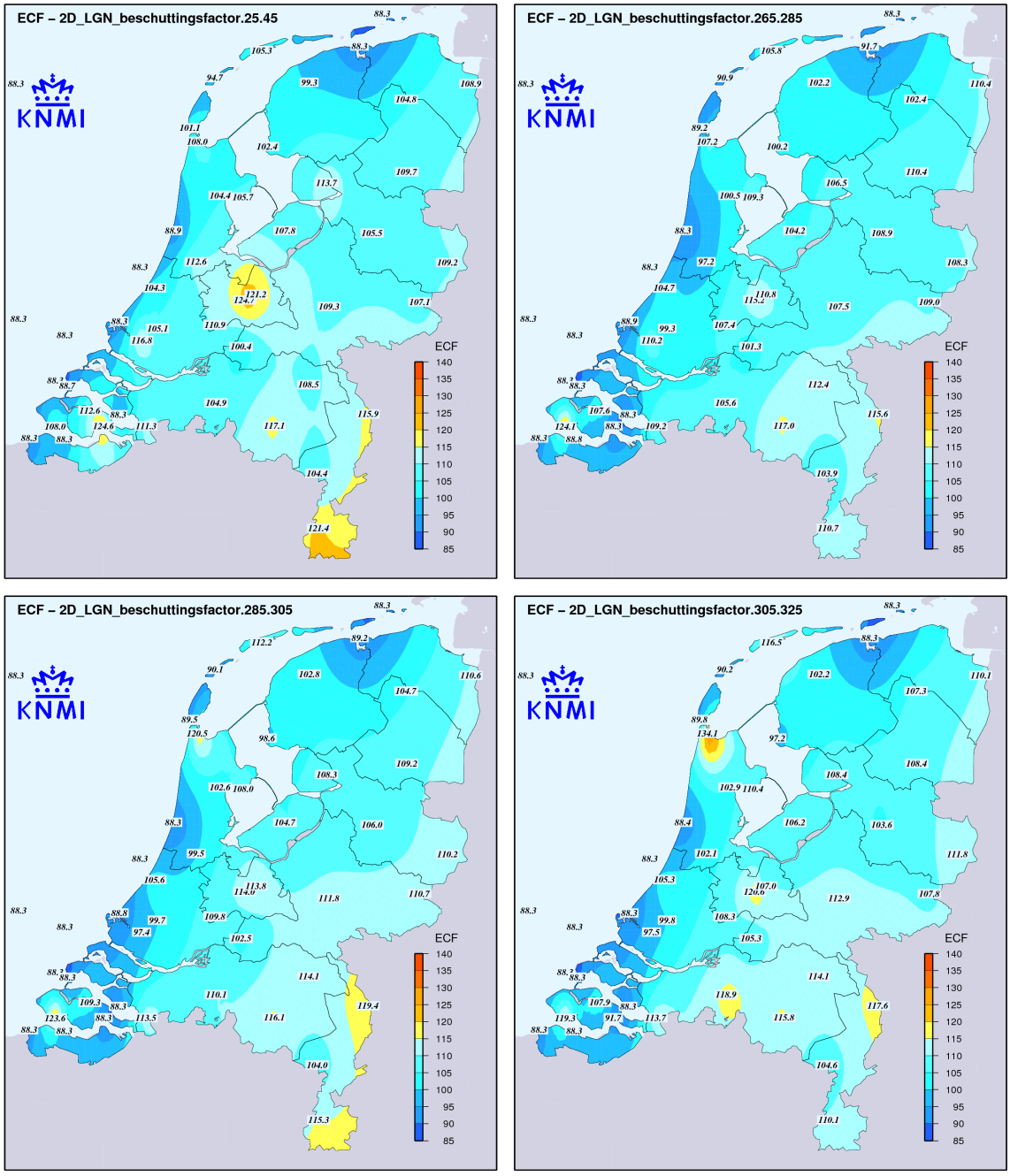


Figure C.1.3: *Directional exposure correction factors, based on land use maps. The wind direction sectors are denoted at the top line of each figure.*

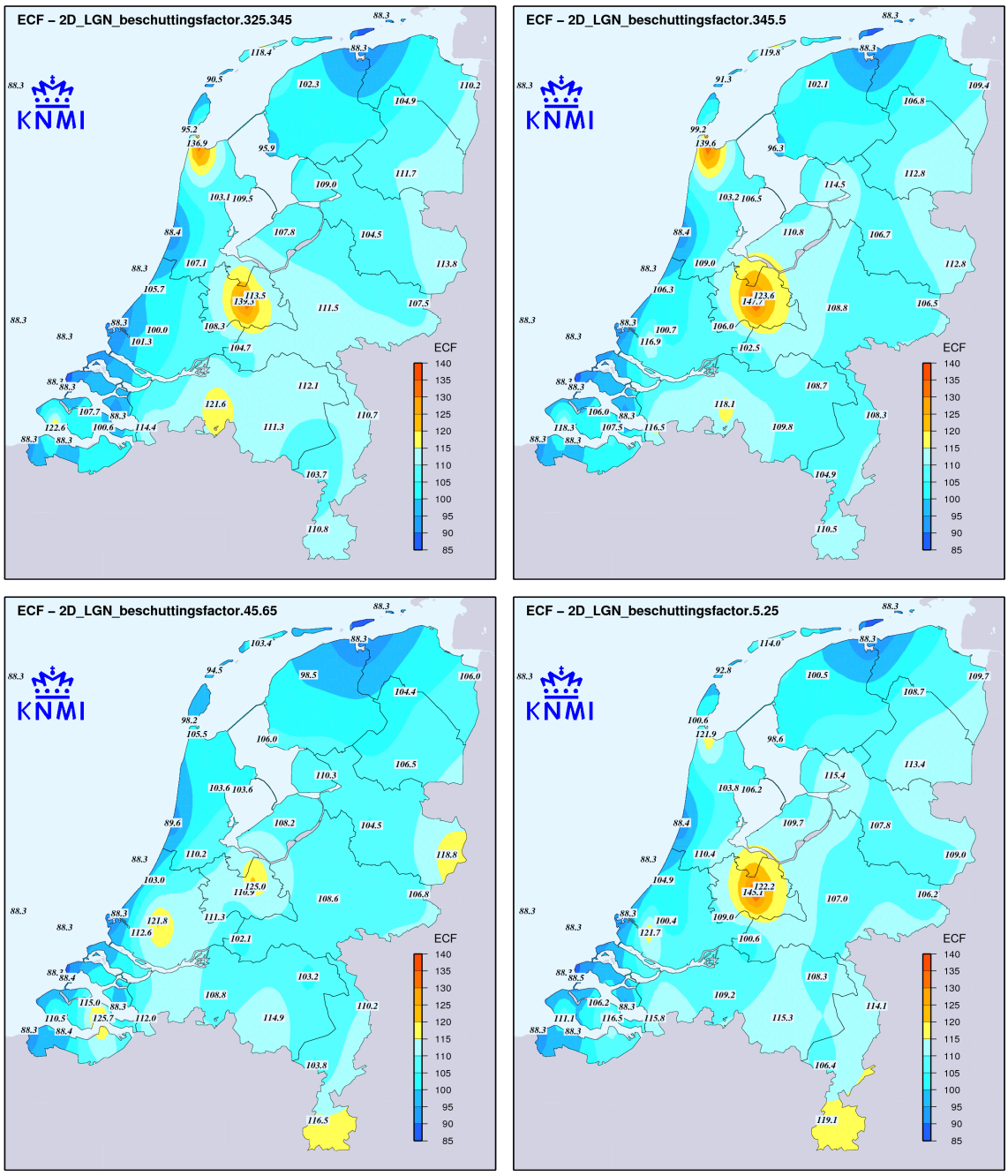


Figure C.1.4: *Directional exposure correction factors, based on land use maps. The wind direction sectors are denoted at the top line of each figure.*

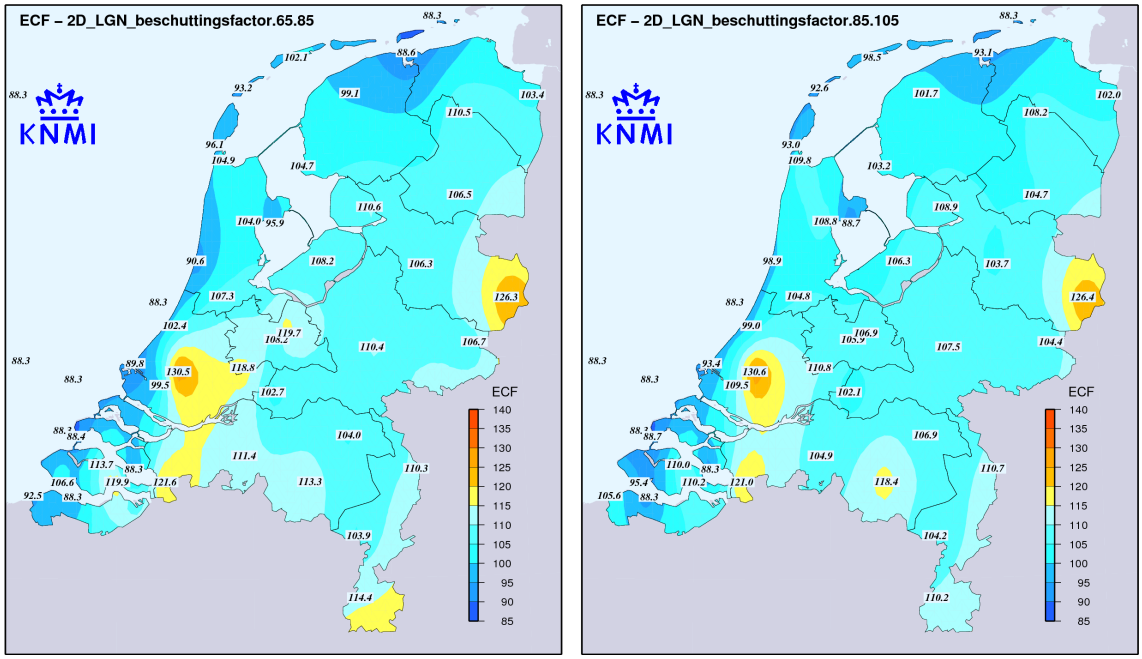


Figure C.1.5: *Directional exposure correction factors, based on land use maps. The wind direction sectors are denoted at the top line of each figure.*

## C.2 1 hour gustiness analysis

Figures C.2.1, C.2.2, C.2.3, C.2.4 and C.2.5 show the spatial distribution exposure correction factors per wind direction sector. Exposure correction factors are calculated based on 1 hour gustiness analysis.

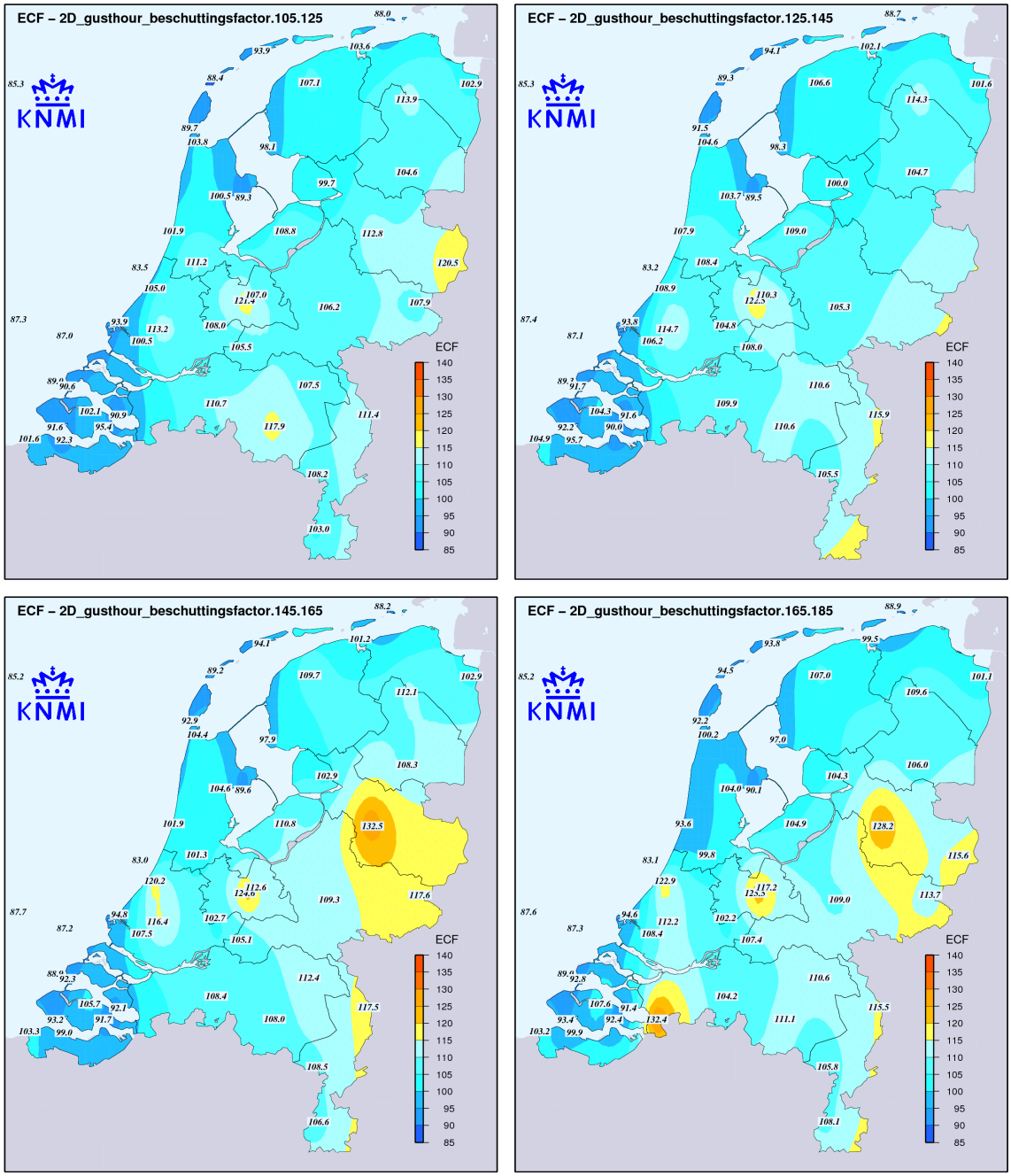


Figure C.2.1: *Directional exposure correction factors, based on* 1 *hour gustiness analysis. The wind direction sectors are denoted at the top line of each figure. In case the sensor height deviates from* 10 *m, the exposure correction factors have been adjusted, assuming a logarithmic wind profile with a roughness length derived from omnidirectional* $\sigma_u$ *analysis (see Section 3.3.3).*

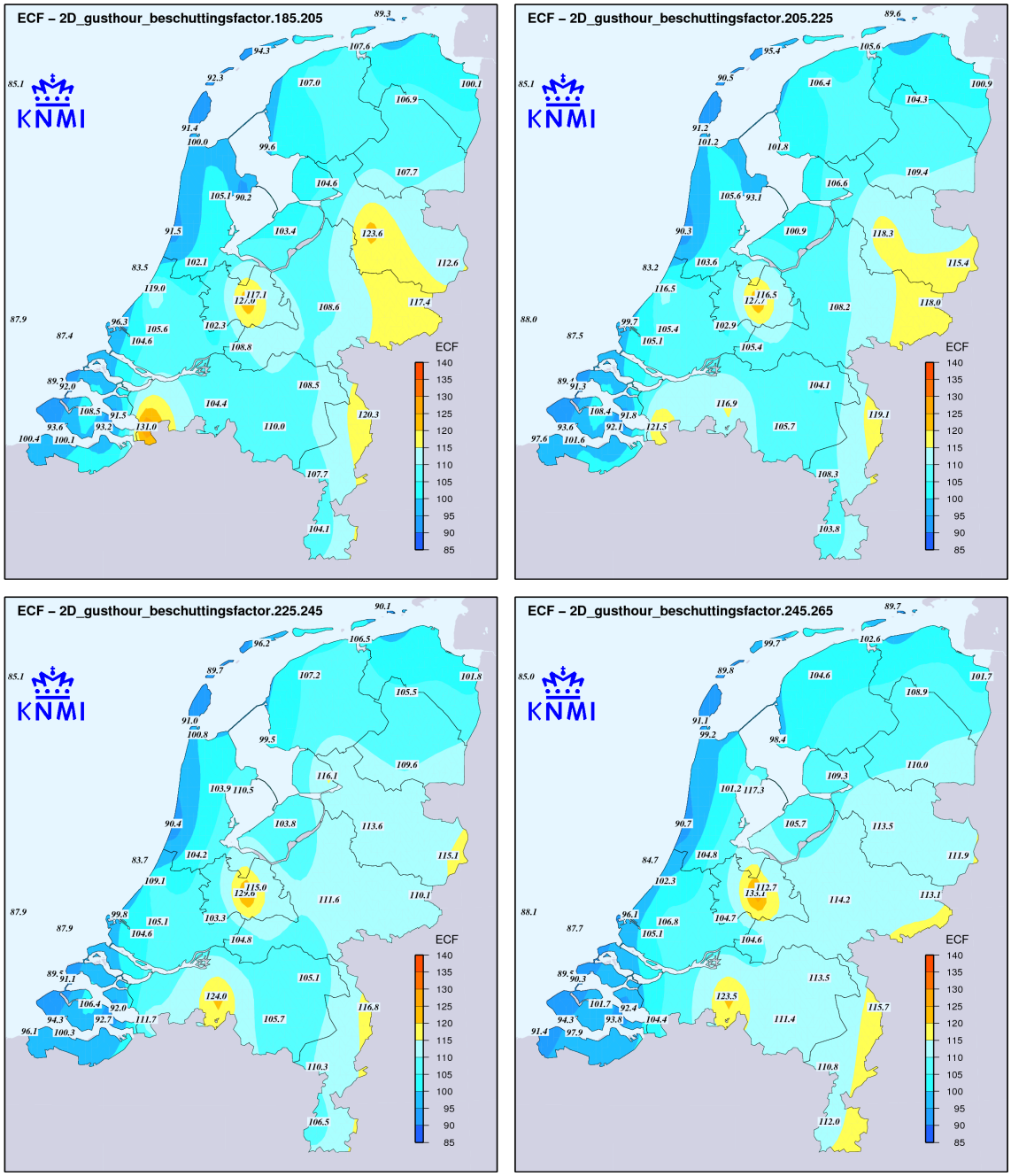


Figure C.2.2: *Directional exposure correction factors, based on* 1 *hour gustiness analysis. The wind direction sectors are denoted at the top line of each figure. In case the sensor height deviates from* 10 *m, the exposure correction factors have been adjusted, assuming a logarithmic wind profile with a roughness length derived from omnidirectional* $\sigma_u$ *analysis (see Section 3.3.3).*

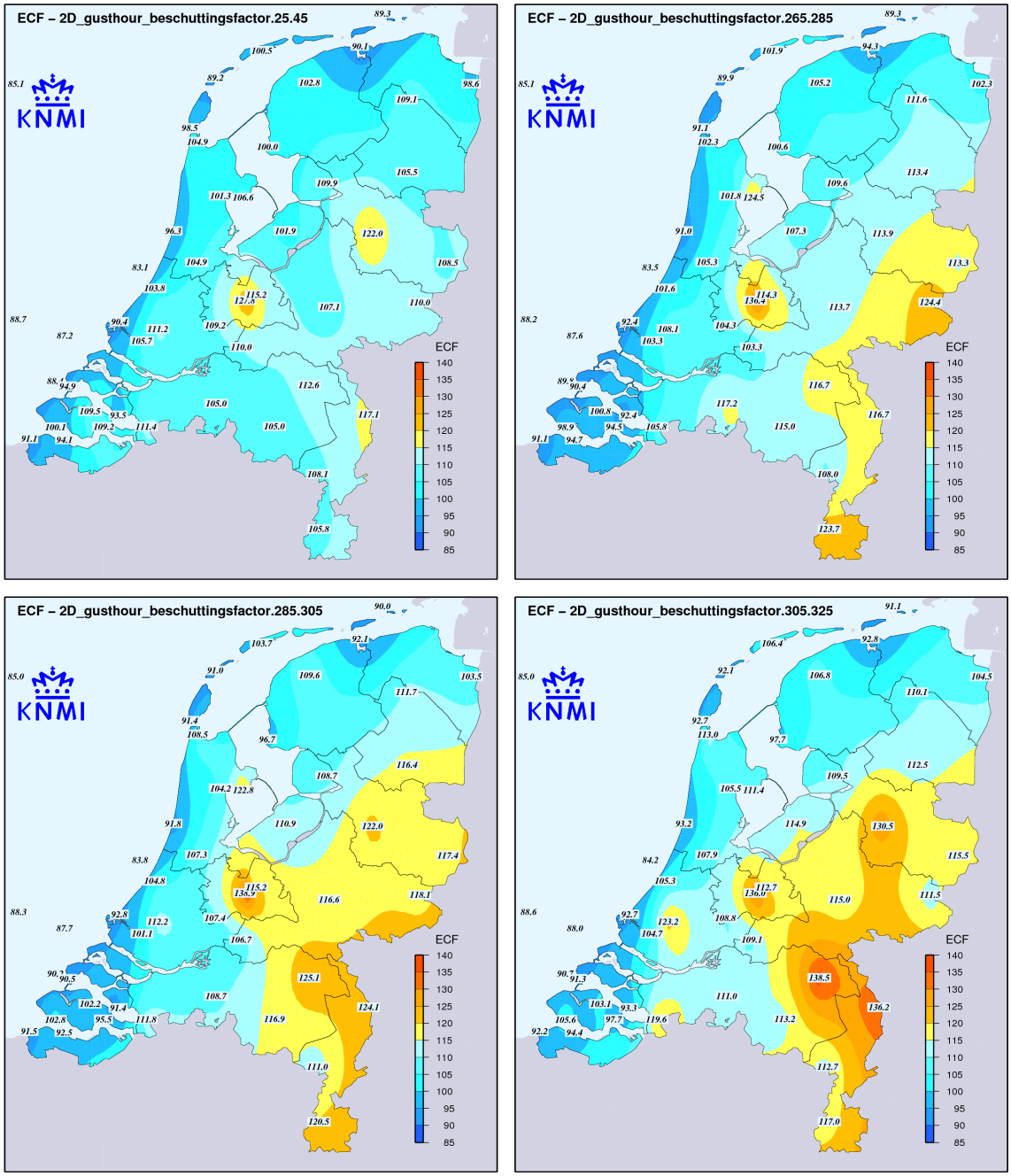


Figure C.2.3: *Directional exposure correction factors, based on* 1 *hour gustiness analysis. The wind direction sectors are denoted at the top line of each figure. In case the sensor height deviates from* 10 *m, the exposure correction factors have been adjusted, assuming a logarithmic wind profile with a roughness length derived from omnidirectional* $\sigma_u$ *analysis (see Section 3.3.3).*

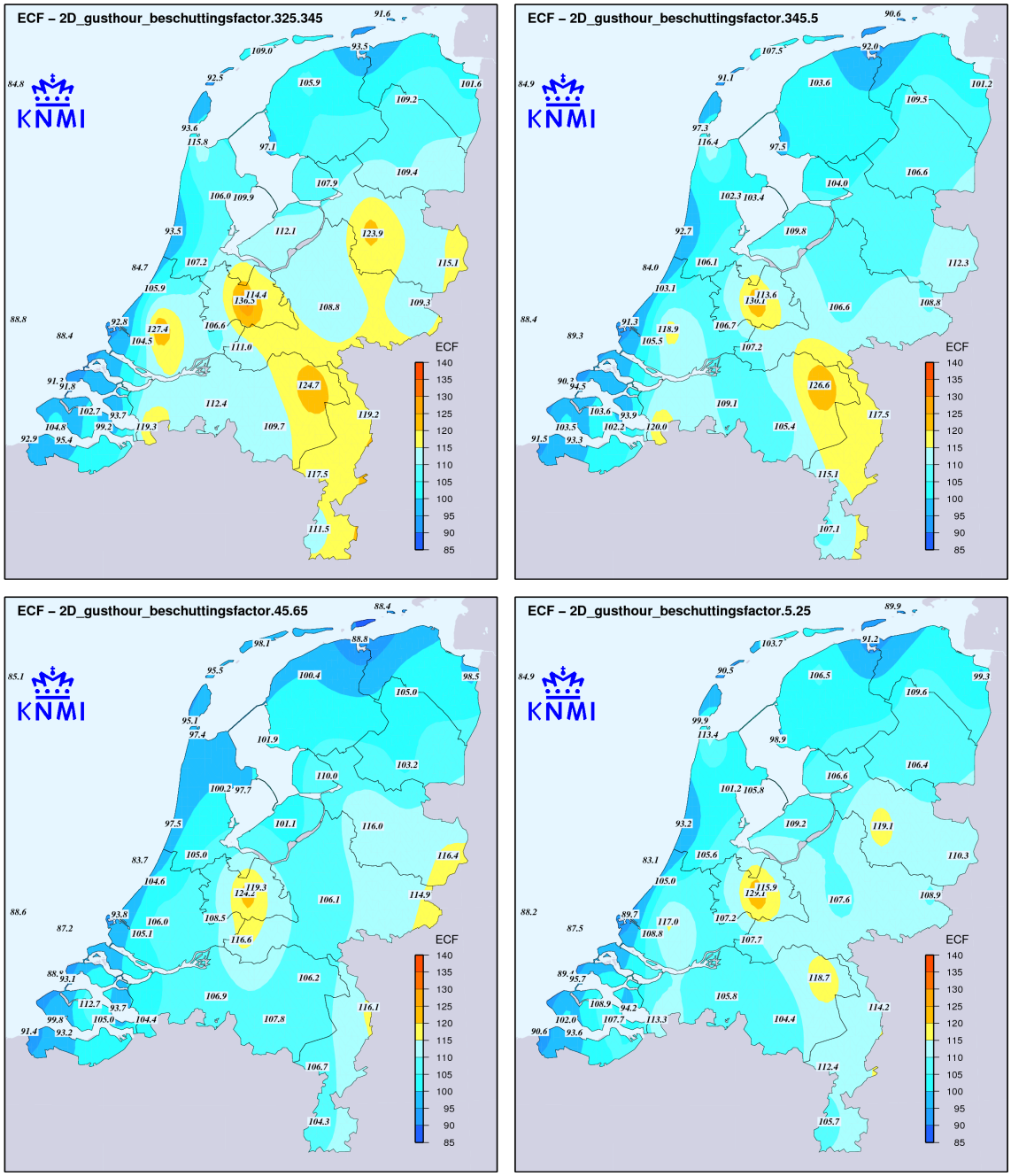


Figure C.2.4: *Directional exposure correction factors, based on* 1 *hour gustiness analysis. The wind direction sectors are denoted at the top line of each figure. In case the sensor height deviates from* 10 *m, the exposure correction factors have been adjusted, assuming a logarithmic wind profile with a roughness length derived from omnidirectional* $\sigma_u$ *analysis (see Section 3.3.3).*

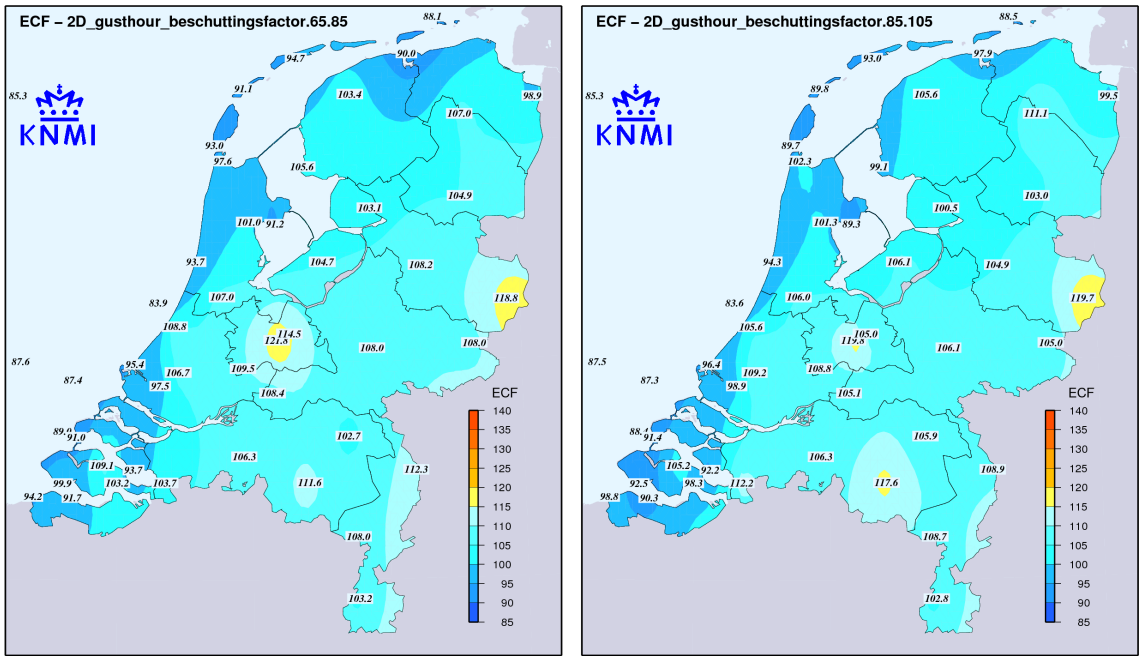


Figure C.2.5: *Directional exposure correction factors, based on* 1 *hour gustiness analysis. The wind direction sectors are denoted at the top line of each figure. In case the sensor height deviates from* 10 *m, the exposure correction factors have been adjusted, assuming a logarithmic wind profile with a roughness length derived from omnidirectional* $\sigma_u$ *analysis (see Section 3.3.3).*

## C.3 $\sigma_u$ analysis

Figures C.3.1, C.3.2, C.3.3, C.3.4 and C.3.5 show the spatial distribution exposure correction factors per wind direction sector. Exposure correction factors are calculated based on $\sigma_u$ analysis.

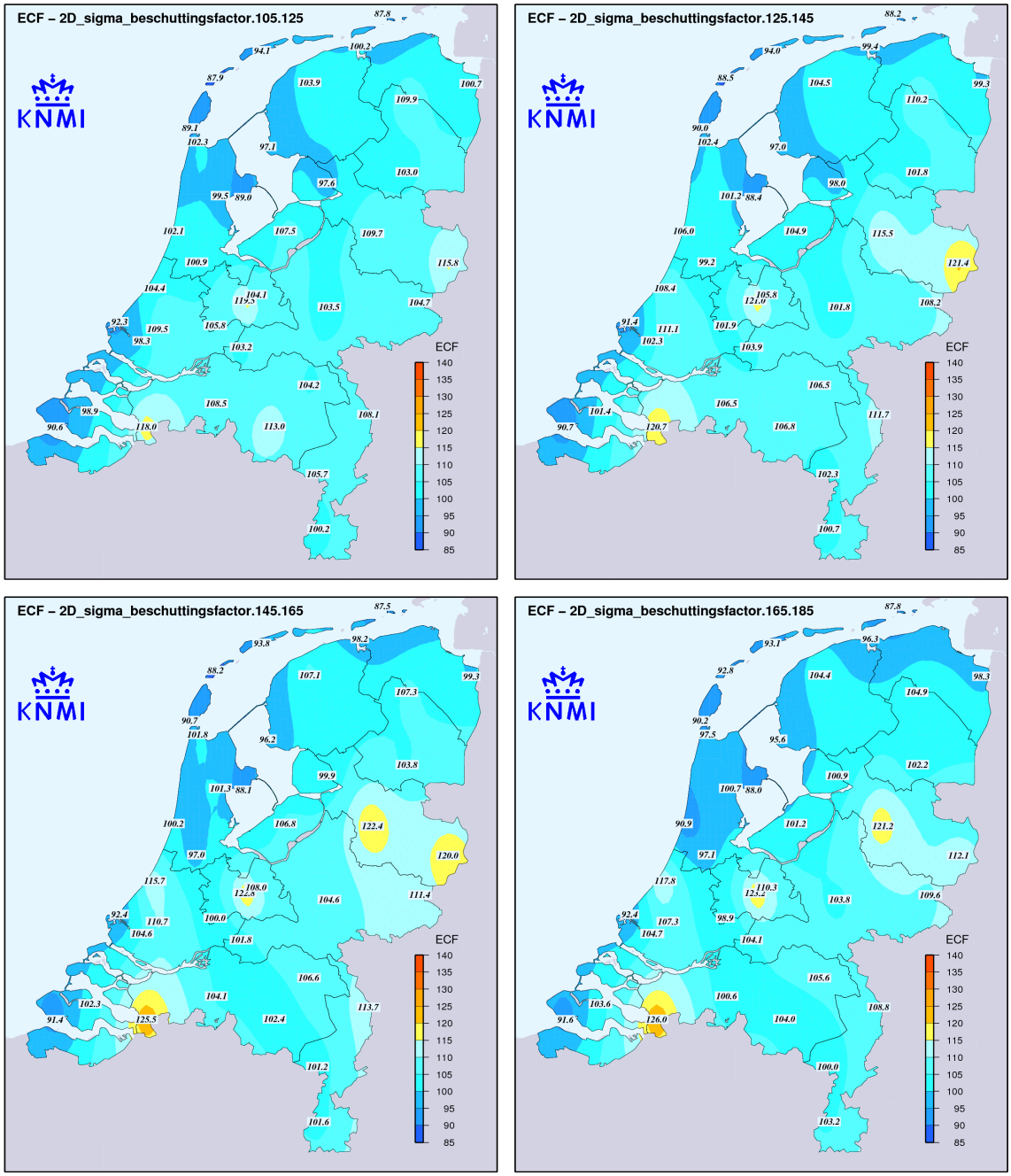


Figure C.3.1: *Directional exposure correction factors, based on $\sigma_u$ analysis. The wind direction sectors are denoted at the top line of each figure. In case the sensor height deviates from 10 m, the exposure correction factors have been adjusted, assuming a logarithmic wind profile with a roughness length derived from omnidirectional $\sigma_u$ analysis (see Section 3.3.3).*

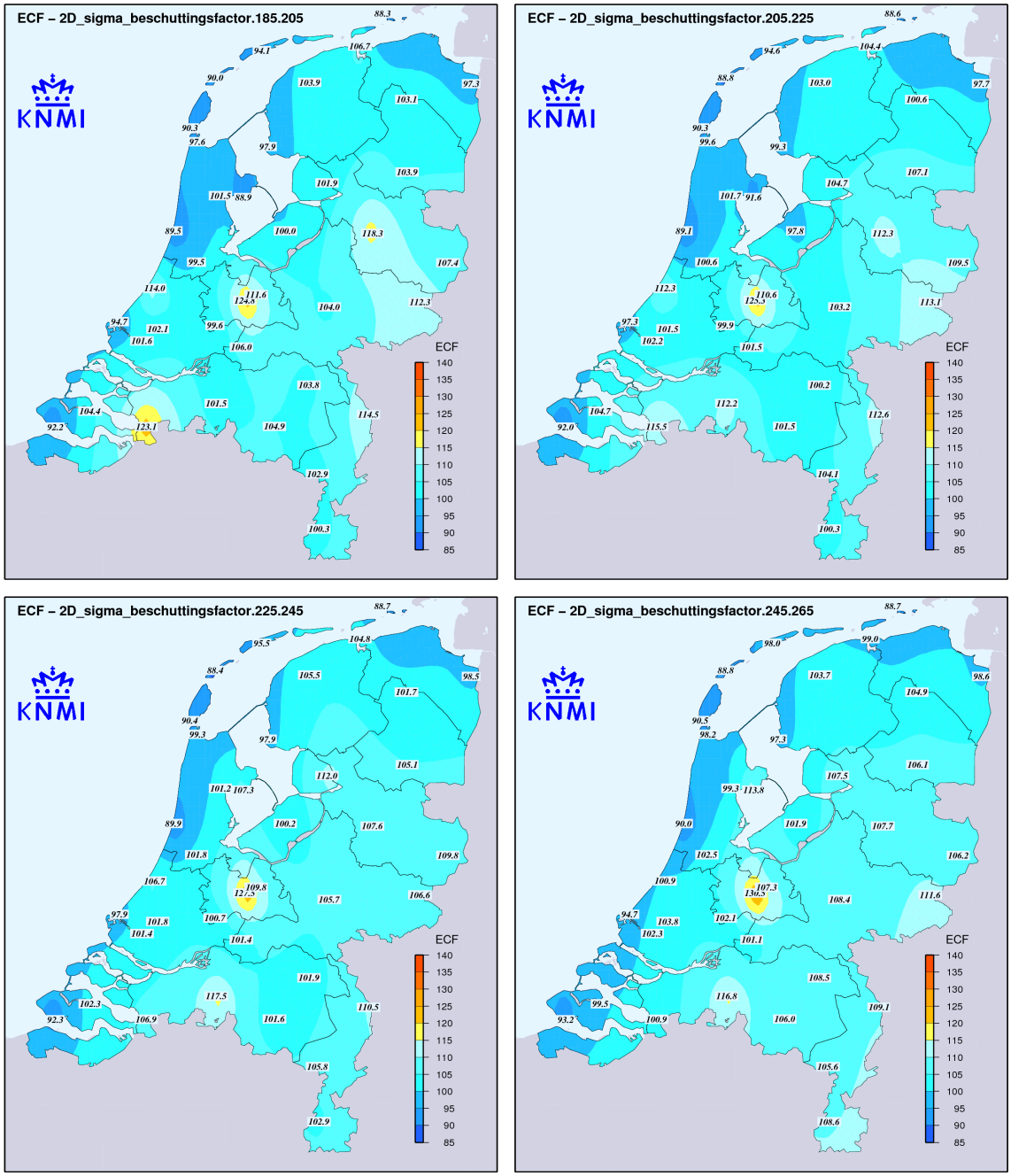


Figure C.3.2: *Directional exposure correction factors, based on $\sigma_u$ analysis. The wind direction sectors are denoted at the top line of each figure. In case the sensor height deviates from 10 m, the exposure correction factors have been adjusted, assuming a logarithmic wind profile with a roughness length derived from omnidirectional $\sigma_u$ analysis (see Section 3.3.3).*

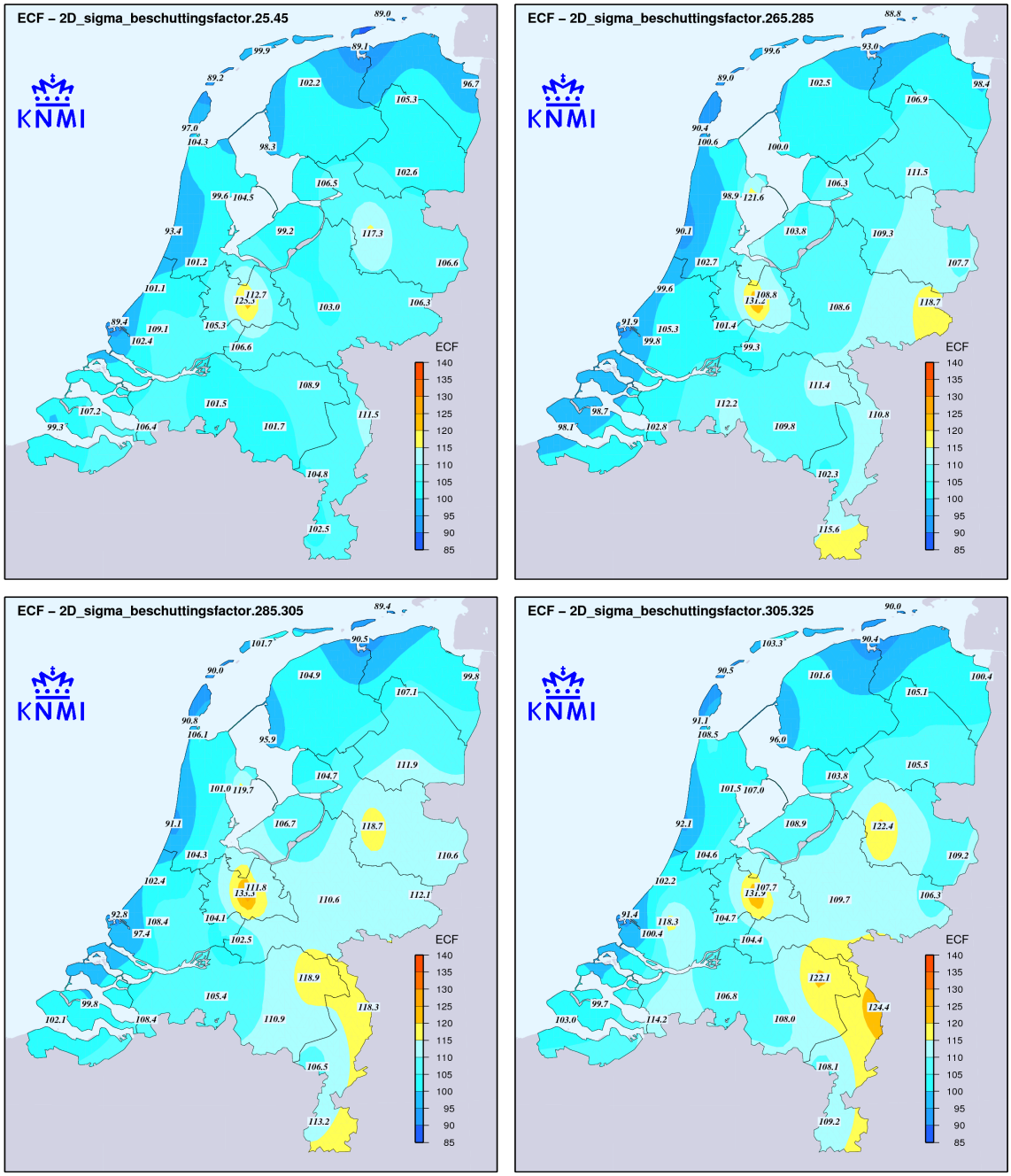


Figure C.3.3: *Directional exposure correction factors, based on $\sigma_u$ analysis. The wind direction sectors are denoted at the top line of each figure. In case the sensor height deviates from 10 m, the exposure correction factors have been adjusted, assuming a logarithmic wind profile with a roughness length derived from omnidirectional $\sigma_u$ analysis (see Section 3.3.3).*

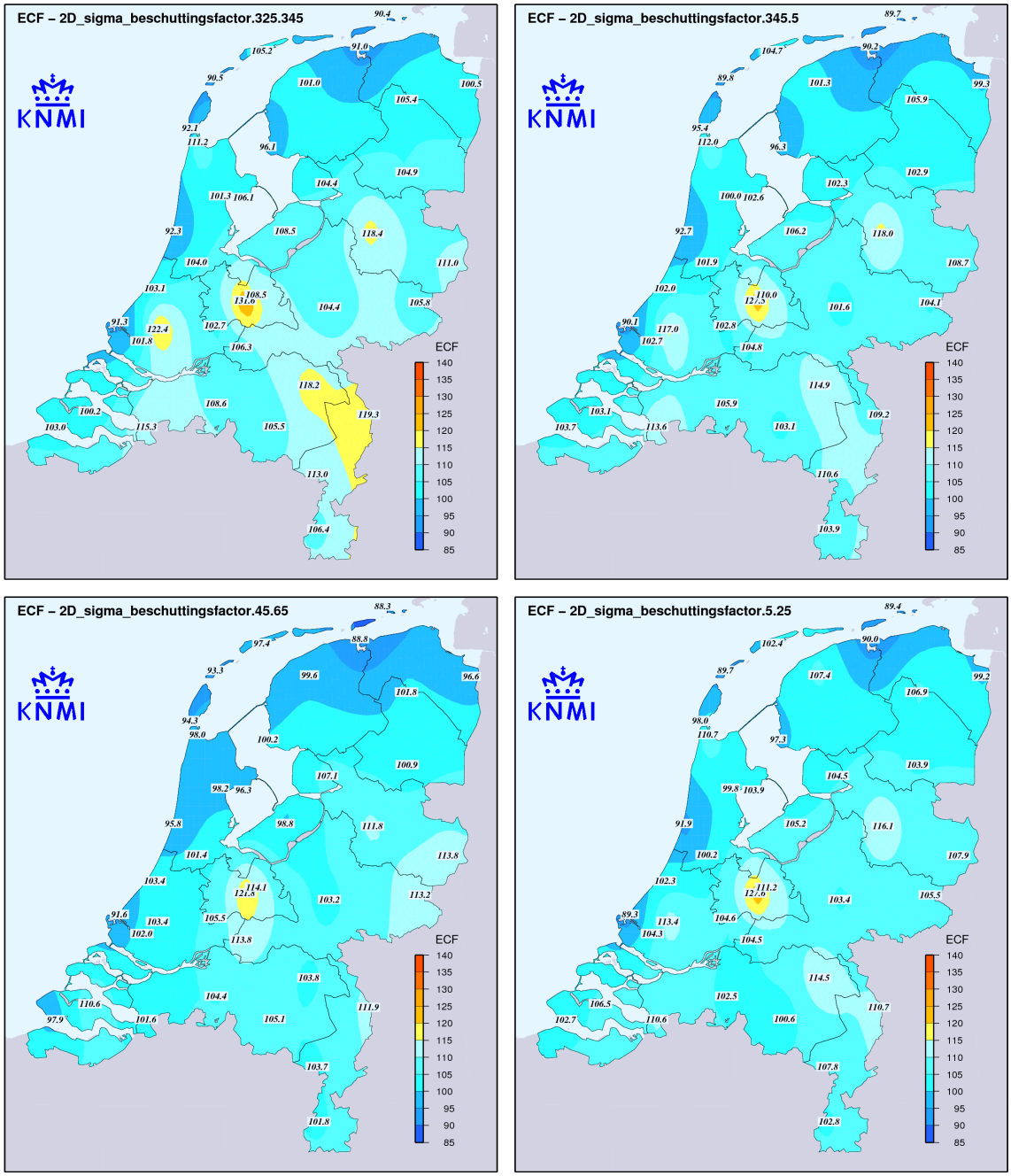


Figure C.3.4: *Directional exposure correction factors, based on $\sigma_u$ analysis. The wind direction sectors are denoted at the top line of each figure. In case the sensor height deviates from 10 m, the exposure correction factors have been adjusted, assuming a logarithmic wind profile with a roughness length derived from omnidirectional $\sigma_u$ analysis (see Section 3.3.3).*

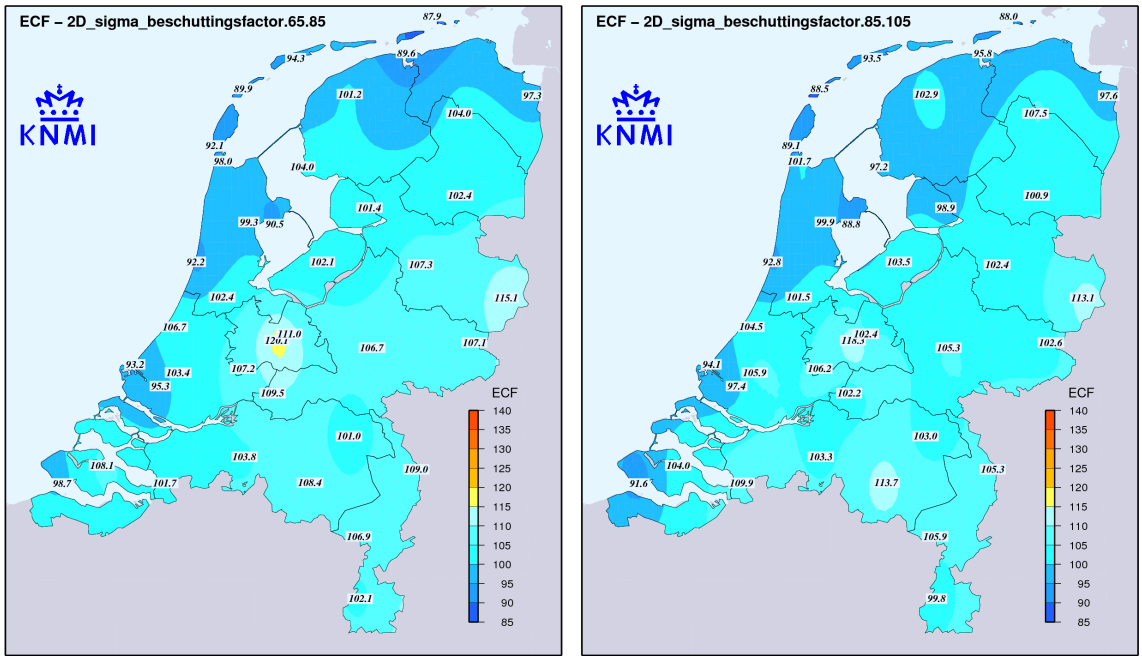


Figure C.3.5: *Directional exposure correction factors, based on $\sigma_u$ analysis. The wind direction sectors are denoted at the top line of each figure. In case the sensor height deviates from* 10 *m, the exposure correction factors have been adjusted, assuming a logarithmic wind profile with a roughness length derived from omnidirectional $\sigma_u$ analysis (see Section 3.3.3).*

# Appendix D

# Directional fit of exposure correction factors

Figures D.0.1, D.0.2 and D.0.3 show the directional relationships between exposure correction factors based on 1 hour gustiness analysis and $\sigma_u$ analysis.

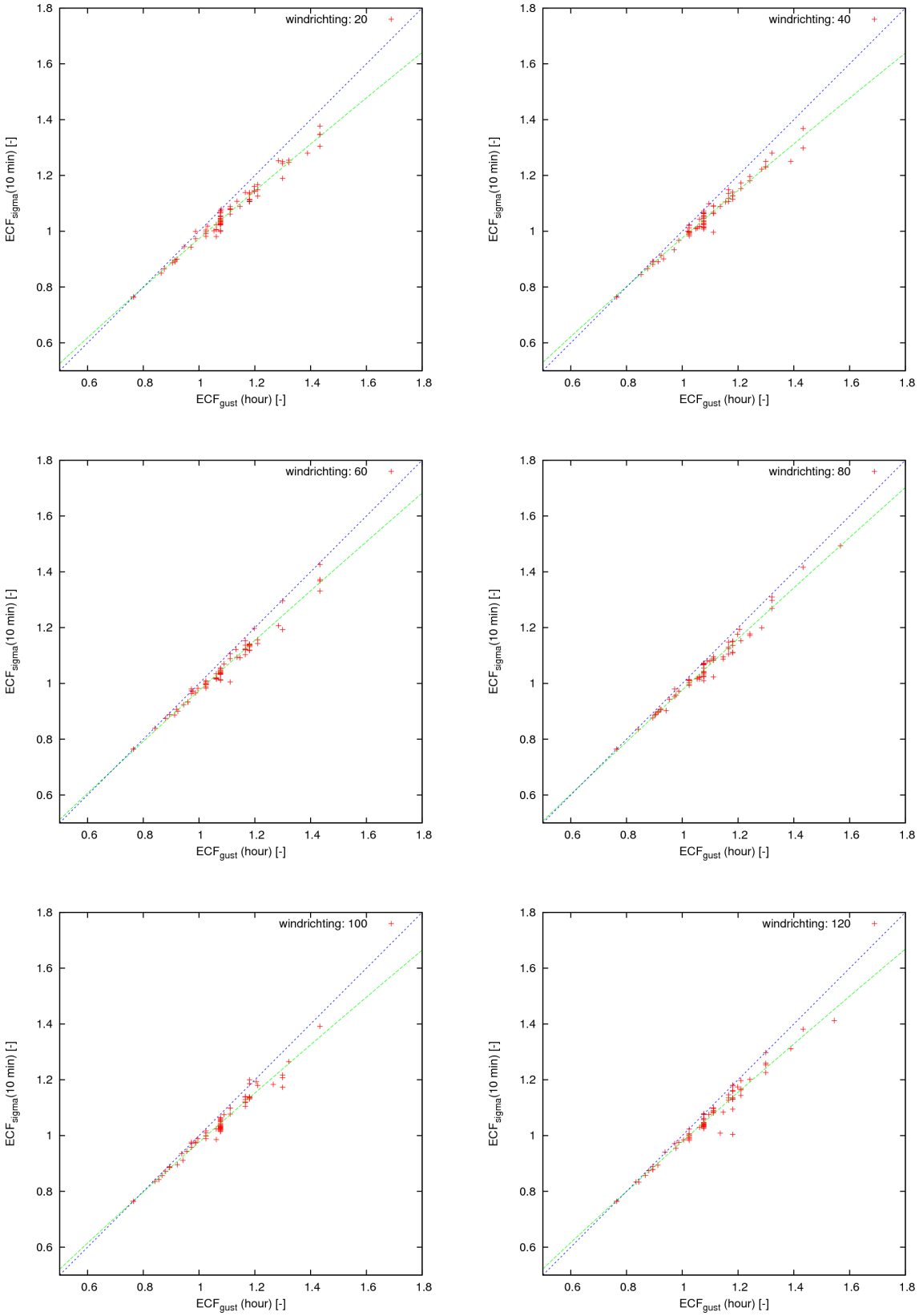


Figure D.0.1: *Plots of relation between exposure correction factors from gustiness analysis and* $\sigma_u$ *analysis for* 109 *wind sites in the period 2003-2008 for each wind direction sector. Each dot represents an exposure correction factor for a station. The wind direction sectors are denoted at the top line of each figure.*

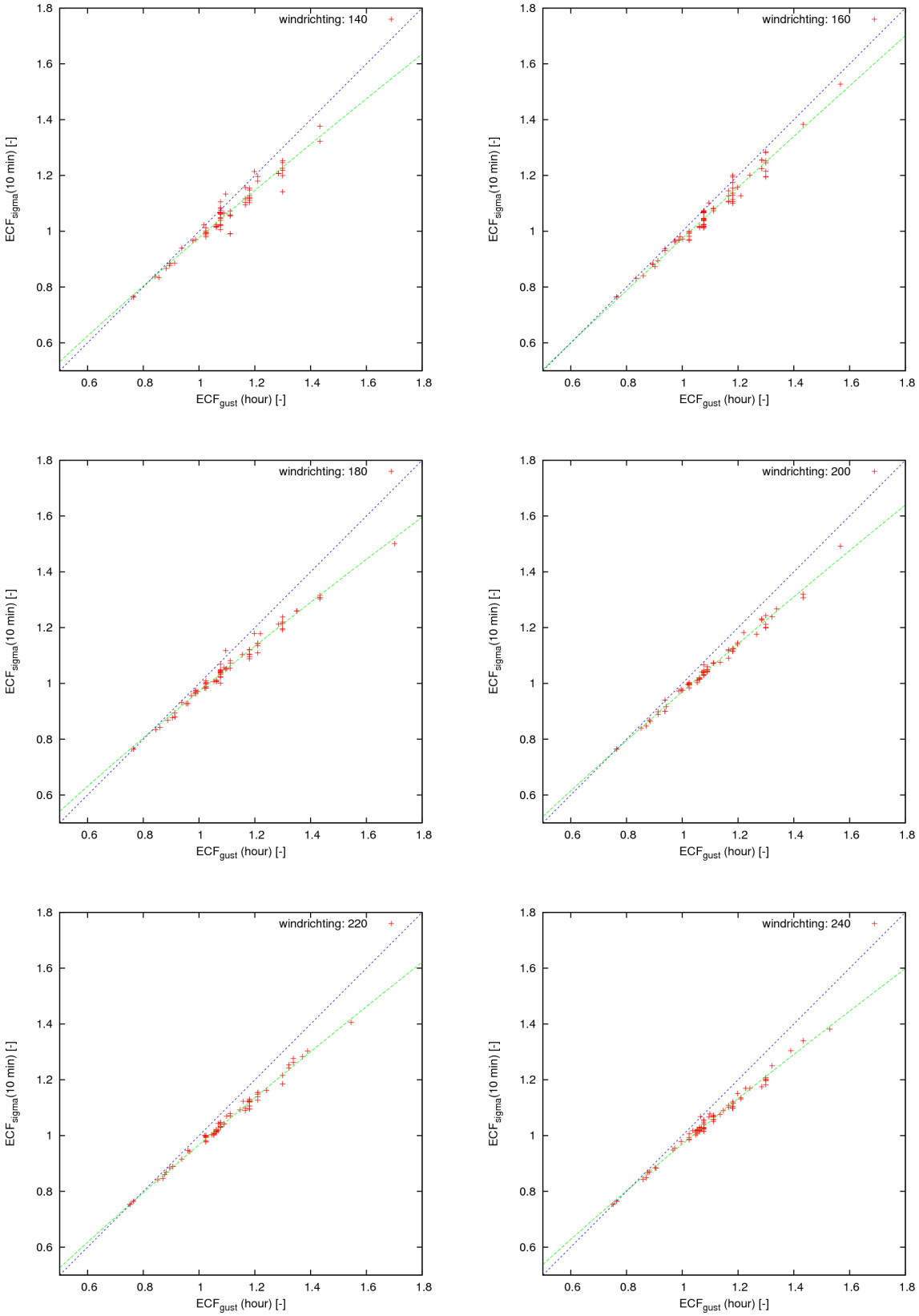


Figure D.0.2: *Plots of relation between exposure correction factors from gustiness analysis and* $\sigma_u$ *analysis for* 109 *wind sites in the period 2003-2008 for each wind direction sector. Each dot represents an exposure correction factor for a station. The wind direction sectors are denoted at the top line of each figure.*

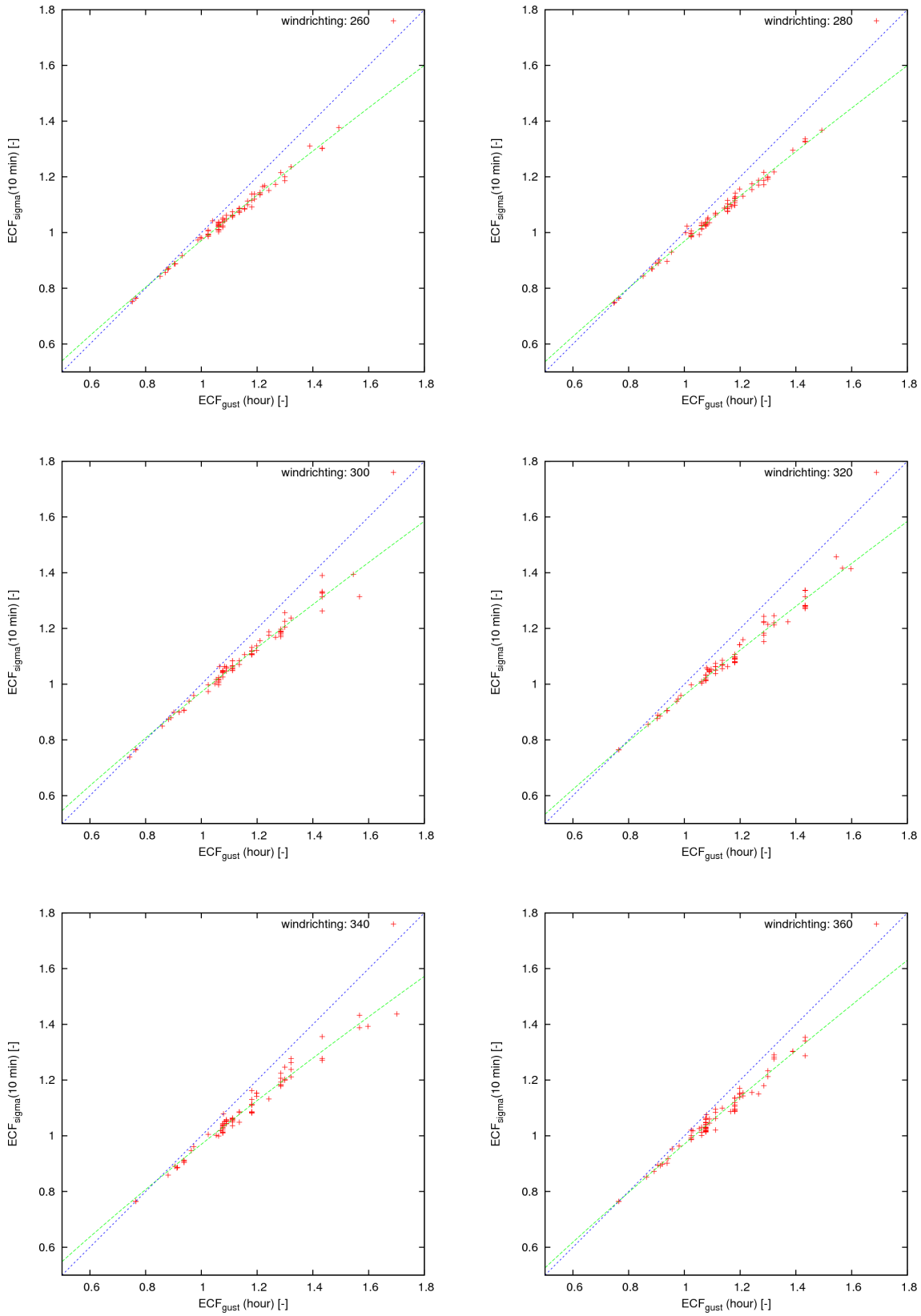


Figure D.0.3: *Plots of relation between exposure correction factors from gustiness analysis and $\sigma_u$ analysis for* 109 *wind sites in the period 2003-2008 for each wind direction sector. Each dot represents an exposure correction factor for a station. The wind direction sectors are denoted at the top line of each figure.*

# Appendix E

# Directional 1000 year return levels of potential wind

## E.1 Original data (*old*)

Figures E.1.1, E.1.2, E.1.3, E.1.4 and E.1.5 show the hourly mean potential wind speed for a return period of 1000 years, per wind direction sector. The exposure correction factors used are based on 1 hour gustiness analysis.

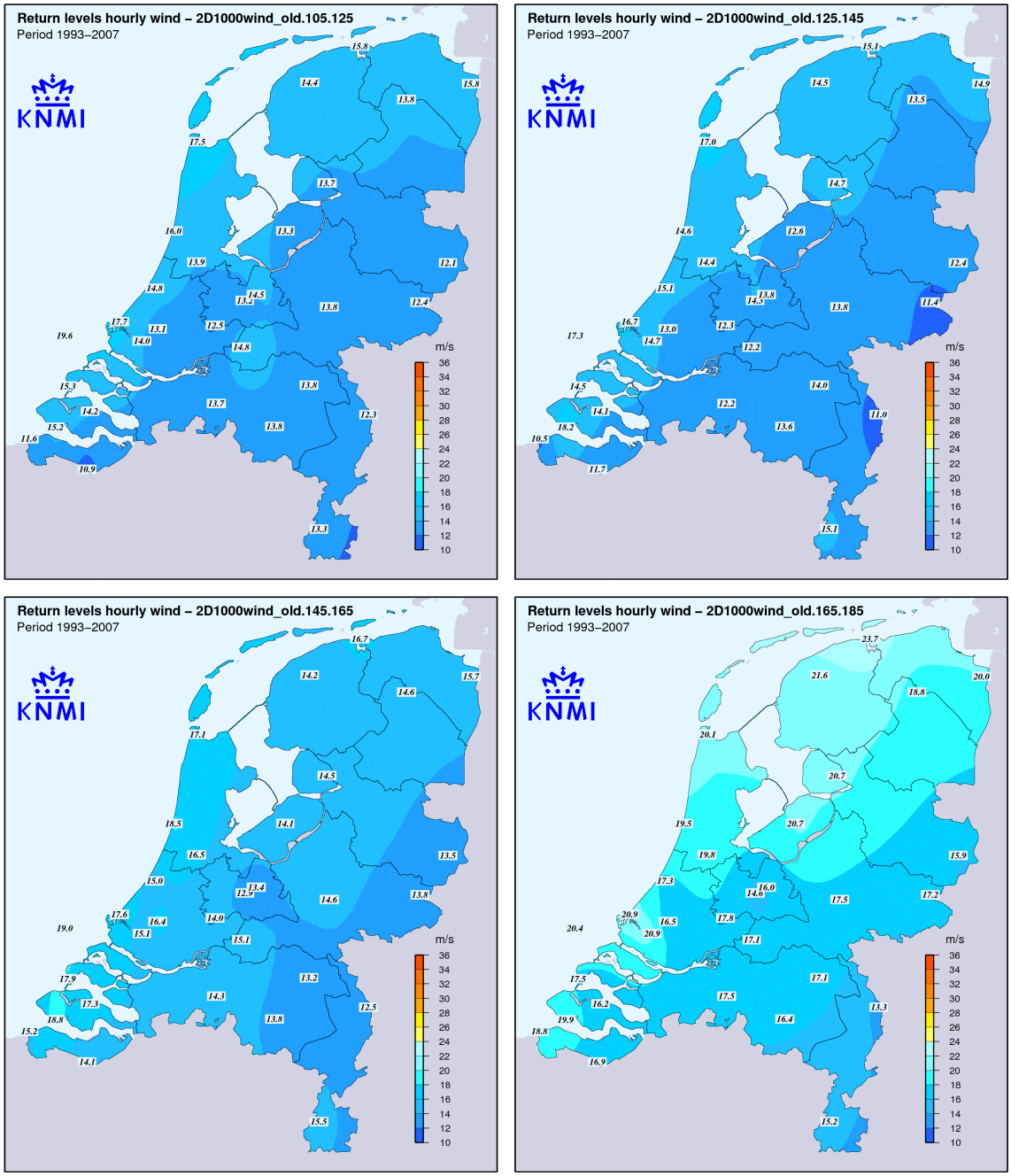


Figure E.1.1: *Directional hourly mean potential wind speeds for a return period of* 1000 *years. The wind direction sectors are denoted at the top line of each figure. Potential wind speed is calculated using exposure correction factors derived from* 1 *hour gustiness analysis. Potential wind speeds are based on a reference roughness length of* 3 *cm.*

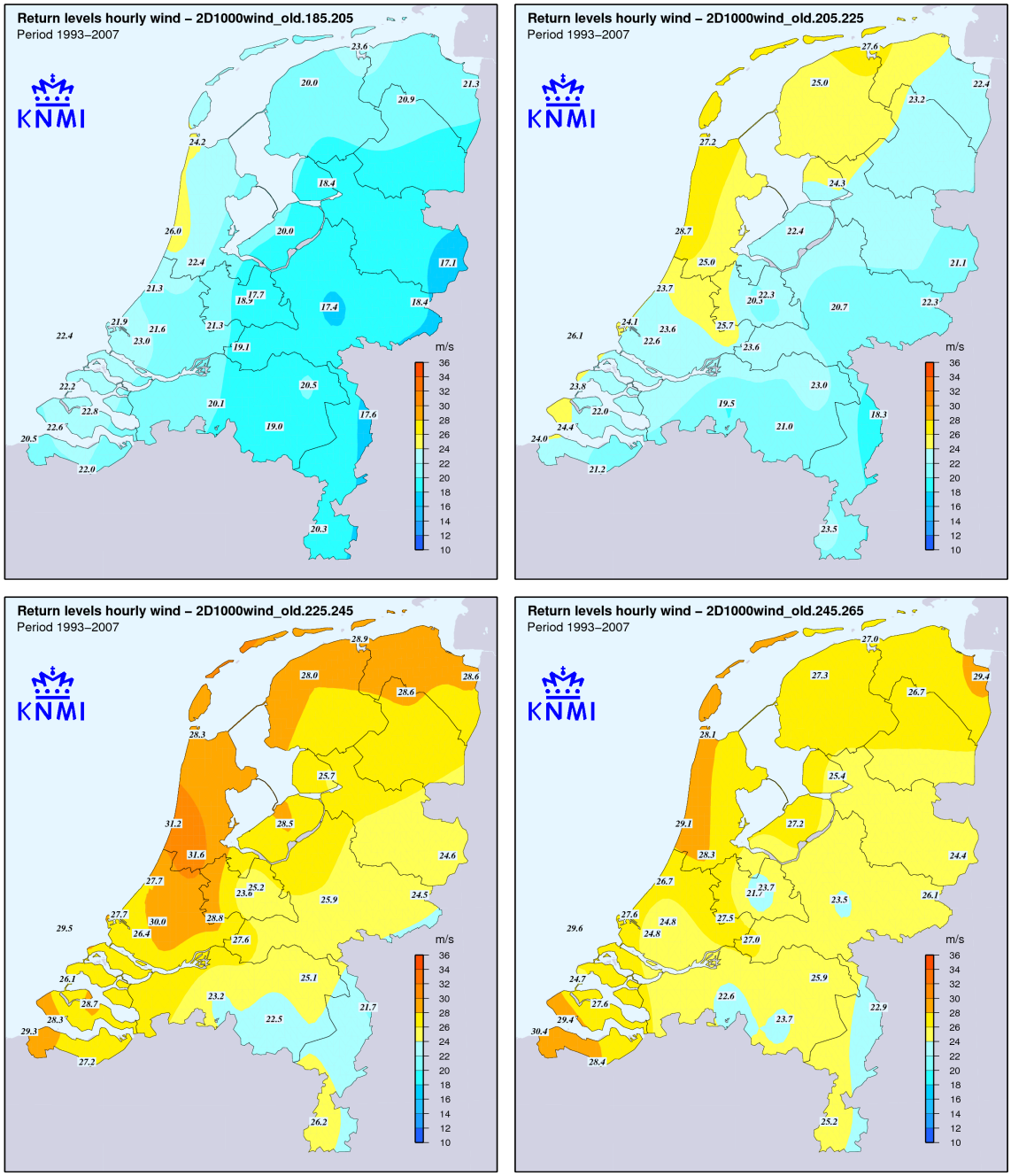


Figure E.1.2: *Directional hourly mean potential wind speeds for a return period of* 1000 *years. The wind direction sectors are denoted at the top line of each figure. Potential wind speed is calculated using exposure correction factors derived from* 1 *hour gustiness analysis. Potential wind speeds are based on a reference roughness length of* 3 *cm.*

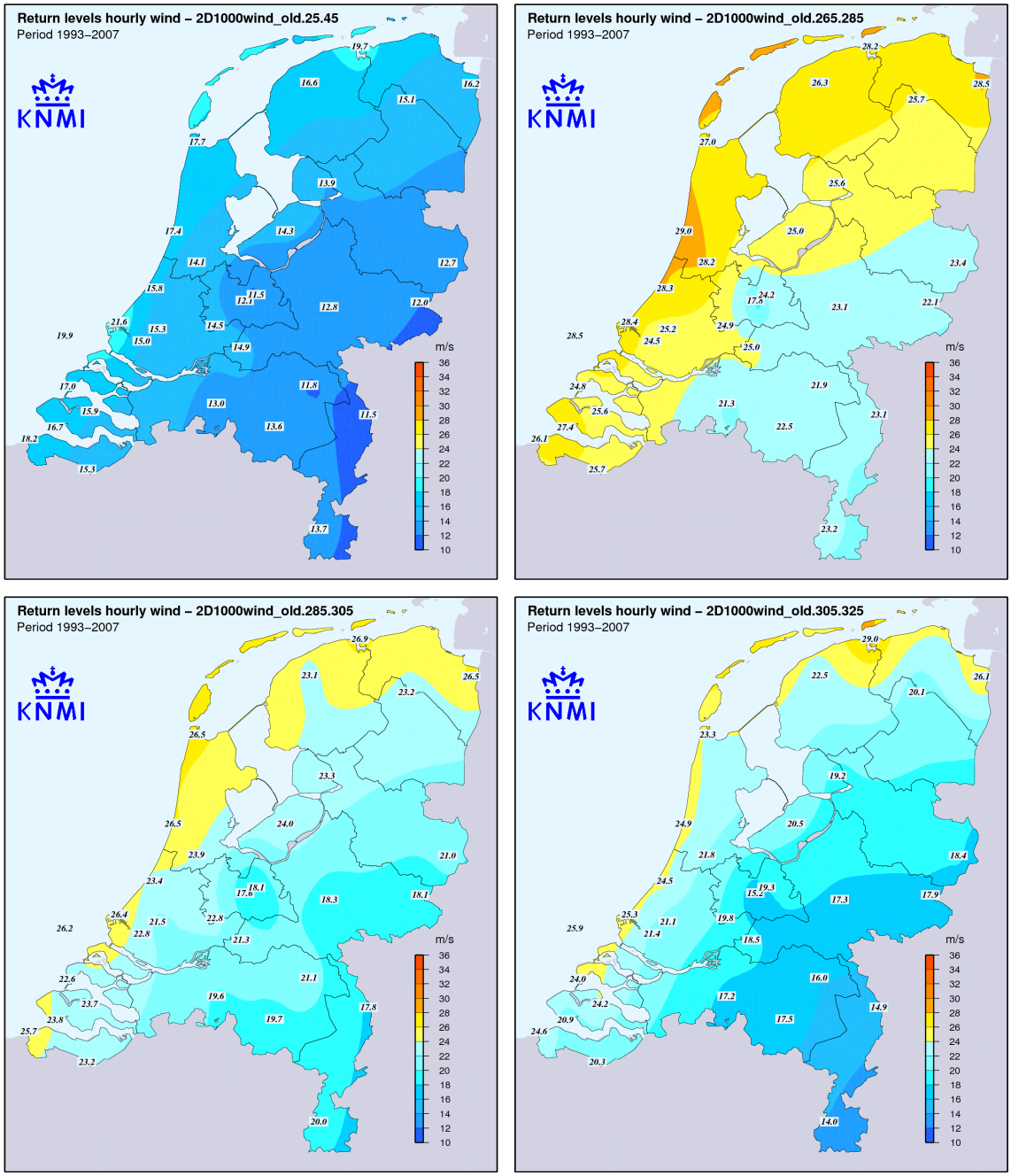


Figure E.1.3: *Directional hourly mean potential wind speeds for a return period of* 1000 *years. The wind direction sectors are denoted at the top line of each figure. Potential wind speed is calculated using exposure correction factors derived from* 1 *hour gustiness analysis. Potential wind speeds are based on a reference roughness length of* 3 *cm.*

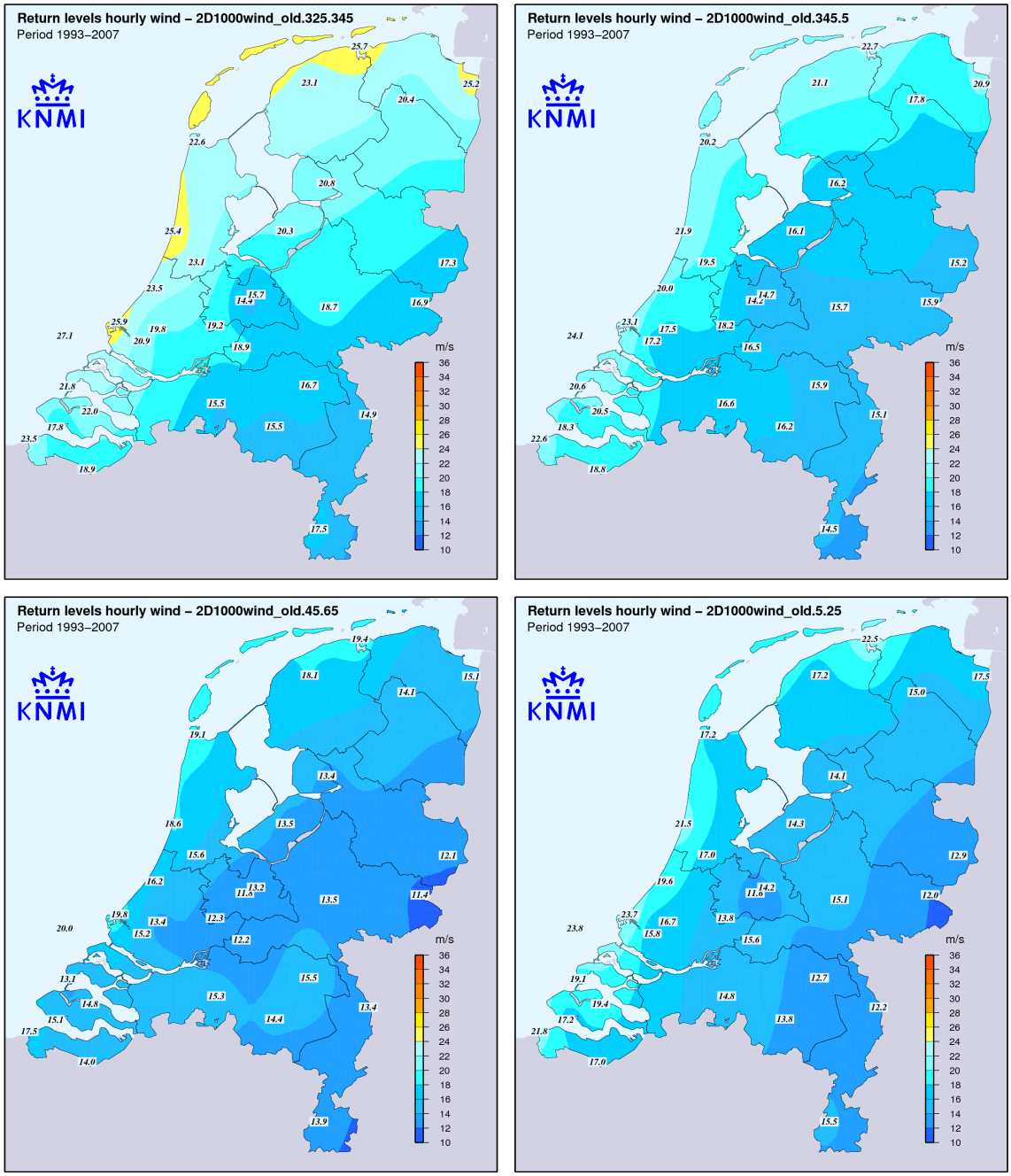


Figure E.1.4: *Directional hourly mean potential wind speeds for a return period of* 1000 *years. The wind direction sectors are denoted at the top line of each figure. Potential wind speed is calculated using exposure correction factors derived from* 1 *hour gustiness analysis. Potential wind speeds are based on a reference roughness length of* 3 *cm.*

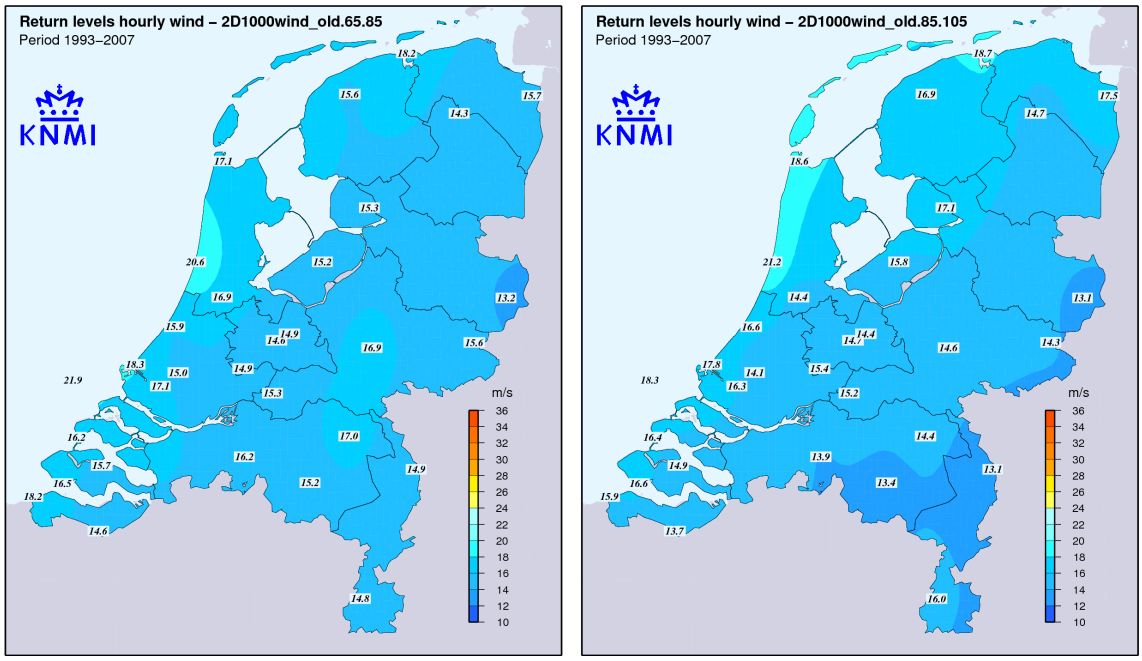


Figure E.1.5: *Directional hourly mean potential wind speeds for a return period of* 1000 *years. The wind direction sectors are denoted at the top line of each figure. Potential wind speed is calculated using exposure correction factors derived from* 1 *hour gustiness analysis. Potential wind speeds are based on a reference roughness length of* 3 *cm.*

## E.2 Corrected data (*new*)

Figures E.2.1, E.2.2, E.2.3, E.2.4 and E.2.5 show the hourly mean potential wind speed for a return period of 1000 years, per wind direction sector. The exposure correction factors are calculated by applying the fit to resemble correction factors found with $\sigma_u$ analysis (see section 4.5).

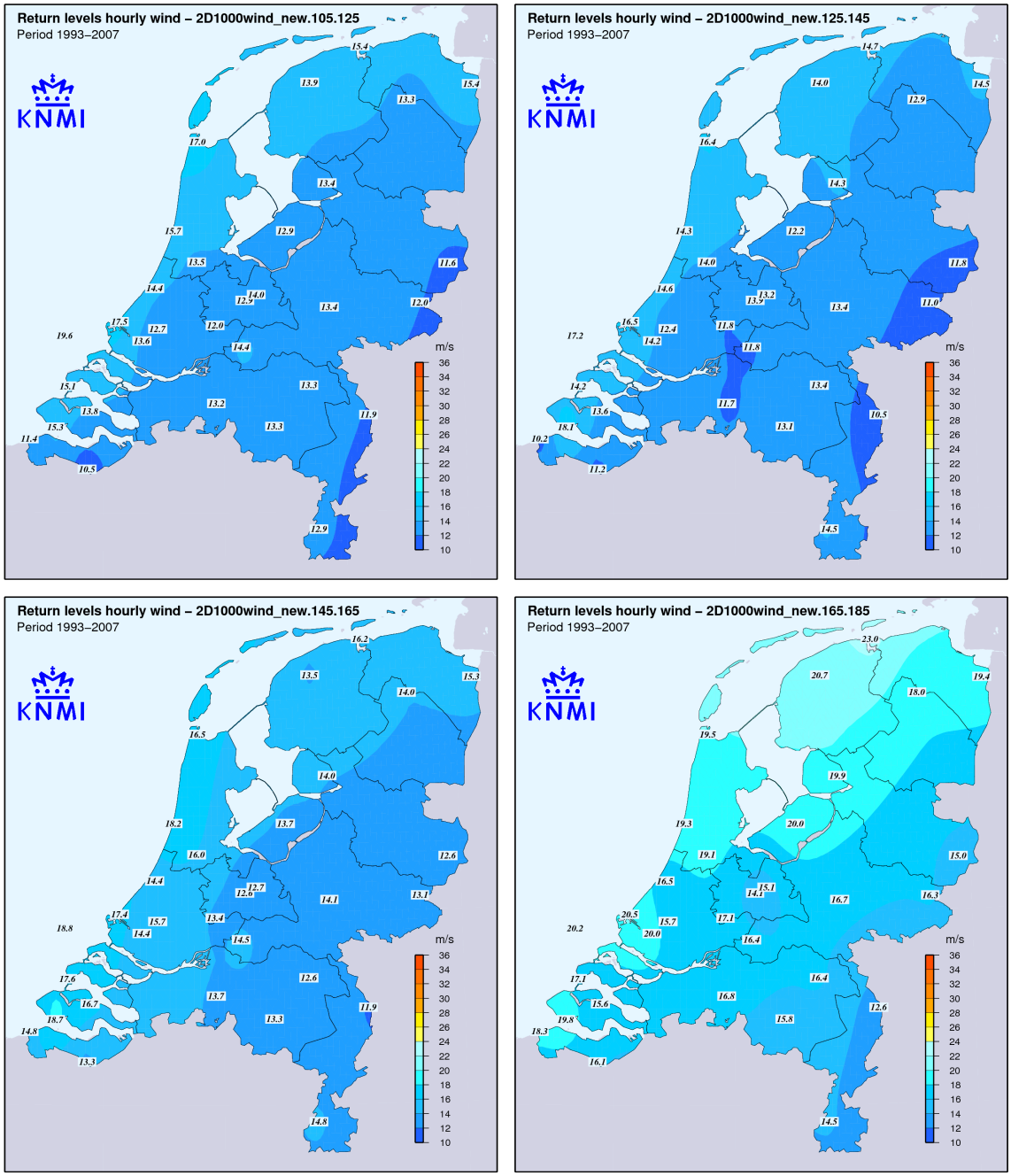


Figure E.2.1: *Directional hourly mean potential wind speeds for a return period of* 1000 *years. The wind direction sectors are denoted at the top line of each figure. Potential wind speed is calculated by applying a fit on exposure correction factors derived from* 1 *hour gustiness analysis to resemble correction factors based on* $\sigma_u$ *analysis. Potential wind speeds are based on a reference roughness length of* 3 *cm.*

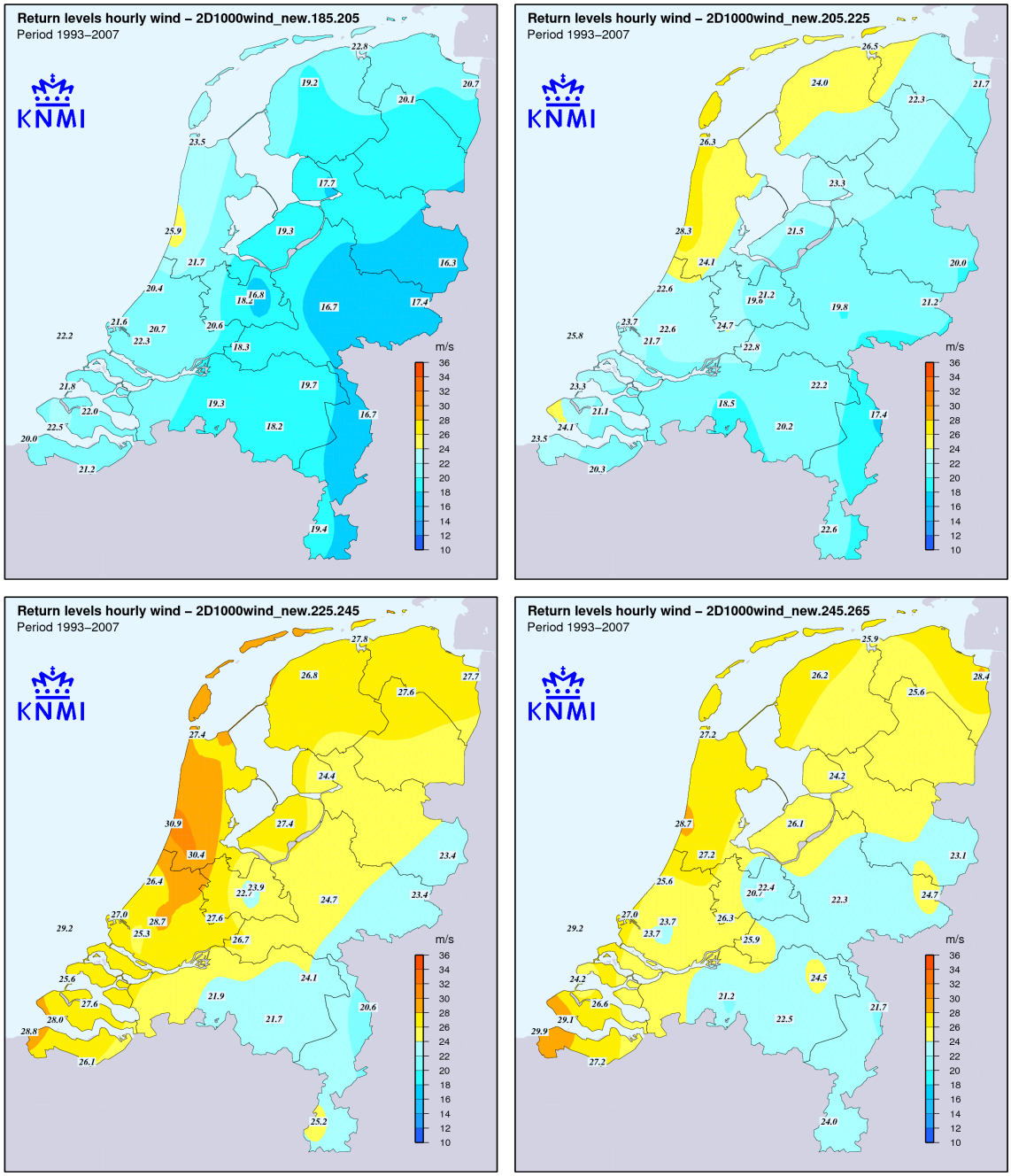


Figure E.2.2: *Directional hourly mean potential wind speeds for a return period of* 1000 *years. The wind direction sectors are denoted at the top line of each figure. Potential wind speed is calculated by applying a fit on exposure correction factors derived from* 1 *hour gustiness analysis to resemble correction factors based on* $\sigma_u$ *analysis. Potential wind speeds are based on a reference roughness length of* 3 *cm.*

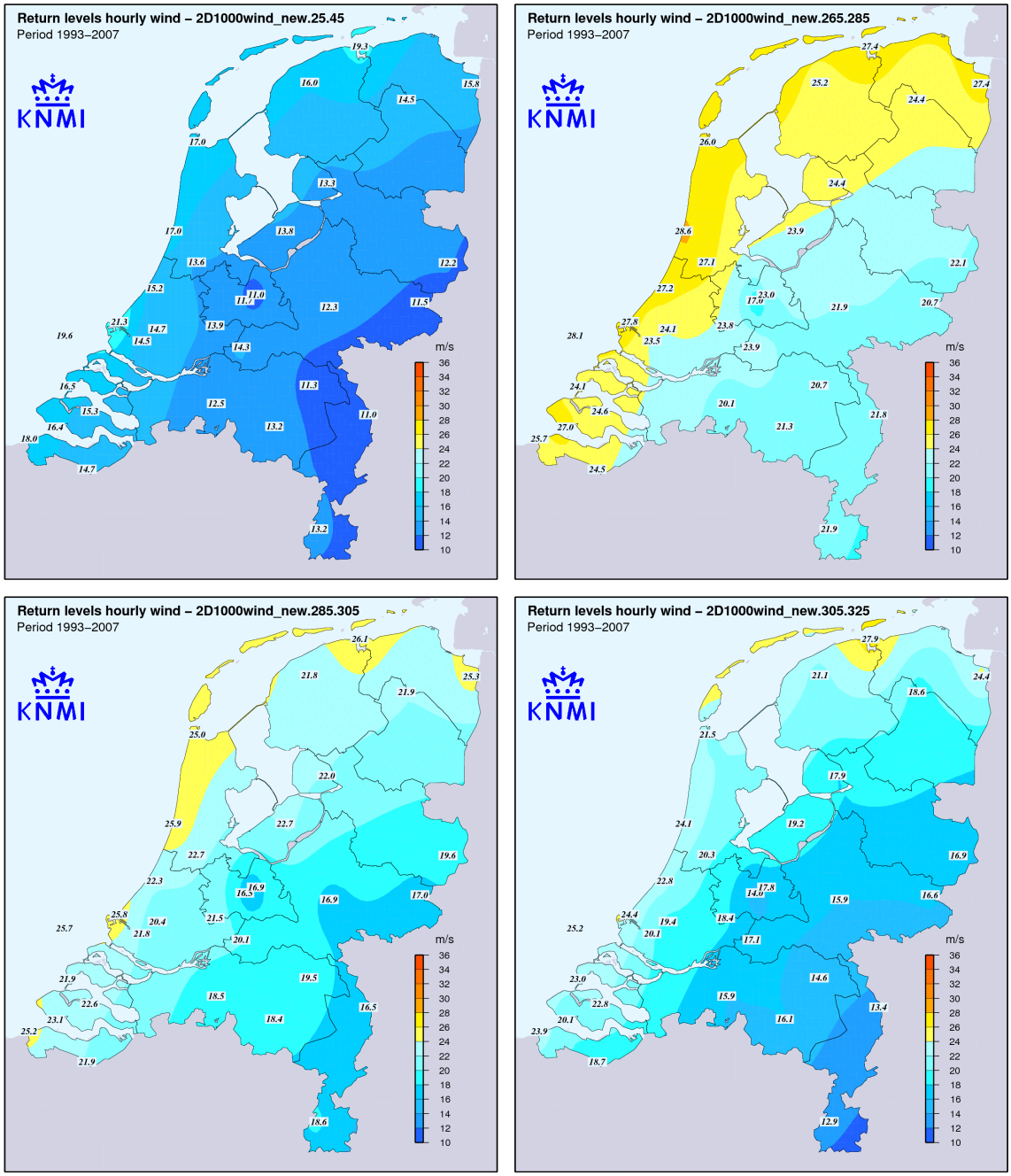


Figure E.2.3: *Directional hourly mean potential wind speeds for a return period of* 1000 *years. The wind direction sectors are denoted at the top line of each figure. Potential wind speed is calculated by applying a fit on exposure correction factors derived from* 1 *hour gustiness analysis to resemble correction factors based on* $\sigma_u$ *analysis. Potential wind speeds are based on a reference roughness length of* 3 *cm.*

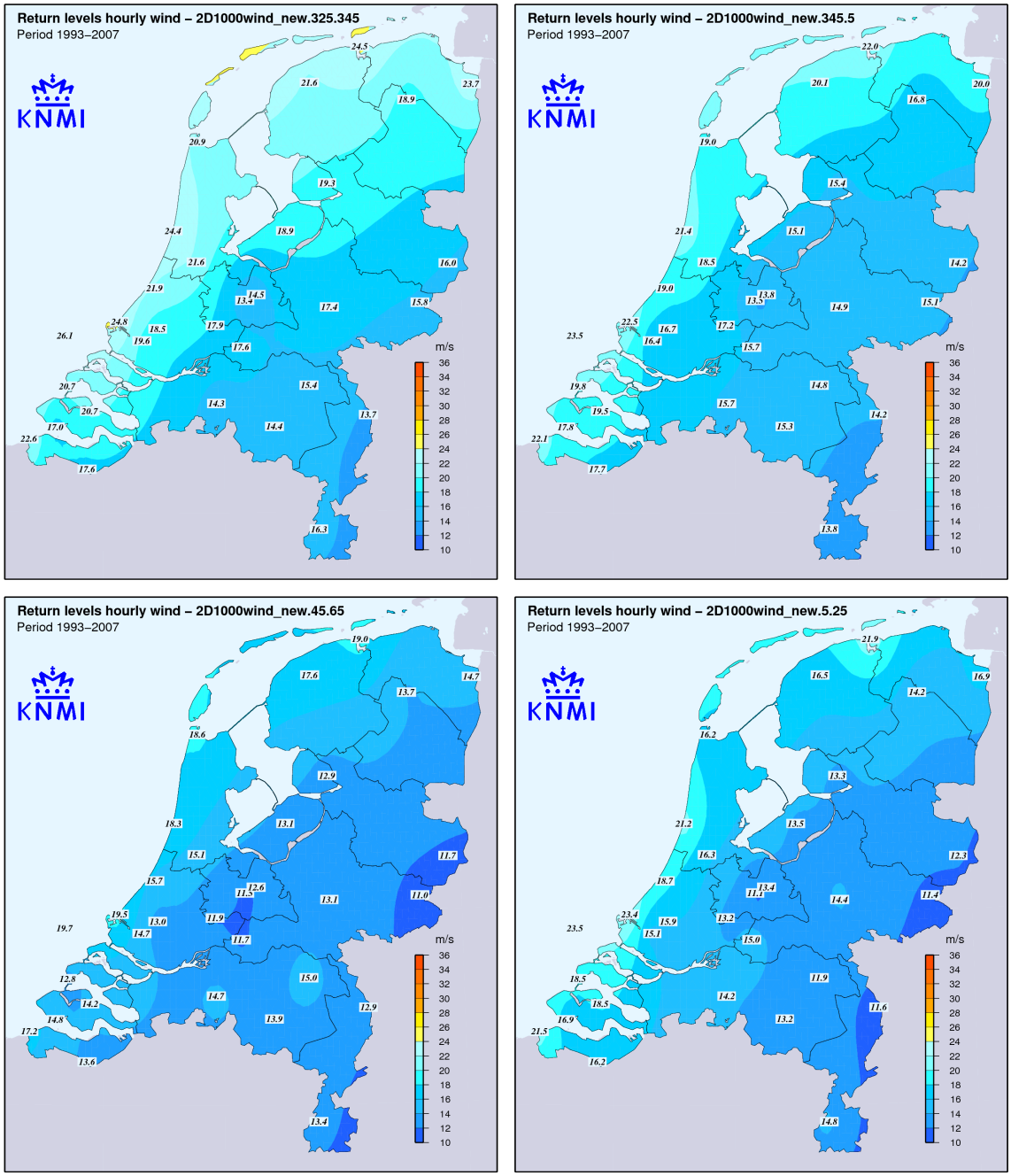


Figure E.2.4: *Directional hourly mean potential wind speeds for a return period of* 1000 *years. The wind direction sectors are denoted at the top line of each figure. Potential wind speed is calculated by applying a fit on exposure correction factors derived from* 1 *hour gustiness analysis to resemble correction factors based on* $\sigma_u$ *analysis. Potential wind speeds are based on a reference roughness length of* 3 *cm.*

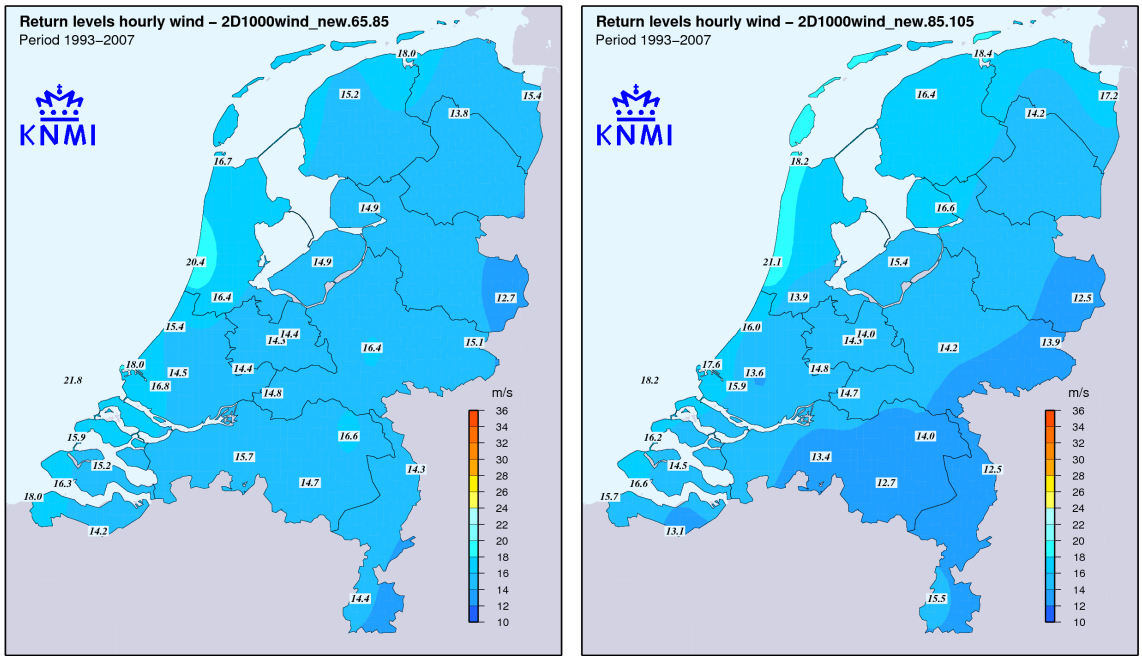


Figure E.2.5: *Directional hourly mean potential wind speeds for a return period of* 1000 *years. The wind direction sectors are denoted at the top line of each figure. Potential wind speed is calculated by applying a fit on exposure correction factors derived from* 1 *hour gustiness analysis to resemble correction factors based on* $\sigma_u$ *analysis. Potential wind speeds are based on a reference roughness length of* 3 *cm.*

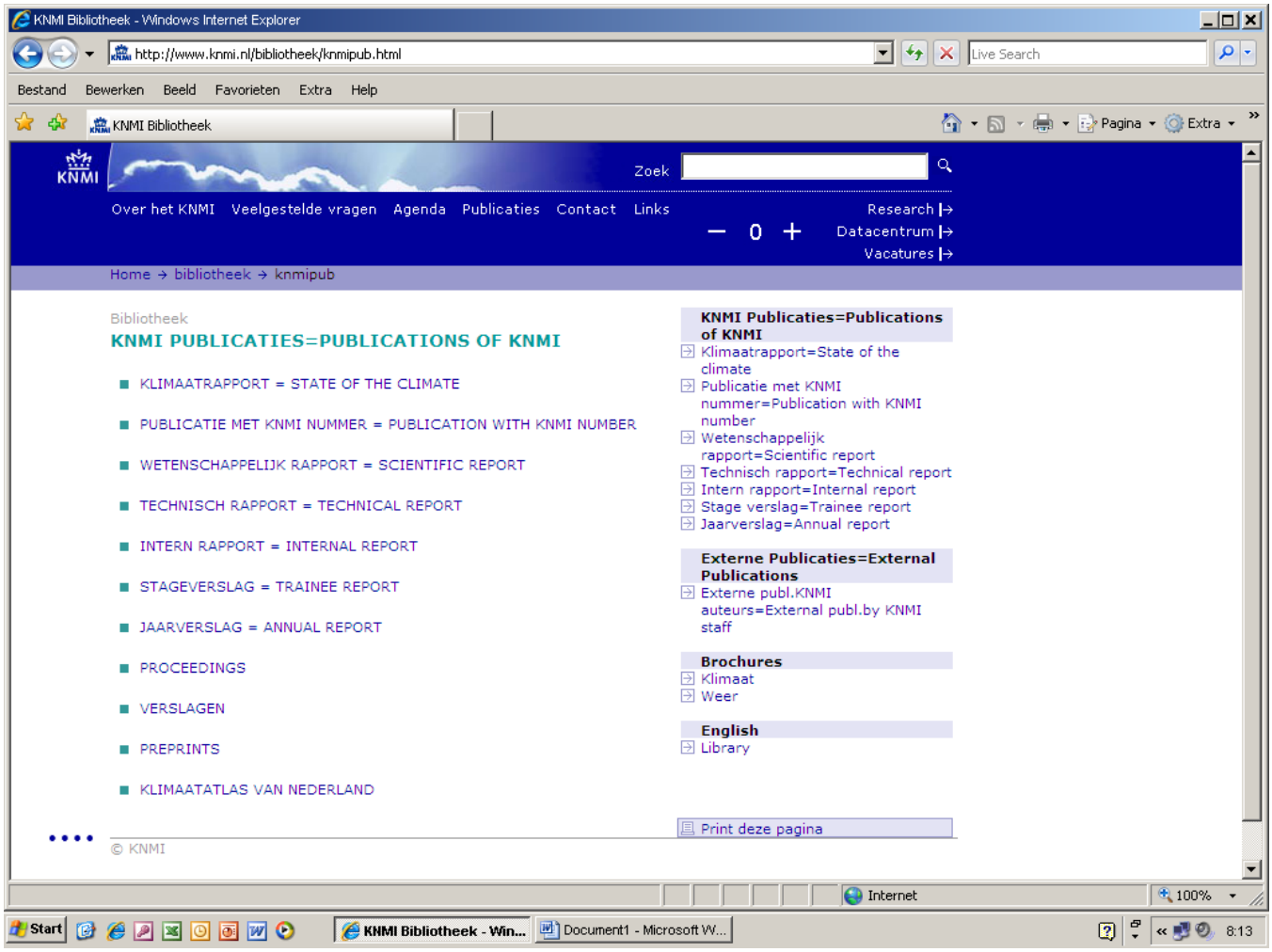


---

All titles of KNMI-publications (and a full text PDF for the most recent ones) can be found on

# http://www.knmi.nl/bibliotheek/knmipub.html

*If you have any questions, please contact us: bibliotheek@knmi.nl*